MATHEMATICAL MODELS FOR VEHICULAR CARBON DIOXIDE EMISSION

Pita Donald

A Dissertation Submitted in Partial Fulfilment of the Requirements for the Degree of Master's in Mathematical and Computer Sciences and Engineering of the Nelson Mandela African Institution of Science and Technology

Arusha, Tanzania

August, 2024

ABSTRACT

The increasing demand for transportation due to a growing global population has led to more vehicles on the road and increased use of fossil fuels, resulting in higher atmospheric carbon dioxide (CO_2) levels and contributing to global warming. Thus, adopting sustainable transportation practices is crucial for achieving climate change goals, specifically the reduction of greenhouse gas emissions to mitigate global warming. This study presents a nonlinear mathematical model to analyze the dynamics and control of atmospheric CO_2 concentration in relation to vehicle emissions. The model is qualitatively analyzed to understand long-term system behavior. Model parameters are calibrated using real-world data on world population, economic activities, atmospheric CO_2, forest biomass, and vehicle numbers. Results describes the dependence between vehicle CO_2 emissions and atmospheric CO_2 levels and impact human population decline. Numerical simulations validate analytical findings, and global sensitivity analysis explores the influence of various parameters on CO_2 dynamics. An optimal control problem is formulated and solved by using Pontryagin's principle, establishing optimality conditions. Solving the problem reveals that reducing vehicle emissions, implementing reforestation efforts, adopting green economy practices, and curbing fossil-fueled vehicle production can cut atmospheric CO_2 levels by 2.866%. Consequently, addressing climate change linked to increased atmospheric CO_2 concentration is achievable through these measures.

DECLARATION

I, Pita Donald do hereby declare to the Senate of Nelson Mandela African Institution of Science and Technology that this thesis is my original work and that it has neither been submitted nor being concurrently submitted for degree award in any other institution.

13 August, 2024

Pita Donald **Date**

(Candidate)

The above declaration is confirmed

13 August, 2024

Dr. Maranya Makuru Mayengo **Date**

(Supervisor 1)

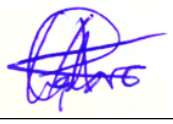

13 August, 2024

Dr. Aristide G. Lambura **Date**

(Supervisor 2)

COPYRIGHT

CERTIFICATION

The undersigned certify that they have read and hereby recommend for acceptance by the Nelson Mandela African Institution of Science and Technology a research report entitled: ***Mathematical Models for vehicular carbon dioxide emission***, in partial fulfilment of the requirements for the degree of Master's in Mathematical and Computer Sciences and Engineering of the Nelson Mandela African Institution of Science and Technology

Dr. Maranya Makuru Mayengo

(Supervisor 1)

Date: 13 August, 2024

Dr. Aristide G. Lambura

(Supervisor 2)

Date: 13 August, 2024

ACKNOWLEDGEMENTS

I express my deepest gratitude to the Almighty God for granting me the remarkable opportunity to embark on the journey of pursuing a Master's Degree at the Nelson Mandela African Institution of Science and Technology (NM-AIST). I am indebted to the National Institute Of Transport (NIT) for their generous financial support, which made my studies at NM-AIST possible.

I extend my sincere appreciation to my esteemed supervisors, Dr. Maranya Mayengo from the Nelson Mandela African Institution of Science and Technology and Dr. Aristide Lambura from Ardhi University. Their unwavering dedication, guidance, timely responses, and invaluable advice played a pivotal role in the successful completion of this study within the stipulated timeframe.

A special acknowledgment is due to the noteworthy contributions of PhD students Ibrahim Fanuel and Mussa Amos. Their encouragement, facilitation, and technical support were instrumental in the accomplishment of this work. My gratitude knows no bounds, and I can only offer heartfelt words of thanks for their indispensable role in this endeavor.

In closing, I wish to express my deepest thanks to my cherished family—my wife, Happy Raphael, my daughter, Grace, and my son, Giovanni. Their boundless encouragement, love, unwavering support, and heartfelt prayers were the pillars that sustained me throughout this academic journey. I am profoundly grateful for their significant contributions.

DEDICATION

I dedicate this work to my dear mother, the late Betelina Sambogo. She was a constant source of strength throughout my entire academic journey, and even though she's no longer here, her influence and support continue to be my guiding force. This work is a way of saying thank you to her for making me strong and determined.

TABLE OF CONTENTS

LIST OF TABLES

LIST OF FIGURES

LIST OF APPENDICES

LIST OF ABBREVIATIONS

AFOLU	Agriculture Forestry and other Land Use
BTS	Bureau of Transportation Statistics
BRT	Bus Rapid Transit
CO_2	Carbon Dioxide
DTReM-LV	Dynamic TRansport emission Model for Lativa
GDP	Gross Domestic Product
GHG	Green House Gas
IEA	International Energy Agency
LHS	Latin Hypercube Sampling.
LRT	Light Railway Transit
LSM	Least-Square Method
NIT	National Institute of Transport
PMP	Pontryagin's Maximum Principle.
PRCC	Partial Rank Correlation Coefficient.
USA	United States of America
UN	United Nations
WBOD	World Bank Open Data
WHO	World Health Organization.

CHAPTER ONE

INTRODUCTION

1.1 Background of the problem

Van Klooster (1947) observed a distinct vapor, which he called ”wood gas” or ”spiritus sylvestris,” when charcoal was burnt in a closed vessel in the 1630s. Joseph Black, a Scottish physician, also noticed a similar gas when heating calcium carbonate ($CaCO_3$), naming it ”fixed air.” He also identified carbon dioxide from exhaled breath (Van Klooster, 1947). In 1803, British chemist John Dalton proposed the composition of carbon dioxide, indicating that it consists of one carbon atom and two oxygen atoms, hence the name ”carbon dioxide” (CO_2).

Carbon dioxide is a chemical compound composed of molecules with one carbon atom covalently double bonded to two oxygen atoms. It exists in a gaseous state at room temperature and is transparent in the atmosphere. Carbon dioxide acts as a Green House Gas, absorbing infrared radiation and contributing to the Green House effect. Emissions of carbon dioxide, often represented as CO_2 emissions, result from various activities such as burning fossil fuels, changes in land use, cement manufacturing and many others. These emissions include not only the combustion of solid, liquid, and gas fuels but also the release of carbon dioxide during processes like gas flaring.

The rise in the world's population and its economic progress have caused a greater need for energy, mainly fulfilled by fossil fuels. This surge in energy requirements has led to higher levels of carbon dioxide (CO_2) emissions, worsening the issues related to climate change (Mohammadi *et al.*, 2020; Appiah *et al.*, 2021). As the population continues to expand, the use of fossil fuels and natural gas for energy production also rises, leading to higher CO_2 emissions.

The global emission of Green House Gases (GHGs) stems from various economic sectors, including energy, industry, building, transport, and agriculture, forestry, and other land use (AFOLU) (Lamb *et al.*, 2021). Excessive harvesting of natural resources leads to an increase in CO_2 emissions and energy consumption (Hussain *et al.*, 2020). Additionally, Hussain *et al.* (2020) performed a causal relationship analysis between CO_2 emissions, energy use, economic growth, natural resource depletion, urbanization, and trade openness. The results from Hussain

et al. (2020), show significant cross-sectional dependencies and heterogeneity between these variables. The study emphasizes that extraction of natural resources increases energy consumption, resulting in increased CO_2 emissions. These GHGs play a crucial role in driving climate change by contributing to the greenhouse effect. Carbon dioxide (CO_2) stands out among Green House Gases (GHGs) due to its significant contribution to climate-related catastrophes (Li *et al.*, 2021). This gas plays a key role in causing various climate-related issues such as ozone layer depletion, droughts, and global warming.

Over the past few decades, there has been a notable rise in the global volume of carbon dioxide (CO_2). One of the major factors contributing to this increase is the human population, as there exists a positive correlation between population size and CO_2 emissions (Mohammadi *et al.*, 2020; Appiah *et al.*, 2021). The expanding demand for energy, primarily met by fossil fuels, is a significant issue accompanying population growth and economic development worldwide (Appiah *et al.*, 2021). As the population continues to grow, so does the usage of fossil fuels and natural gas, consequently leading to an increase in the production of CO_2.

The increasing urban population has a significant positive impact on CO_2 emissions (Majewska & Gierałtowska, 2022). This can be attributed to the higher demand for goods and services driven by population growth, leading to an increase in GDP (Mohammadi *et al.*, 2020). Consequently, the rise in GDP promotes CO_2 emissions within the region. The higher income and expenditure of urban residents contribute to increased CO_2 emissions through greater energy consumption in transportation, including road and air travel (Mohammadi *et al.*, 2020). This high demand for mobility results in the utilization of fossil fuels as an energy source in the transportation sector, thereby contributing to the atmospheric concentration of CO_2.

The concentration of CO_2 in the atmosphere is significantly influenced by the energy sector (Verma *et al.*, 2021). Verma *et al.* (2021) developed a model to analyze CO_2 emissions from the energy sector, raising concerns about the potential difficulty in stabilizing atmospheric CO_2 levels under conditions of high energy consumption and CO_2 emission rates from this sector. The study suggests that mitigating atmospheric CO_2 levels requires minimizing energy consumption. Notably, the transportation sector is one of the major consumers of fossil fuels as an energy source. For example, urban transportation constituted 23% of overall energy-related emissions. (Zhao *et al.*, 2016), and globally, the transportation sector contributed to 25% of total CO_2 emissions resulting from the combustion of fossil fuels (IEA, 2019).

Among the GHG, Carbon dioxide (CO_2) is accompanied by human activities (Mohammadi *et al.*, 2020). The expanding CO_2 density in the global environment is large because of fossil fuel consumption, and one of the sectors that burn these fossil fuels is transportation (Zhao *et al.*, 2016). Burning fossil fuels releases CO_2 into the atmosphere, and the remaining volume of CO_2 emitted is either absorbed or stored by forest biomass and other natural processes (Yeh & Liao, 2017).

In recent years the world experienced vast climate changes, which resulted to disasters like global warming, floods, drought and other climate change related problems. GHGs are the key drivers of global warming which produces greenhouse effects. Among the GHG which contribute significantly to the global warming, CO_2 is the prominent example (Yoro & Daramola, 2020). Indeed, a strong correlation exists between a country's economic status and its carbon dioxide (CO_2) emissions. Developed countries tend to exhibit higher energy consumption, largely derived from burning fossil fuels, leading to increased carbon dioxide emissions (Ritchie *et al.*, 2020).

According to data from Ritchie *et al.* (2020), approximately 86% of global carbon dioxide emissions originate from the richest half of the world's countries, comprising high-income and middle-upper-income nations. In contrast, the bottom half, consisting of low-income and lower-middle-income countries, contributes only about 14% to global carbon dioxide emissions. The poorest countries make a negligible contribution to global carbon dioxide emissions as depicted in Fig. 1 . This disparity can be attributed to various factors, such as higher industrial activity, advanced transportation infrastructure, and energy-intensive sectors in wealthier countries. While acknowledging that variations exist within each income group due to factors like energy efficiency and government policies, the general trend underscores the larger share of carbon dioxide emissions from higher-income countries.

Despite the variety of studies devoted to the characterization, dynamics and forecast of CO_2 emissions, it is necessary to take into consideration the dynamic relationship between atmospheric CO_2 concentration, human population, human economic activities, forest biomass, and vehicle population and consider strategies for controlling the rise in atmospheric CO_2 concentration by formulating an optimal control problem. This study aims to cut down the atmospheric CO_2 concentration related to vehicle emissions by bringing together a mathematical framework and using available mitigation techniques to reduce CO_2 emissions from the transportation sec-

tor.

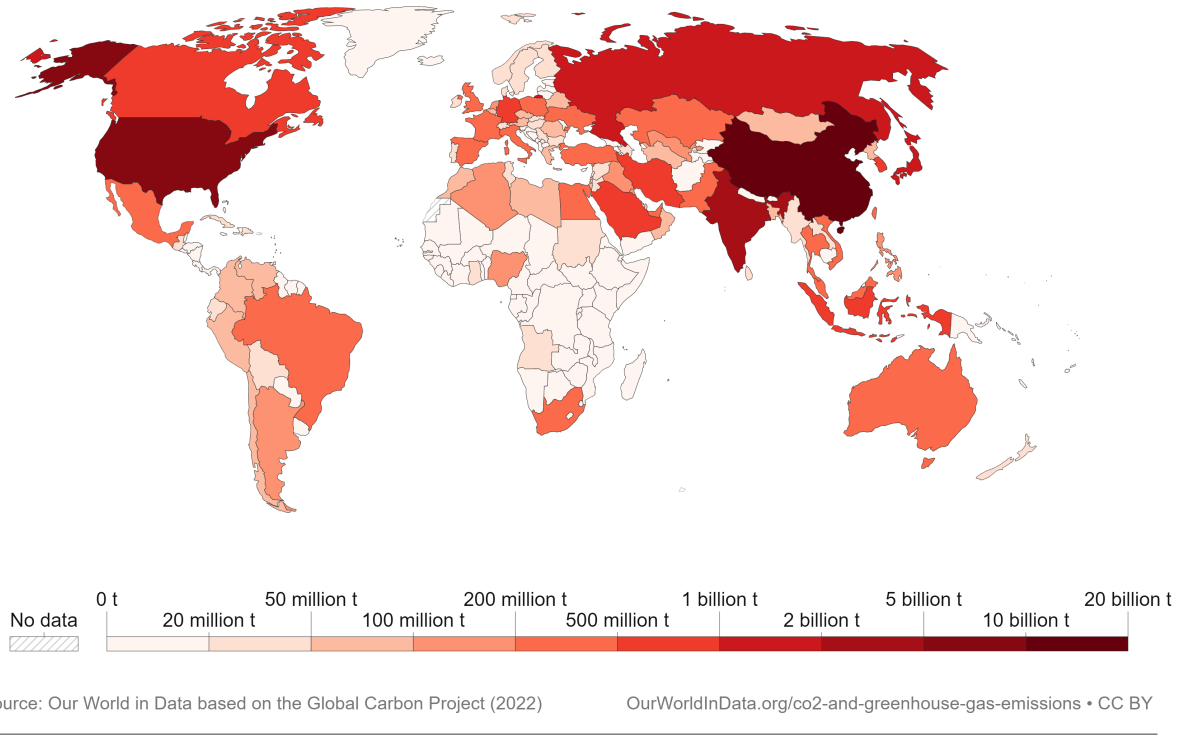

Figure 1: World annual Carbon dioxide (CO_2) emissions from fossil fuels and Industry, 2021

1.2 Statement of the problem

Recently, the rapid increase in the number of fossil-fueled vehicles, driven by population and GDP growth, has significantly contributed to CO_2 emissions resulting to an elevated concentration of CO_2 in the atmosphere, and climate-related issues (Zhao *et al.*, 2016). The increased number of vehicles burning fossil fuels is closely linked to increased CO_2 concentration, further exacerbating climate change and causing habitat loss and biodiversity decline (Mohammadi *et al.*, 2020).

The transportation industry plays a major role in the emission of CO_2 due to the combustion of fossil fuels, which contributes to the buildup of atmospheric CO_2 concentrations (Li *et al.*, 2021; Zhao *et al.*, 2016; Pedreira *et al.*, 2022). Transportation sector alone is accounted to contribute approximately 23% of the world CO_2 emission of which road transportation contribute 73% (Tan & Gao, 2015; Zhao *et al.*, 2016; IEA, 2019). As a result, climate-related concerns like ozone layer depletion, droughts, and global warming have become more pronounced.

The development of mathematical models for vehicular CO_2 emissions is crucial for comprehensively understanding and effectively managing the environmental impact of transportation systems. Previous studies have attempted to capture the relationship between CO_2 emissions, energy usage, and human population, as evidenced by models such as those proposed by (Li *et al.*, 2021; Verma *et al.*, 2021). However, these models frequently neglect to account for significant interactions with pivotal factors, including economic activities, vehicle population and forest biomass.

In this study, we aim to address these limitations by developing a deterministic mathematical model that integrates the dynamics of vehicular CO_2 emissions with the complex interplay of human population dynamics, economic activities, and forest biomass dynamics. By incorporating optimal control techniques, our model will enable us to not only predict CO_2 emissions more accurately but also identify optimal strategies for mitigating emissions while balancing socio-economic needs and environmental conservation efforts. By bridging the gap between existing models and the real-world complexities of transportation systems, our research seeks to provide policymakers and urban planners with a valuable tool for designing effective strategies to reduce carbon emissions and promote sustainable development.

1.3 Rationale of the study

The growing human population and economic expansion have intensified the demand for mobility in both human transportation and the movement of goods and services. This surge in mobility has consequently amplified global transportation activities, with vehicles being the primary facilitators of this demand. However, a significant drawback of heightened transportation activities is the increased concentration of atmospheric CO_2, with adverse environmental effects when present in large volumes. This study aims to develop a mathematical model that captures the dynamic relationships among atmospheric CO_2 levels, human population, economic activities, forest biomass, and the population of vehicles. Additionally, the study seeks to apply a mathematical framework to optimize the mitigation of vehicle CO_2 emissions, thus formulating an optimal control problem.

This study provides environmentalists, policymakers, government officials, researchers, and society at large with valuable insights into effective strategies for mitigating the rise in atmospheric CO_2 concentration and its detrimental impact on the environment. The anticipated find-

ings are expected to contribute to the ongoing discourse on climate change mitigation policies and serve as an alert to society about utilizing available environmentally friendly transportation options.

1.4 Research objective

1.4.1 General objective

The main objective of this study is to develop and analyze mathematical models describing the dynamics and possible controls of vehicular Carbon dioxide (CO_2) emissions.

1.4.2 Specific objectives

The specific objectives of the study are:

(i) To develop and analyze vehicular CO_2 emission models

(ii) To estimate model parameters

(iii) To validate the vehicular CO_2 emission model

(iv) To determine the optimal control strategies for mitigating vehicular CO_2 emission

1.5 Research questions

This research was guided by following questions:

(i) How can the pattern of CO_2 emissions be mathematically modeled?

(ii) What methods are there for estimating model parameters using the data at hand?

(iii) Using the available data set, how can the model be validated?

(iv) What kind of controls might be put in place to lessen CO_2 emissions from vehicles?

1.6 Significance of the study

This research holds significance for environmentalists, policymakers, governments, international organizations, researchers, and society at large in several key aspects. Firstly, it aids in comprehending the parameters that drive the dynamics of atmospheric CO_2, facilitating informed decisions regarding the imposition of control measures. Secondly, by implementing

optimal control measures, the study furnishes policymakers and governments with insights to formulate policies and design programs aimed at mitigating vehicle CO_2 emissions to attain 13^{th} SDGs. Lastly, for researchers, this study contributes to existing literature, offering new knowledge and providing a foundation for further exploration into the dynamics and control of atmospheric CO_2 concentration resulting from vehicle emissions.

1.7 Delineation of the study

This study does not solely consider the impact of alternative transportation options, such as shared mobility facilities and other modes of transport, on atmospheric CO_2 dynamics. Rather, it establishes a foundation for predicting the long-term effects of increased vehicular CO_2 emissions on atmospheric CO_2 concentrations and human populations. Additionally, it provides a mathematical framework for implementing available mitigation options to reduce CO_2 emissions from vehicles.

CHAPTER TWO

LITERATURE REVIEW

2.1 Introduction

In recent times, complexity sciences in which mathematical modeling is among of it, has gained prominence as a tool for addressing various challenges in different communities like saving human lives as pointed out by Helbing *et al.* (2014). Among several, options mathematical modeling tools can be helpful in selection of the best options from set of alternatives. For instance optimal control theory can be applied to make an informed decision for the best allocation of control strategies to a particular problem. Numerous researchers have made efforts to solve societal issues by employing mathematical models, such as epidemiological problems, ecological problems, and pests management problems. This section outlines significant studies that have employed mathematical models to analyze the dynamics of atmospheric CO_2, mathematical models for optimizing CO_2 emissions control, as well as statistical and other models for studying and managing atmospheric CO_2 levels.

2.2 Models for atmospheric CO_2 dynamics and emissions

A non-linear mathematical model, consisting a system of differential equations, applied to examine the impact of genetically modified trees on controlling atmospheric CO_2 concentration (Verma & Verma, 2021) . The study findings indicated that the plantation of genetically modified trees expands the forest's capacity to store CO_2, resulting in a depletion of CO_2 concentration in the atmosphere. Furthermore, a non-linear deterministic mathematical model was developed by Caetano *et al.* (2008) to describe the dynamics between CO_2 emission, Gross Domestic Product (GDP), and forest area. The model revealed that increasing the rate of reforestation and adopting clean energy sources like renewable energy significantly reduce CO_2 concentration in the atmosphere. It was also observed that increasing forest biomass facilitates the reduction of CO_2 concentration, while excessive forest harvesting accelerates CO_2 concentration. Similar findings highlighted that, motivating society to expand forest biomass can lead to the depletion of CO_2 concentration (Devi & Gupta, 2019). Additionally, the study suggests that shifting to clean energy technologies instead of relying on fossil fuels can contribute to reducing atmospheric CO_2 concentration.

Also, a non-linear mathematical model was utilized to investigate the dynamics of atmospheric CO_2 concentration, human population, and forest biomass (Misra & Verma, 2013). The findings indicated that the human population experiences a decline as a result of increased CO_2 emissions from their daily activities. Furthermore, the depletion of forest biomass caused by population growth contributes to the acceleration of atmospheric CO_2 concentration. Excessive deforestation leads to high CO_2 concentration in the atmosphere, while the implementation of reforestation strategies helps stabilize CO_2 concentration. The study suggests that mitigation policies should prioritize the development of more energy-efficient appliances and promote behavioral changes in society to encourage energy conservation.

Furthermore, a deterministic mathematical model to study the achievement of sustainable forest management was conducted (Misra & Lata, 2015). The study considered human population overgrowth and the development activities as the source of forest biomass depletion. The study proposed that, to reduce the population pressure, economic efforts should be employed to provide incentives such as fuel efficient stoves, biogas, subsidies on goods that are alternative of forest resources. The study suggested to plant genetically engineered plants in order to conserve forest resources.

The dynamics of CO_2 gas in relation to the absorption or storage capacity of plants was analyzed by using a non-linear mathematical model (Devi & Gupta, 2019). It suggests that increasing the population of plants with a high capacity to absorb or store CO_2 can lead to a depletion of CO_2 concentration in the atmosphere. Conversely, when deforestation occurs at a high rate, it results in a rapid increase in atmospheric CO_2 concentration. The study emphasizes the importance of categorizing plant populations based on their capacity to absorb or store CO_2 and prioritizing the plantation of forest biomass, which acts as a significant CO_2 sequester.

A Dynamic TRansport emission Model for Lativa (DTReM-LV model) developed by the Institute of Energy Systems and Environment (Barisa & Rosa, 2018). The model consists of a system dynamics based on computer simulation model for mitigating of CO_2 emission from road transportation sector in Lativa. It suggests the use of alternative fuel vehicles, public transport use and subsidy on the alternative fuel vehicles for sustainable transportation.

Inline with the United Nation (UN) goals to attain low emissions that will disappear from 2040's with no direct removal of atmospheric CO_2. Jaoua (2019) proposed an exponential

model for reduction and stabilization of CO_2 emissions the simulations of the model concurred with the UN climate simulations. Jaoua (2019) quantified the global warming wit time to determine the moment when the UN goals will be attained. Also, a Box-Jenkins methodology for predicting the trend of atmospheric CO_2 emissions using data from NOAA (2020) was employed and findings revealed that, the global atmospheric CO_2 concentration shows higher increasing trend for the up coming years (Jawahar Farook & Senthamarai Kannan, 2014).

Regarding deforestation, the study by Misra *et al.* (2015) also highlights it as a core cause of increased atmospheric CO_2 concentration. They propose a non-linear mathematical model to study the impact of reforestation and the delay between measuring forest biomass and implementing reforestation efforts. The findings suggest that increasing forest biomass through reforestation leads to a decrease in atmospheric CO_2 concentration. This is because a higher forest biomass enhances the absorption or storage of CO_2, resulting in a depletion of atmospheric CO_2.

The study by Verma *et al.* (2021) established a dynamic relationship between energy use, atmospheric CO_2 concentration, and human population. It employs optimal control measures to identify effective ways of reducing atmospheric CO_2. The study proposes that switching to low CO_2 energy sources, such as renewable energy, can reduce the cost of mitigating CO_2 emissions. Additionally, behavioral changes in society to reduce energy consumption are seen as a way to deplete CO_2 emissions.

While existing literature has delved into various aspects of atmospheric dynamics and carbon dioxide (CO_2) emissions, a critical void emerges in the specific exploration of mathematical models dedicated to studying the intricate dynamics of atmospheric CO_2 concentration concerning vehicular emissions. This gap is particularly noteworthy given the pressing global concern of rising greenhouse gas levels and the significant contribution of transportation activity to this environmental challenge. The proposed study seeks to bridge this gap by introducing a non-linear mathematical model designed explicitly to scrutinize the dynamics of atmospheric CO_2 concentration, with a focused emphasis on the nuanced interplay between vehicle emissions and their impact on atmospheric CO_2. By incorporating available mitigation options, the research aims to provide a comprehensive understanding of the dynamics involved, offering insights crucial for developing targeted strategies to reduce and manage CO_2 emissions from vehicles. This endeavor is pivotal not only for advancing the scientific understanding of at-

mospheric dynamics but also for informing practical interventions to curb the environmental impact of vehicular emissions.

CHAPTER THREE
MATERIALS AND METHODS

3.1 Introduction

In this chapter, mathematical models for CO_2 emission from vehicles are formulated and analyzed. Firstly, a deterministic model is formulated by using non-linear ordinary differential equations and the boundedness of model solution is tested. The steady state values of the model system was computed and their stability properties was established. Secondly, model parameters for the basic model was estimated using actual data sets by employing Least square method. Lastly, an optimal control problem was formulated and solved numerically.

3.2 Basic model formulation

When formulating the system of nonlinear ordinary differential equations, five state variables were taken into consideration. These equations were utilized to model the dynamics of atmospheric CO_2 concentration concerning human population, economic activities, forest biomass, and vehicle population. The following assumptions underlie the formulation of model (6):

(i) Previous scholars (Misra *et al.*, 2015; Verma & Verma, 2021; Misra & Verma, 2013; Misra & Lata, 2015) have discussed the assumption that, human population follows a logistic growth pattern and it is depleting due to negative impacts caused by increased atmospheric CO_2 concentration like global warming and other climate related issues. Also, it is growing due to extraction of forest resources.

(ii) Human economic activities is assumed to grow as human population increases, also it is assumed to be proportional to vehicle population and it is assumed to deplete naturally. Furthermore, human economic activities is assumed to be quantified by GDP.

(iii) Atmospheric CO_2 concentration is assumed to grow due to human economic activities, vehicle population and natural processes such as volcanic eruption and it is depleting due to forest biomass through photosynthesis process and natural processes.

(iv) Forest biomass is assumed to grow logistically and is depleting due to anthropogenic activities (Misra *et al.*, 2015; Verma & Verma, 2021; Misra & Verma, 2013; Misra & Lata, 2015).

(v) Vehicle population is assumed to grow due to demand for mobility of both humans, goods and services and it depletes naturally.

3.3 Model description

The system of non-linear ordinary differential equations is used to describe the dynamics of atmospheric CO_2 concentration. The model is made up of five distinct compartments, namely, human population (N), human economic activities (H), atmospheric CO_2 concentration (C), forest biomass (B) and vehicle population (V) at a time t. It is assumed that the human population grows logistically and depletes due to the adverse impact of increased atmospheric CO_2 concentration by a rate α (Misra & Lata, 2015; McMichael *et al.*, 2006). Also, it is assumed that human population increases due to consumption of forest resources by a rate ω (Misra & Lata, 2015). Using these assumptions, the dynamics of human population is governed by the Equation (1) and parameter descriptions are in Table 2.

$$\dot{N} = rN\left(1 - \frac{N}{L}\right) + \omega\psi NB - \alpha CN \tag{1}$$

Human economic activities are assumed to expand in response to population growth, as it drives increased demand for goods and services, and depletes naturally by a rate η. The growth of human activities is assumed to be influenced by the number of vehicles by the rate τ. As number of vehicle increases, it stimulates various economic sectors and promotes overall economic growth. This, in turn, leads to an expansion of human activities and their impact on the environment. Additionally, we assume that the growth of human economic activities is quantified by the Gross Domestic Product (GDP). The GDP serves as an indicator of economic performance and reflects the overall value of goods and services produced within a country. As GDP increases, it signifies a higher level of economic activity, including industrial, commercial, and agricultural sectors. The dynamics of human economic activities can be modeled by the Equation (2) and its parameters are detailed in Table 2.

$$\dot{H} = sN + \tau V - \eta H \tag{2}$$

The atmospheric CO_2 concentration is assumed to increase due to the growing number of vehicles and human activities by rates γ and σ respectively. Additionally, CO_2 concentration

in the atmosphere is naturally depleted through ocean sinking and absorbed by forest through photosynthesis process (Roosa & Jhaveri, 2020; Pal & Ghosh, 2023). The growth rate of atmospheric CO_2 resulting from natural processes, such as respiration of living organisms, volcanic eruptions, and changes in ocean circulation, is assumed to be constant (Misra & Lata, 2015). The dynamics of atmospheric CO_2 is governed by Equation (3) and parameters are described in a Table 2.

$$\dot{C} = C_0 + \gamma V + \sigma H - \rho BC - \pi C \tag{3}$$

It is presumed that forest biomass adheres to the principles of logistic growth and depletes due to human population growth. Its dynamics is governed by Equation (4) and parameters are explained in a Table 2.

$$\dot{B} = \theta B\left(1 - \frac{B}{K}\right) - \psi NB \tag{4}$$

In the region of consideration, the vehicle population is assumed to have a growth rate of β and naturally depletes, by the rate ξ. Vehicle population dynamics is modeled by Equation (5).

$$\dot{V} = \beta N - \xi V \tag{5}$$

Consequently, we formulate the following system of equations of non linear differential equation as presented in a system (6).

$$\begin{cases} \dot{N} = rN\left(1 - \frac{N}{L}\right) + \omega\psi NB - \alpha CN \\ \dot{H} = sN + \tau V - \eta H \\ \dot{C} = C_0 + \gamma V + \sigma H - \rho BC - \pi C \\ \dot{B} = \theta B\left(1 - \frac{B}{K}\right) - \psi NB \\ \dot{V} = \beta N - \xi V \end{cases} \tag{6}$$

Where:

$$N(0) \geq 0, H(0) \geq 0, C(0) > 0, B(0) \geq 0, V(0) \geq 0 \tag{7}$$

Model state variables and model parameters are described in Table 1 and Table 2 respectively.

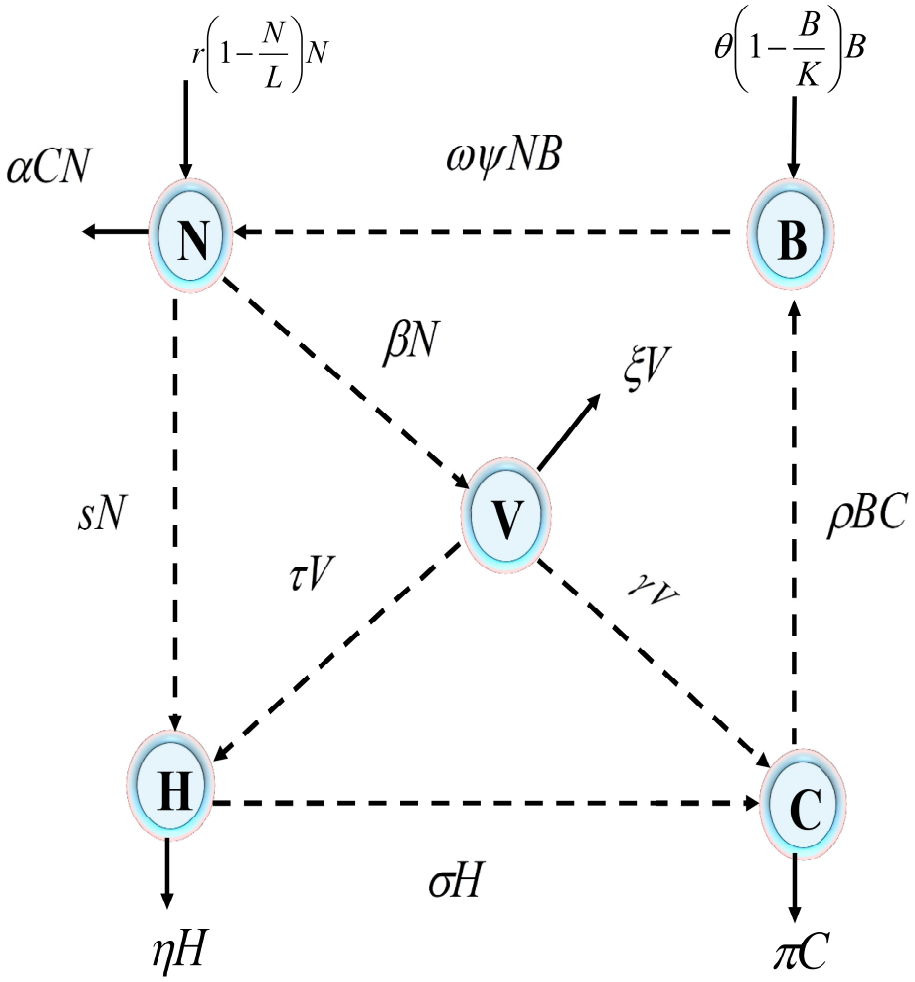

Figure 2: Schematic diagram for the mathematical model

Table 1: Model state variables and their respective description

Variable	Description
$N(t)$	Human population
$H(t)$	Human economic activities
$C(t)$	Atmospheric CO_2 concentration
$B(t)$	Forest Biomass
$V(t)$	Vehicle population

Table 2: Model parameters and description

Parameter	Description
r	Intrinsic human population growth rate
L	Human population carrying capacity
α	Mortality rate coefficient due to enhanced CO_2
s	Economic activities growth rate due to population
τ	Human economic activities growth rate due to vehicle population
η	Human economic activities depletion rate constant
C_0	Emission rate of CO_2 from natural and respiration processes
γ	CO_2 vehicle emission rate constant
σ	Human economic activities CO_2 emission rate
ρ	CO_2 depletion rate coefficient due to forest biomass
π	Natural CO_2 depletion rate coefficient
θ	Forest biomass intrinsic growth rate coefficient
K	Forest area carrying capacity
ψ	Deforestation rate coefficient
β	Vehicle's population growth rate due to demand for mobility
ξ	Vehicle depletion rate coefficient
ω	Human population growth rate coefficient due forest harvesting

3.4 Basic model analysis

In this section we study the long-term behavior of the non-linear ordinary differential equation system (6). The equilibrium points were obtained using Maple 2019 software and we use stability theory to discuss their stability. The equilibrium point of the dynamical system is the point at which the model does not change with time (Layek *et al.*, 2015). If the system reaches this point, it will remain at this equilibrium state persistently. The system (6) has four non-negative equilibrium points which were obtained by equating the rate of change equals to zero.

3.4.1 Boundedness of model solutions

In this section we show that the solutions of a system (6) with initial start (7) are bounded by using a standard comparison theorem for differential equations (Freedman & So, 1985). In the Lemma (3.1), we find the region of attraction, which is an invariant region that attracts all solutions of the model system (6) with initial start (7).

Lemma 3.1

The set $\Omega = \{(N,H,C,B,V) \in \mathbb{R}^5 : 0 \leq N \leq N_m; 0 \leq H \leq H_m; 0 < C \leq C_m; 0 \leq B \leq B_m;\ 0 \leq V \leq V_m$, where $N_m = L + \dfrac{\omega\psi KL}{r}$, $H_m = \dfrac{sN_m}{\eta}$, $C_m = \dfrac{\eta C_0 + s\sigma N_m}{\eta(\rho K + \pi)}$, $B_m = K$, $V_m = \dfrac{\beta N_m}{\xi}$ form the region of attraction for the system (6) which attract all solutions initiating in the interior of positive orthant.

Proof for Lemma (3.1):

From the fourth equation of model system (6), we have Equation (8):

$$\frac{dB}{dt} \leq \theta B\left(1 - \frac{B}{K}\right). \tag{8}$$

By comparing the above differential inequality with the following differential equation:

$$\frac{dB}{dt} = \theta B\left(1 - \frac{B}{K}\right). \tag{9}$$

and using standard comparison theorem, we have Equation (10):

$$B(t) \leq \frac{K}{1 + \left(\dfrac{K}{B(0)} - 1\right)e^{-}\theta t}. \tag{10}$$

Let $\varepsilon > 0$ be given. Then $\exists_{t_0 \geq 0}$ such that:

$$B(t) \leq K + \varepsilon \qquad \forall_{t \geq t_0}. \tag{11}$$

This gives

$$\limsup_{t \to \infty} B(t) \leq B_m. \tag{12}$$

Now from the first equation of the model system (6), we have:

$$\frac{dN}{dt} \leq (r + \omega\psi(K + \varepsilon))N - \frac{rN^2}{L} \qquad \forall_{t \geq t_0}. \tag{13}$$

Using the same argument as previously, $\exists_{t_1 \geq t_0}$ such that:

$$N(t) \leq (r + \omega\psi(K+\varepsilon))\frac{L}{r} + \varepsilon = N_\varepsilon \quad , \quad \forall_{t \geq t_1 \geq t_0}. \tag{14}$$

Hence

$$\limsup_{t\to\infty} N(t) \leq N_m. \tag{15}$$

From second equation in the model system (6), we get the following:

$$\frac{dH}{dt} \leq sN_\varepsilon - \eta H \qquad \forall_{t \geq t_1}. \tag{16}$$

Then we have

$$H(t) \leq \frac{sN_\varepsilon}{\eta} + \varepsilon = H_\varepsilon \quad , \quad \forall_{t \geq t_2 \geq t_1}. \tag{17}$$

Hence

$$\limsup_{t\to\infty} H(t) \leq H_m. \tag{18}$$

From third equation of the model system(6),

$$\frac{dC}{dt} \leq C_0 + \sigma H\varepsilon - \rho(K+\varepsilon)C - \pi C \qquad \forall_{t \geq t_2}. \tag{19}$$

$\exists_{t_3 \geq t_2}$ such that:

$$C(t) \leq \frac{C_0 + \sigma H_\varepsilon}{\rho(K+\varepsilon)+\pi} + \varepsilon = C_\varepsilon \qquad \forall_{t \geq t_3 \geq t_2}. \tag{20}$$

Hence

$$\limsup_{t\to\infty} C(t) \leq C_m. \tag{21}$$

Similarly, it can be easily shown that $\limsup_{t\to\infty} V(t) \leq \frac{\beta N_m}{\xi}$. Thus, the Lemma 3.1 is proved.

3.4.2 Equilibrium analysis

The long-term behavior of the system (6) was established by using stability theory. The feasible equilibrium points are obtained and their stability properties are established. The model system (6) has two non-negative trivial solutions $E_1\left(0,0,\frac{C_0}{\pi},0,0\right)$ and $E_2\left(0,0,\frac{\theta C_0}{K\rho+\pi},K,0\right)$ and two non-trivial solutions $E_3(N_3,H_3,C_3,0,V_3)$ and $E^*(N^*,H^*,C^*,B^*,V^*)$.

It can be noted that the existence of E_1 and E_2 is obvious. Further more the existence of equilibria E_3 and E^* depend on the satisfaction of condition (22).

$$r > \frac{\alpha C_0}{\pi} \tag{22}$$

Existence of E_3

To prove the existence of E_3 we solved the system (23) to obtain algebraic equations for N_3, H_3, C_3 and V_3, using approach employed by Verma *et al.* (2021). Consider the system (23) below:

$$\begin{cases} r\left(1-\dfrac{N_3}{L}\right)-\alpha C_3=0 \\ sN_3+\tau V_3-\eta H_3=0 \\ C_0+\gamma V_3+\sigma H_3-\pi C_3=0 \\ \beta N_3-\xi V_3=0 \end{cases} \tag{23}$$

From system (23) we have the following equations:

$$V_3=\frac{\beta N_3}{\xi}. \tag{24}$$

$$C_3=\frac{\eta\xi C_0+(\gamma\beta\eta+\sigma(s\xi+\tau\beta))N_3}{\pi\xi\eta}=f(N_3). \tag{25}$$

$$H_3=\frac{s\xi N_3+\tau\beta N_3}{\eta\xi}. \tag{26}$$

On the other hand, the first equation provides $g(N_3)$ such that:

$$g(N_3)=r\left(1-\frac{N_3}{L}\right)-\alpha f(N_3). \tag{27}$$

By using Equation (27), we analyze $g(N_3)$ in three different scenarios as follows:

(a) When $N_3=L+\dfrac{\omega\psi KL}{r}$ we have the following:

$$-\left(\omega\psi KL+\frac{\eta\xi C_0 r+(\gamma\beta\eta+\sigma(s\xi+\tau\beta))(rL+\omega\psi KL)}{\pi r\xi\eta}\right)<0.$$

(b) At $N_3 = 0$, a function $g(N_3)$ is given by:

$$g(0) = \alpha\left(\frac{r}{\alpha} - \frac{C_0}{\pi}\right).$$

Since $g\left(L + \frac{\omega\psi KL}{r}\right) < 0$, there exist a positive root N_3 in the interval of $0 < N_3 < L + \frac{\omega\psi KL}{r}$ if and only if $g(0) > 0$. Clearly, this requirement is met upon satisfaction of condition (22).

(c) For uniqueness of $N = N_3$, we need to prove that $g'(N_3) < 0$. Considering Equation (27) and some algebraic simplifications, it can be easily shown that:

$$g'(N_3) = -\left(\frac{r}{L} + \alpha\frac{\gamma\beta\eta + \sigma(s\xi + \tau\beta)}{\pi\xi\eta}\right) < 0.$$

Thus, a unique positive root, say $N = N_3$ of the Equation (27) lies on interval $0 < N_3 < L + \frac{\omega\psi KL}{r}$. Substituting $N = N_3$ into Equations (24)–(26) we get the appropriate values of $V = V_3$, $C = C_3$ and $H = H_3$. Hence, it can be concluded that an equilibrium point E_3 exists, whenever the condition (22) holds.

Existence of E^*

Interior equilibrium point E^* of the system (6) can be obtained by solving the system (28).

$$\begin{cases} r\left(1 - \frac{N^*}{L}\right) - \alpha C^* + \omega\psi B^* = 0 \\ sN^* + \tau V^* - \eta H^* = 0 \\ C_0 + \gamma V^* + \sigma H^* - \rho B^* C^* - \pi C^* = 0 \\ \theta\left(1 - \frac{B^*}{K}\right) - \psi N^* = 0 \\ \beta N^* - \xi V^* = 0 \end{cases} \tag{28}$$

The solution of the system (28) establishes the following results:

$$V^* = \frac{\beta N^*}{\xi} \tag{29}$$

$$H^* = \frac{(s\xi + \tau\beta)N^*}{\xi\eta} \tag{30}$$

$$B^* = \frac{K}{\theta}(\theta - \psi N^*) \tag{31}$$

$$C^* = \frac{\eta C_0 \xi + \eta\gamma\beta N^* + \sigma N^*(s\xi + \tau\beta)}{\eta\xi(\rho B^* + \pi)} \tag{32}$$

$$h(N^*, B^*) = r\left(1 - \frac{N^*}{L}\right) - \frac{\alpha}{\eta\xi\pi}(\xi\eta C_0 + \xi\gamma\beta N^* + \sigma N^*(s\xi + \tau\beta)) + \omega\psi B^* \tag{33}$$

From Equation (33) when no forest resources ($B^* = 0$) we get the following function of N^*

$$f(N^*) = r\left(1 - \frac{N^*}{L}\right) - \frac{\alpha}{\eta\xi\pi}(\xi\eta C_0 + \xi\gamma\beta N^* + \sigma N^*(s\xi + \tau\beta)). \tag{34}$$

By using Equation (34) $f(N^*)$ can be analyzed as follows:

(a) We evaluate a function $f(N^*)$ at $N^* = 0$ to get the following:

$$f(0) = \alpha\left(\frac{r}{\alpha} - \frac{C_0}{\pi}\right) > 0$$

(b) When $N^* = L + \dfrac{\omega\psi KL}{r}$ we have the following:

$$-\left[\omega\psi K + \frac{\alpha}{\eta\xi\pi r}[r\xi\eta C_0 + (rL + \omega\psi KL)(\xi\gamma\beta + (s\xi + \tau\beta)\sigma)]\right] < 0$$

There exists a positive root $N = N^*$ of Equation (34) in the interval $(0, L + \dfrac{\omega\psi KL}{r})$ under condition (22).

(c) For uniqueness of $N = N^*$, we need $f'(N^*) < 0$, that is:

$$f'(N^*) = -\left(\frac{r}{L} + \frac{\alpha}{\eta\xi\pi}(\xi\gamma\beta + \sigma(s\xi + \tau\beta))\right) < 0$$

Thus, a unique positive root, say N^* of the Equation (34) lies on interval $0 < N^* < L + \dfrac{\omega\psi KL}{r}$. Substituting the obtained value of N^* into Equations (29), (30) and (31) and performing algebraic simplifications we get the appropriate values of V^*, B^* and H^*. Since the values of N^* and B^* are known, then to obtain the value of C^* we substitute N^* and B^* into Equation (32) and we conclude that an interior point E^* exists under condition (22).

3.4.3 Stability analysis

In this section the behaviors of different equilibrium points of the model system are analyzed. From the system (6) the Jacobian matrix is given by:

$$J = \begin{pmatrix} r\left(1-\frac{N}{L}\right)-\frac{rN}{L}-\alpha C+\omega\psi B & 0 & -\alpha N & \omega\xi N & 0 \\ s & -\eta & 0 & 0 & \tau \\ 0 & \sigma & -\rho B-\pi & -\rho C & \gamma \\ -\psi B & 0 & 0 & \theta\left(1-\frac{B}{K}\right)-\frac{\theta B}{K}-\psi N & 0 \\ \beta & 0 & 0 & 0 & -\xi \end{pmatrix}. \tag{35}$$

At the equilibrium point $E_1\left(0,0,\frac{C_0}{\pi},0,0\right)$ the corresponding Jacobian matrix J_{E_1}, resulted from evaluating matrix J through E_1 is given by:

$$J_{E_1} = \begin{pmatrix} \alpha\left(\frac{r}{\alpha}-\frac{C_0}{\pi}\right) & 0 & 0 & 0 & 0 \\ s & -\eta & 0 & 0 & \tau \\ 0 & \sigma & -\pi & \frac{-\rho C_0}{\pi} & \gamma \\ 0 & 0 & 0 & \theta & 0 \\ \beta & 0 & 0 & 0 & -\xi \end{pmatrix}. \tag{36}$$

The eigenvalues of a matrix J_{E_1} are $\lambda_1=-\xi$, $\lambda_2=\theta$, $\lambda_3=-\eta$, $\lambda_4=-\pi$ and $\lambda_5=\frac{r}{\alpha}-\frac{C_0}{\pi}>0$. The equilibrium point E_1 is unstable since it have at least one positive eigenvalues, that is $\lambda_2>0$ and $\lambda_5>0$.

Similarly, evaluating matrix J at E_2, the following matrix is established.

$$J_{E_2} = \begin{pmatrix} \frac{K^2\omega\psi\rho+K\pi\psi\omega+Kr\rho+\pi r-\alpha C_0}{\rho K+\pi} & 0 & 0 & 0 & 0 \\ s & -\eta & 0 & 0 & \tau \\ 0 & \sigma & -K\rho-\pi & \frac{-C_0\rho}{\rho K+\pi} & \gamma \\ -\psi K & 0 & 0 & -\theta & 0 \\ \beta & 0 & 0 & 0 & -\xi \end{pmatrix}. \tag{37}$$

The eigenvalues of J_{E_2} are $\lambda_1=-\xi$, $\lambda_2=-\theta$, $\lambda_3=-\eta$, $\lambda_4=-(K\rho+\pi)$, and $\lambda_5=$

$\frac{K^2\omega\psi\rho + K\pi\psi\omega + Kr\rho + \pi r - \alpha C_0}{\rho K + \pi}$. Clearly, upon utilizing condition (22), $\lambda_5 > 0$ making E_2 unstable.

At the equilibrium point E_3, we establish a matrix J_{E_3}, such that:

$$J_{E_3} = \begin{pmatrix} -\frac{rN_3}{L} & 0 & -\alpha N_3 & \omega\psi N_3 & 0 \\ s & -\eta & 0 & 0 & \tau \\ 0 & \sigma & -\pi & -\rho C_3 & \gamma \\ 0 & 0 & 0 & -(\psi N_3 - \theta) & 0 \\ \beta & 0 & 0 & 0 & -\xi \end{pmatrix}. \tag{38}$$

$$N_3 > \frac{\theta}{\psi} \tag{39}$$

Upon satisfaction of condition (39) all the entries at the main diagonal will be negative, we utilize the Gershgorin's Theorem by columns of the matrix to deduce sufficient conditions for local stability of E_3 (Devi & Gupta, 2019). As such, E_3 is proved to be asymptotically stable upon satisfaction of conditions in Equation (40).

$$\begin{cases} \frac{L}{r}(s+\beta) < N_3 < \frac{\pi}{\alpha} \\ \sigma < \eta \\ \frac{\rho C_m + \theta}{\psi(\omega+1)} < N_3 < \frac{\rho C_m - \theta}{\psi(\omega-1)} \\ \tau + \gamma < \xi \end{cases} \tag{40}$$

Where C_m is defined in Lemma 3.1.

Theorem 3.1

The equilibrium point E_3, if exists, is locally asymptotically stable if conditions in Equation (40) are satisfied.

At the interior equilibrium point E^*, the Jacobian matrix J, was evaluated to get a matrix J_{E^*}, such that:

$$J_{E^*} = \begin{pmatrix} -\frac{rN^*}{L} & 0 & -\alpha N^* & \omega\psi N^* & 0 \\ s & -\eta & 0 & 0 & \tau \\ 0 & \sigma & -\rho B^* - \pi & -\rho C^* & \gamma \\ -\psi B^* & 0 & 0 & -\frac{\theta B^*}{K} & 0 \\ \beta & 0 & 0 & 0 & -\xi \end{pmatrix}. \tag{41}$$

Clearly, all entries in the main diagonal of J_{E^*} are negative. We use the Gershgorin's Theorem by columns of the matrix to deduce the local stability of E^* (Devi & Gupta, 2019). As such, E^* is proved to be locally asymptotically stable upon satisfaction of conditions in Equation (42).

$$\begin{cases} N^* > \max\left\{\frac{L}{r}(\beta - \psi K), \frac{L}{r}(\psi K - \beta)\right\} \\ \sigma < \eta \\ N^* < \frac{\rho K - \pi}{\alpha} \\ \frac{\rho C_m - \theta}{\omega\psi} < N^* < \frac{\theta + \rho C_m}{\omega\psi} \\ \tau + \gamma < \xi \end{cases} \tag{42}$$

Where C_m is defined in Lemma (3.1).

Theorem 3.2

The interior equilibrium point E^*, if exists, is locally asymptotically stable if conditions (42) are satisfied.

Theorem 3.3

The interior equilibrium point E^*, if exists, is globally asymptotically stable in Ω if conditions 43 – 45 are satisfied.

$$\omega^2 > \frac{9\rho^2}{4\theta(\rho K + \pi)} \tag{43}$$

$$\tau^2 > \frac{s^2\xi^2}{9\beta^2} \tag{44}$$

$$L < \max\left\{\frac{16\omega\eta^2 r(C^*)^2(\rho K + \pi)}{81\sigma^2 s^2}, \frac{4r(\rho K + \pi)}{9\alpha^2}, \frac{16\xi^2\omega r(\rho K + \pi)(C^*)^2}{81\sigma^2 s^2}\right\} \tag{45}$$

The proof of theorem (3.3):

To analyze the global stability of the interior equilibrium E^*, we use Lyapunov stability theory. Consider the following scalar valued positive definite function:

$$\begin{aligned} U &= \left(N - N^* - N^* \ln \frac{N^*}{N}\right) + \frac{1}{2}k_1 (H - H^*)^2 + \frac{1}{2}k_2 (C - C^*)^2 \\ &\quad + \frac{1}{2}k_3 \left(B - B^* - B^* \ln \frac{B^*}{B}\right) + \frac{1}{2}k_4 (V - V^*)^2 \end{aligned} \tag{46}$$

Where k_1, k_2, k_3 and k_4 are suitable positive constants to be determined later.

Differentiating U with respect to t we have the following:

$$\frac{dU}{dt} = \frac{\partial U}{\partial N}\left(\frac{dN}{dt}\right) + \frac{\partial U}{\partial H}\left(\frac{dH}{dt}\right) + \frac{\partial U}{\partial C}\left(\frac{dC}{dt}\right) + \frac{\partial U}{\partial B}\left(\frac{dB}{dt}\right) + \frac{\partial U}{\partial V}\left(\frac{dV}{dt}\right) \tag{47}$$

Performing algebraic operations we get the following:

$$\begin{aligned} \frac{dU}{dt} &= -\frac{r}{L}(N - N^*)^2 - \eta k_1 (H - H^*)^2 - k_2 (\rho K + \pi)(C - C^*)^2 - \frac{\theta k_3}{K}(B - B^*)^2 \\ &\quad - \xi k_4 (V - V^*)^2 - \alpha (C - C^*)(N - N^*) + \psi (\omega - k_3)(B - B^*)(N - N^*) \\ &\quad + s k_1 (H - H^*)(N - N^*) + \tau k_1 (V - V^*)(H - H^*) + \gamma k_2 (V - V^*)(C - C^*) \\ &\quad + \sigma k_2 (H - H^*)(C - C^*) + \beta k_4 (N - N^*)(V - V^*) - k_2 \rho C^* (B - B^*)(C - C^*) \\ &\quad + \beta k_4 (N - N^*)(V - V^*) \end{aligned} \tag{48}$$

Choosing $k_1 = \frac{4r\eta}{9s^2L}$, $k_2 = \frac{1}{C^*}$, $k_3 = \omega$ and $k_4 = \frac{4r\xi}{9\beta^2 L}$, $\frac{dU}{dt}$ is negative definite under conditions 43 – 45, hence the Theorem (3.3) is proved.

3.4.4 Ecological interpretation of stability analysis

Equilibrium points E_1 and E_2 represent different situations regarding the extinction of the human population and the presence or absence of forest biomass. The point E_1 signifies the extinction of forest biomass, while E_2 represents a situation where forest biomass exists. The absence of human population would lead to the cessation of human-related activities, resulting in a lack of stabilization in atmospheric CO_2 concentration. Only natural processes such as volcanic eruptions will contribute to CO_2 emissions, resulting in a natural depletion of atmospheric CO_2 concentration. However, the analysis reveals further that the forest will rapidly grow up to its carrying capacity, acting as a sink for CO_2 absorption. The atmospheric CO_2 concentration will solely depend on natural processes and will naturally deplete.

The equilibrium point E_3 illustrates a situation where forest biomass no longer exists. In such a scenario, the emitted CO_2 will undergo some degree of natural absorption, while the remaining portion will persist in the atmosphere. This state is achieved when the natural growth rate of the human population exceeds the mortality rate resulting from the natural release of CO_2.

The interior equilibrium point E^* takes into account the coexistence of human population, economic activities, atmospheric CO_2 concentration, forest area, and vehicle population. To achieve this balance, the natural growth rate of the human population needs to exceed the mortality rate caused by natural CO_2 emissions. Moreover, specific conditions for the global stability of E^* must be met to ensure the stability of the atmospheric CO_2 concentration. When these conditions are satisfied, the forest biomass can absorb the existing atmospheric CO_2, safeguarding the environment, while the remaining CO_2 gradually decreases. These interpretations emphasize how human actions and natural processes interact, highlighting the critical importance of maintaining the necessary conditions to uphold the stability of atmospheric CO_2 concentration and environmental well-being.

3.5 Optimal control problem

According to the UNCCC (2023), it was announced that, despite of an ongoing efforts placed to cut down GHG emissions, there is a rise of 9% during year 2023. Also, it was noted that, the world experiences high temperature values due to an increased GHG emissions. To lower the world temperature not more than 1.5 degrees celcius, we need to cut off GHG emissions by 45%. In order to attain the United Nations 13^{th} Sustainable Development Goal (SDG's), it is important to cut down CO_2 emissions from vehicles. This can be controlled by cutting down the emission rate of CO_2 from vehicles in operation, employing technological options to cut down CO_2 from produced vehicles, mainly vehicles that burns fossil fuels, reforestation efforts to increase forest cover to expand CO_2 absorption capacity and practicing green economy policies. The implementation of strategies that reduces the atmospheric CO_2 along with fulfilling the demand for mobility of both human being, services and goods is desirable. These strategies can be derived by employing an optimal control theory. The parameters μ_1, μ_2, μ_3 and μ_4 are the function of time in the interval $[0, T]$, where T is the period for applying these control strategies. To formulate an optimal control problem, technique employed by Verma *et al.* (2021) was adopted. In the model system (49) control parameters μ_1 represents the efficiency

of mitigation options to cut down CO_2 emission rate per unit vehicle, μ_2 is the reforestation rate to increase forest capacity to absorb atmospheric CO_2, μ_3 is the efficiency of mitigation options to cut down fossil fueled vehicle production and μ_4 represents Eco-efficiency or green economy implementation rate to cut down CO_2 emissions from human economic activities.

$$\begin{cases} \dot{N} = rN\left(1-\frac{N}{L}\right) + (1-\mu_2)\,\omega\psi NB - \alpha CN \\ \dot{H} = sN + \tau V - \eta H \\ \dot{C} = C_0 + (1-\mu_1)\,\gamma V + (1-\mu_4)\,\sigma H - \rho BC - \pi C \\ \dot{B} = \theta B\left(1-\frac{B}{K}\right) - (1-\mu_2)\,\psi NB \\ \dot{V} = (1-\mu_3)\,\beta N - \xi V \end{cases} \tag{49}$$

Where $N(0) \geq 0$, $H(0) \geq 0$, $C(0) > 0$, $B(0) \geq 0$ and $V(0) \geq 0$.

The aim here is to minimize atmospheric CO_2 concentration and the cost of implementing reforestation campaign. Here we use a the objective function J as follows:

$$J = min_{\mu_i \in \mathscr{U}} \int_0^T \left[a_1 C(t) + a_2\mu_1^2(t) + a_3\mu_2^2(t) + a_4\mu_3^2(t) + a_5\mu_4^2(t)\right] dt \tag{50}$$

From Equation (50), a_1, a_2 ,a_3, a_4 and a_5 are positive weight parameters. Here we look for a pair of control $\left(\mu_1^*(t), \mu_2^*(t), \mu_3^*(t), \mu_4^*(t)\right)$ in the control set $\mathscr{U}$ = { $\mu_1(t)$,$\mu_2(t)$,$\mu_3(t)$,$\mu_4(t)$: $\mu_1(t)$, $\mu_2(t)$,$\mu_3(t)$ and $\mu_4(t)$ are measurable, $0 \leq \mu_1(t) \leq \mu_{1max}$, $0 \leq \mu_2(t) \leq \mu_{2max}$, $0 \leq \mu_3(t) \leq \mu_{3max}$, $0 \leq \mu_4(t) \leq \mu_{4max}$ for $t \in [0,T]$ } which minimizes the function J subject to the system (49).

3.5.1 Existence of optimal control

Theorem 3.4

Given $J(\mathscr{U})$ subject to the system (6) with non-negative initial conditions of the state variables, there exists an optimal control $\mu^* = \left(\mu_1^*(t), \mu_2^*(t), \mu_3^*(t), \mu_4^*(t)\right) \in \mathscr{U}$ which minimizes an objective function J subject to the system (6) in interval $[0,T]$.

Proof: To establish the existence of an optimal control, we rely on results from previous scholars (Fleming & Rishel, 2012). The boundedness of solutions to the system (49) guarantees

the existence of a solution within the system. Notably, both the control and state variables are constrained to be positive, ensuring physical feasibility.

Moreover, the necessary convexity of the objective functional in $\mu_1(t)$, $\mu_2(t)$, $\mu_3(t)$, and $\mu_4(t)$ is satisfied. This convexity property is essential for facilitating the identification of optimal solutions. The right-hand side of the equations in the system (49) is bounded by a linear function of the control and state variables. Additionally, there exist constants b_1, b_2, b_3, b_4, $b_5 > 0$ and $\ominus > 1$ such that the inequality (51) holds.

$$a_1C(t) + a_2\mu_1(t)^2 + a_3\mu_2^2(t) + a_4\mu_3^2(t) \leq b_1 + \left(b_2|\mu_1(t)|^2 + b_3|\mu_2(t)|^2 + b_4|\mu_3(t)|^2 + b_5|\mu_4(t)|^2\right)^{\ominus}/2 \tag{51}$$

Here, b_1 depends on the upper bound of C, while b_2, b_3, b_4, b_5 are determined based on system parameters. This inequality ensures that the objective functional remains bounded, which is crucial for the existence of an optimal control.

Furthermore, the control set $\mathscr{U}$ is convex and closed by definition. The boundedness of solutions to the system (49) further ensures the compactness of $\mathscr{U}$, which is a prerequisite for the existence of an optimal control.

Therefore, by combining the boundedness of solutions, convexity of the objective functional, and the compactness of the control set, we conclude that there exists at least one optimal control strategy μ^* that minimizes the objective function over the specified time horizon. This establishes the existence of an optimal control within the formulated problem.

3.5.2 Characterization of optimal control

To determine necessary conditions on the optimal control problem, we applied Pontryagin's principle (Pontryagin, 2018). The principle change the system of differential equations into a minimization problem to point wise minimization problem by using Lagrange or Hamiltonian function with respect to controls. The Hamiltonian for control problem is denoted by $\mathscr{H}$ as shown in Equation (52).

$$\begin{aligned}\mathscr{H} &= a_1C(t)+a_2\mu_1^2(t)+a_3\mu_2^2(t)+a_4\mu_3^2(t)+a_5\mu_4^2(t)\\ &+\lambda_1\left(rN\left(1-\frac{N}{L}\right)+(1-\mu_2)\omega\psi NB-\alpha CN\right)+\lambda_2\left(sN+\tau V-\eta H\right)\\ &+\lambda_3\left(C_0+(1-\mu_1)\gamma V+(1-\mu_4)\sigma H-\rho BC-\pi C\right)\\ &+\lambda_4\left(\theta B(1-\frac{B}{K})-(1-\mu_2)\psi NB\right)+\lambda_5\left((1-\mu_3)\beta N-\xi V\right)\end{aligned} \tag{52}$$

Where λ_1, λ_2, λ_3, λ_4 and λ_5 are the adjoint variables. A system of differential equations corresponding to these variables is obtained as follows:

$$\begin{cases}\dot{\lambda_1} &= -\dfrac{\partial\mathscr{H}}{\partial N}=\left(\dfrac{2rN}{L}-r-(1-\mu_2)\psi\omega B+\alpha C\right)\lambda_1-\lambda_2 s+(1-\mu_2)\psi\lambda_4 B-(1-\mu_3)\beta\lambda_5\\ \dot{\lambda_2} &= -\dfrac{\partial\mathscr{H}}{\partial H}=\eta\lambda_2-(1-\mu_4)\sigma\lambda_3\\ \dot{\lambda_3} &= -\dfrac{\partial\mathscr{H}}{\partial C}=-a_1+\alpha\lambda_1 N+\rho\lambda_3 B+\pi\lambda_3\\ \dot{\lambda_4} &= -\dfrac{\partial\mathscr{H}}{\partial B}=\rho\lambda_3 C-\omega\psi\lambda_1 N-\left(\theta-\dfrac{2\theta B}{K}-(1-\mu_2)\psi N\right)\lambda_4\\ \dot{\lambda_5} &= -\dfrac{\partial\mathscr{H}}{\partial V}=\xi\lambda_5-\tau\lambda_2-(1-\mu_1)\gamma\lambda_3\end{cases} \tag{53}$$

The transversality conditions are $\lambda_1(T)=\lambda_2(T)=u_3(T)=\lambda_4(T)=\lambda_5(T)=0$, and the optimal control pair $\left(\mu_1^*,\mu_2^*,\mu_3^*,\mu_4^*\right)$ is characterized by using the following optimality conditions:

$$\frac{\partial\mathscr{H}}{\partial\mu_1}=0,\ \frac{\partial\mathscr{H}}{\partial\mu_2}=0\ ,\ \frac{\partial\mathscr{H}}{\partial\mu_3}=0\ ,\ \frac{\partial\mathscr{H}}{\partial\mu_4}=0$$

at $\mu_1=\mu_1^*$, $\mu_2=\mu_2^*$, $\mu_3=\mu_3^*$ and $\mu_4=\mu_4^*$, on the set $\{t\in[0,T]:0\leq\mu_1(t)\leq\mu_{1max},0\leq\mu_2(t)\leq\mu_{2max},0\leq\mu_3(t)\leq\mu_{3max},0\leq\mu_4(t)\leq\mu_{4max}\}$. This results to the following:

$$\mu_1^*=\frac{\gamma\lambda_3 V}{2a_2}\ ,\ \mu_2^*=\frac{(\omega\lambda_1-\lambda_4)\psi NB}{2a_3}\ ,\ \mu_3^*=\frac{\beta\lambda_5 N}{2a_4}\ ,\ \mu_4^*=\frac{\sigma\lambda_2 H}{2a_5}$$

On the interior set of $\mathscr{U}$, the optimal control μ_1^*, μ_2^*, μ_3^* and μ_4^* are characterized as:

$$\mu_1^* = \begin{cases} 0 & if \quad \dfrac{\lambda_3 \gamma V}{2a_2} \leq 0 \\ \dfrac{\lambda_3 \gamma V}{2a_2} & if \quad 0 < \dfrac{\lambda_3 \gamma V}{2a_2} < 0 \\ \mu_{1max} & if \quad \dfrac{\lambda_3 \gamma V}{2a_2} \geq \mu_{1max} \end{cases} \tag{54}$$

$$\mu_2^* = \begin{cases} 0 & if \quad \dfrac{(\omega\lambda_1 - \lambda_4)\,\psi NB}{2a_3} \leq 0 \\ \dfrac{(\omega\lambda_1 - \lambda_4)\,\psi NB}{2a_3} & if \quad 0 < \dfrac{(\omega\lambda_1 - \lambda_4)\,\psi NB}{2a_3} < 0 \\ \mu_{2max} & if \quad \dfrac{(\omega\lambda_1 - \lambda_4)\,\psi NB}{2a_3} \geq \mu_{2max} \end{cases} \tag{55}$$

$$\mu_3^* = \begin{cases} 0 & if \quad \dfrac{\lambda_5 \beta N}{2a_4} \leq 0 \\ \dfrac{\lambda_5 \beta N}{2a_4} & if \quad 0 < \dfrac{\lambda_5 \beta N}{2a_4} < 0 \\ \mu_{3max} & if \quad \dfrac{\lambda_5 \beta N}{2a_4} \geq \mu_{3max} \end{cases} \tag{56}$$

$$\mu_4^* = \begin{cases} 0 & if \quad \dfrac{\sigma\lambda_2 H}{2a_5} \leq 0 \\ \dfrac{\sigma\lambda_2 H}{2a_5} & if \quad 0 < \dfrac{\sigma\lambda_2 H}{2a_5} < 0 \\ \mu_{4max} & if \quad \dfrac{\sigma\lambda_2 H}{2a_5} \geq \mu_{4max} \end{cases} \tag{57}$$

Theorem 3.5

The optimal control pair $(\mu_1^*, \mu_2^*, \mu_3^*, , \mu_4^*)$ minimizing a function J subject to the system (49) over a set $\mathscr{U}$ is given by:

$$\mu_1^* = \max\{\min\left(\frac{\lambda_3 \gamma V}{2a_2}, \mu_{1max}\right), 0\} \tag{58}$$

$$\mu_2^* = \max\{\min\left(\frac{(\omega\lambda_1 - \lambda_4)\,\psi NB}{2a_3}, \mu_{2max}\right), 0\} \tag{59}$$

$$\mu_3^* = \max\{\min\left(\frac{\lambda_5 \beta V}{2a_4}, \lambda_{3max}\right), 0\} \tag{60}$$

$$\mu_4^* = \max\{\min\left(\frac{\sigma\lambda_2 H}{2a_5}, \lambda_{4max}\right), 0\} \tag{61}$$

The optimality system consists of state equations and the adjoint equations together with the characterization of optimal control pair, initial condition and the transversality conditions. Therefore the following is the optimality system:

$$\begin{cases} \dot{N} = rN\left(1 - \frac{N}{L}\right) + (1-\mu_2^*)\,\omega\psi NB - \alpha CN \\ \dot{H} = sN + \tau V - \eta H \\ \dot{C} = C_0 + (1-\mu_1^*)\,\gamma V + (1-\mu_4^*)\,\sigma H - \rho BC - \pi C \\ \dot{B} = \theta B\left(1 - \frac{B}{K}\right) - (1-\mu_2^*)\,\psi NB \\ \dot{V} = \left(1-\mu_3^*\right)\beta N - \xi V \\ \dot{\lambda_1} = \left(\frac{2Nr}{L} - r - \psi\omega B + \alpha C\right)\lambda_1 - \lambda_2 s + (1-\mu_2)\,\psi B\lambda_4 - (1-\mu_3)\,\beta\lambda_5 \\ \dot{\lambda_2} = \eta\lambda_2 - \sigma\lambda_3 \\ \dot{\lambda_3} = -a_1 + \alpha N\lambda_1 + \rho B\lambda_3 + \pi\lambda_3 \\ \dot{\lambda_4} = \rho C\lambda_3 - \omega\psi N\lambda_1 - \left(\theta - \frac{2B\theta}{K} - (1-\mu_2)\psi N\right)\lambda_4 \\ \dot{\lambda_5} = \xi\lambda_5 - \tau\lambda_2 - (1-\mu_1)\gamma\lambda_3 \end{cases} \tag{62}$$

Where $\mu_1^*(t)$, $\mu_2^*(t)$, $\mu_3^*(t)$and $\mu_4^*(t)$ are given in Equations 58, 59 , 60 and 61 respectively, and $N(0) \geq 0$, $H(0) \geq 0$, $C(0) > 0$, $B(0) \geq 0$ and $V(0) \geq 0$ and $\lambda_i(T) = 0\ \forall_{i\in\{1,2,3,4,5\}}$.

CHAPTER FOUR

RESULTS AND DISCUSSION

4.1 Introduction

In this chapter, we conducted numerical simulations for both the basic model and the optimal control problem outlined in section 3.3. We then provided a brief discussion of the results. Our analysis involved parameter estimations and sensitivity analysis to better understand how each model parameter influences the solutions. We numerically simulated the optimal control problem to evaluate the most effective strategies for mitigating vehicle CO_2 emissions. The goal is to combat the adverse impact of increased atmospheric CO_2.

4.2 Parameter estimation and model fitting

The parameter estimation process involved adjusting the model's parameters to best align with time series data from various sources. These data encompassed world population (WBOD, 2018), atmospheric CO_2 concentration (Tans, 2020; Etheridge *et al.*, 1996; Ritchie *et al.*, 2020; NOAA, 2020), forest area (FAO, 2018), the number of vehicles produced (BTS, 2019), and Gross Domestic Product (GDP) (WBOD, 2019). We calculated the precise parameter values using the least squares method, which minimizes the total squared differences between the model's predictions and the observed data.

To perform this optimization, we employed a built-in MATLAB function called *(fminsearch)*, which implements unconstrained nonlinear minimization using the Nelder-Mead algorithm, yielding candidates serving as local minimizers for the sum of squared residuals (Gao & Han, 2010). The selection of initial parameter values was guided by conditions outlined in the qualitative analysis section.

Additionally, apart from the data-driven parameter estimation, we adopted values of $L = 11$, $C_0 = 5$, and K = 750 000 from previous scholars (Verma *et al.*, 2021; Misra & Verma, 2013; Verma & Misra, 2016). For the intrinsic human population growth rate (r), we referred to data from WBOD (2018), considering a range of 0.02 to 0.03 per year as discussed in Verma *et al.* (2021). This range provides an estimate for the value of r that aligns with the available data

and existing literature. We initiated the model with a starting time of 1994 and initial values as follows: $N(0) = 5.66315$ billion people, $H(0) = 2787.67662$ billion US$, $C(0) = 358.96ppm$, $B(0) = 4099.2026$ million hectares, and $V(0) = 49.658288$ million vehicles.

To test the validity of the model, R-squared values were employed as done by Verma *et al.* (2021). The R-squared values for actual data and model predictions of human population, human economic activities, atmospheric CO_2 concentration, forest biomass, and vehicle production are 0.955471914, 0.94694, 0.981052, 0.9535782, and 0.9275, respectively. These values indicate a robust correlation between the real data and the model predictions. The real and model projections of the variables N, H, C, B and V are shown in Fig. 3. It is evident from Fig. 3 that there is a close alignment between the model projections and the actual data, which ensures the validity of the model.

Furthermore, we applied statistical metrics to assess the performance of our model, including the Root Mean Squared Error Normalized (RMSEN) and the Nash-Sutcliffe Efficiency index (NSE). RMSEN, as it approaches zero, serves as a positive indicator of the model's effectiveness. To classify model performance, we follow the criteria established in previous research (Ferreira *et al.*, 2020; Léonidas *et al.*, 2023), where RMSEN is considered excellent if it is less than or equal to 10%, good between 10% and 20%, reasonable between 20% and 30%, and poor if it exceeds 30%.

On the other hand, the coefficient of efficiency (NSE) quantifies the overall deviation between real and predicted values from the actual data (R_i) and its mean (R). The NSE value can range from $-\infty$ to $+1$, with higher values indicating efficient model predictions. By using Equation (25), we calculated NSE to be 0.9343, suggesting efficient model predictions. Additionally, employing Equation (24), we obtained an RMSEN value of 2.6027%, further supporting the assessment of excellent model predictions.

In Equation (24), R_i represents the actual data value, R denotes the mean of actual data points, S_i represents the model's predicted data points, and n signifies the number of observations.

$$RMSEN = 100 \times \frac{1}{R}\sqrt{\frac{1}{n} \times \sum_{i=1}^{n}(R_i - S_i)^2} \tag{24}$$

$$NSE = 1 - \frac{\sum_{i=1}^{n} (R_i - S_i)^2}{\sum_{i=1}^{n} (R_i - R)^2} \tag{25}$$

Additionally, to assess the robustness of model fitting, we calculated a 95% confidence interval for the parameter estimates, as detailed in Table 3. The narrow width of these confidence intervals suggests the reliability of the model parameter estimates. Notably, the value of r falls within the range specified by Verma *et al.* (2021), providing further support for the credibility of the parameter estimation. The combination of these tests confirms the robustness of the model's parameter estimates, affirming its suitability for predictive purposes.

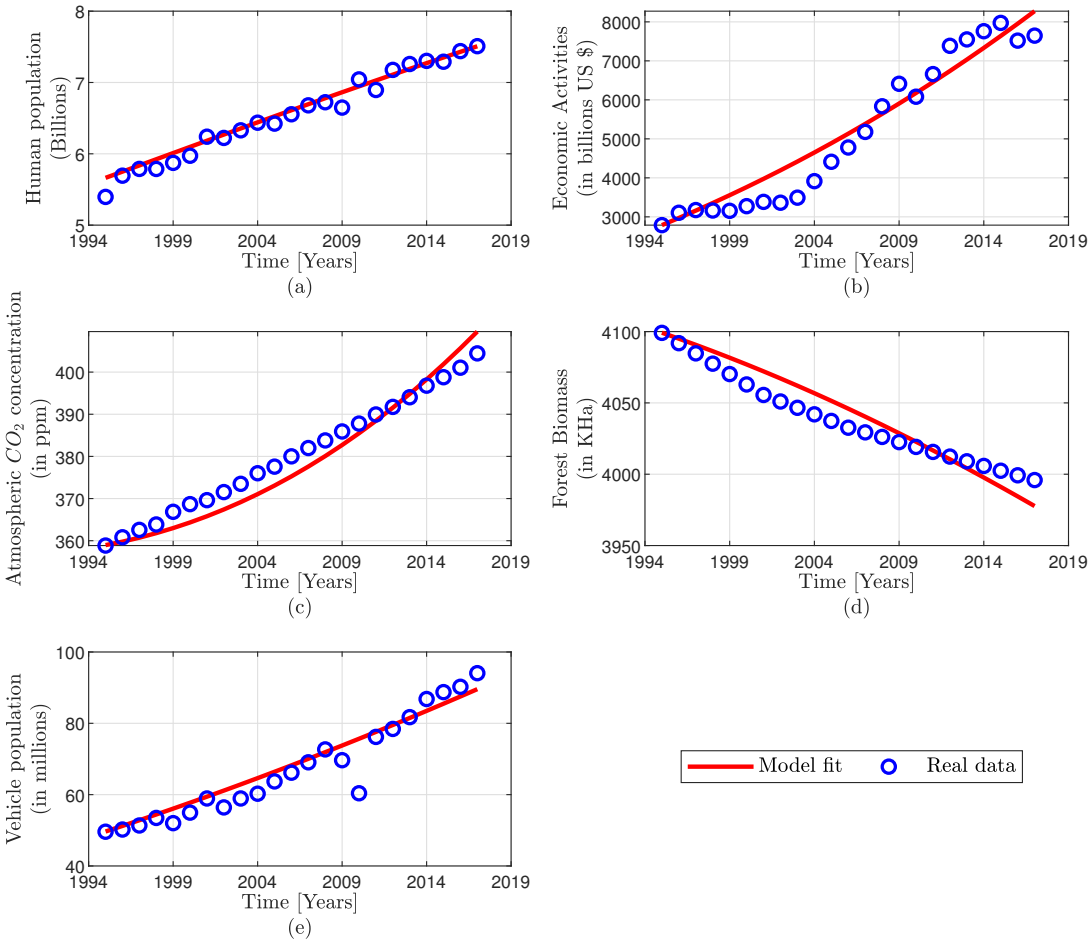

Figure 3: A comparison depicting the actual data alongside the solution of model system (6) for the adjusted data set, demonstrating the striking agreement between the model's output and the observed data

Table 3: Estimated model parameters and their respective 95% confidence intervals

Par	Baseline	Source	Interval	Estimated
r	0.026	(Verma *et al.*, 2021)	[0.022645 0.03378]	0.0285245
α	0.000001	(Verma & Misra, 2016)	$[7.4\times10^{-7}\ 1.3\times10^{-6}]$	0.0000010551
τ	3.94	Assumed	-	3.94
s	0.035	(Caetano *et al.*, 2008)	[0.018 0.046]	0.03374
γ	4.9337×10^{-7}	Assumed	$[1.6\times10^{-8}\ 2.3\times10^{-8}]$	1.3657×10^{-8}
σ	0.000576	Assumed	[0.00052 0.00079]	0.0007897
η	6.67×10^{-7}	Assumed	-	6.67×10^{-7}
π	0.016	(Verma & Misra, 2016)	[0.0097 0.022]	0.016232
θ	0.0523	Assumed	[0.00091 0.00113]	0.0012025
β	0.0729	Assumed	[0.27 0.301]	0.27534
ψ	0.26×10^{-3}	Assumed	[0.000348 0.0004031]	0.389×10^{-3}
ρ	4.8×10^{-9}	(Verma & Misra, 2016)	$[0.87\times10^{-6}\ 1.5\times10^{-6}]$	3.86657×10^{-7}
ξ	1.0676×10^{-6}	Assumed	$[8.4\times10^{-6}\ 1.05\times10^{-5}]$	1.50623×10^{-5}
ω	0.001	Assumed	[0.00072517 0.0013074]	0.00094457

4.3 Non-linear stability of an interior equilibrium

To validate feasibility of the model analysis, we utilized MATLAB R2021a and Maple 2015 software. The chosen set of parameters from Table 3 satisfied the condition (22) for the existence of interior equilibrium point E^*. The eigenvalues of the Jacobian matrix corresponding to the equilibrium point E^* were calculated to be $-3.160388, -0.224952, -0.87302, -5.85509\times10^{-7}$, and -0.15062, all of which are negative. This indicates that the equilibrium point E^* is locally asymptotically stable and the conditions 43 – 45 for global stability of E^* is satisfied for estimated parameter values. Furthermore, the solution trajectories of the model (6) is plotted in Fig. 4 and Fig. 5 with different starting values. It can be observed that all trajectories initiated inside the region Ω converge towards the interior equilibrium point E^*. This demonstrates the nonlinear stability behavior of the point E^* in the $N(t)-V(t)-B(t)$ and $N(t)-B(t)-C(t)$ space, as depicted in Fig. 4 and Fig. 5, respectively.

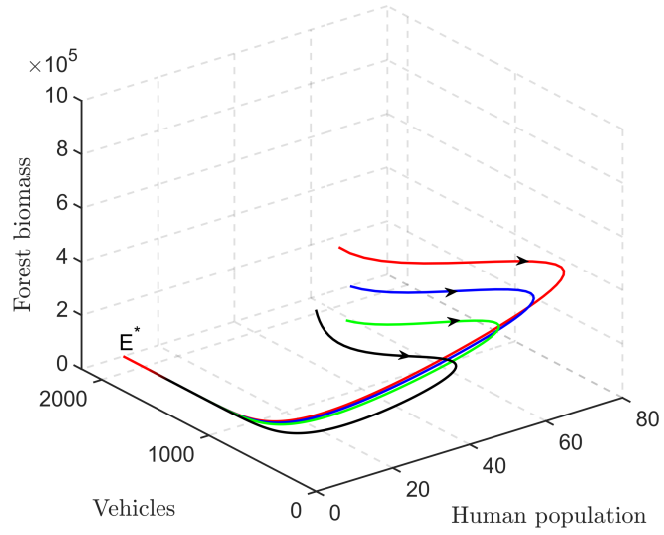

Figure 4: Graphical representation for global stability of an interior equilibrium point E^* in N - B - V plane

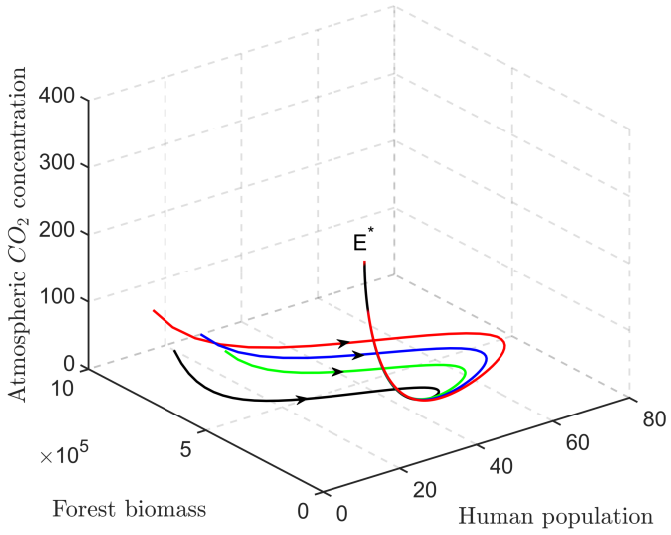

Figure 5: Graphical representation for global stability of an interior equilibrium point E^* in N - B - C plane

4.4 Model parameter sensitivity analysis

In order to grasp the impact of model parameters on the system output, we conducted a global sensitivity analysis (GSA) employing partial ranking correlation coefficient (PRCC) which use Latin Hypercube sampling Monte Carlo simulation (LHS). This approach allows us to assess

how changes in individual parameters can influence the overall model output (Azizi & Mugabi, 2020; Bidah *et al.*, 2020). A positive PRCC suggests that there's a direct correlation between model parameters and its output. This means that when a model parameter's value increases, the model output significantly increases as well, and vice versa for a decrease in parameter value. On the other hand, a negative PRCC implies an inverse relationship between parameter value and the model's predictions (Fanuel *et al.*, 2023).

4.4.1 Sensitivity PRCCs on human population and atmospheric CO_2 concentration

The time-variable Partial Rank Correlation Coefficients (PRCCs) illustrating the influence of model parameters on changes in the atmospheric CO_2 concentration are presented in Fig. 6. We selected PRCC values at different time points, specifically $T = 10$ years, $T = 50$ years, $T = 80$ years, and $T = 100$ years, as summarized in Fig. 7.

Initially, the vehicle emission rates (γ) and the emission rate associated with human economic activities (σ) were less sensitive to variations in the human population as depicted in Fig. 7. However, as time progresses, both γ and σ become more responsive to changes in the human population. This indicates an increasing sensitivity of these parameters to variations in human population, suggesting potential negative consequences, such as elevated CO_2 emissions leading to global warming and other climate-related issues. In Fig. 7 (c), both γ and σ exhibit negative PRCCs, signifying that the amplified anthropogenic emissions contribute to a decline in human population.

The time-variable Partial Rank Correlation Coefficients (PRCCs) representing the influence of model parameters on changes in atmospheric CO_2 concentration are depicted in Fig. 6. Parameters σ, ψ, β, ω, and r exhibit positive PRCCs, while ρ, π, θ, and α display negative PRCCs.

This implies that increased transportation activities contribute to the acceleration of human economic activities, consequently leading to a rise in atmospheric CO_2 concentration. Additionally, a high growth rate in the human population intensifies the demand for mobility in both human activities and the transportation of goods and services, resulting in increased CO_2 emissions.

Conversely, the expansion of forests has a mitigating effect on atmospheric CO_2 concentration,

as highlighted in Fig. 6. The parameter ρ, representing the forest's ability to absorb CO_2, exhibits a negative PRCC with atmospheric CO_2. The declining magnitude of ρ, as illustrated in Fig. 6, indicates a reduction in the forest's capacity to store CO_2 due to ongoing deforestation, making it sensitive to variations in atmospheric CO_2 levels.

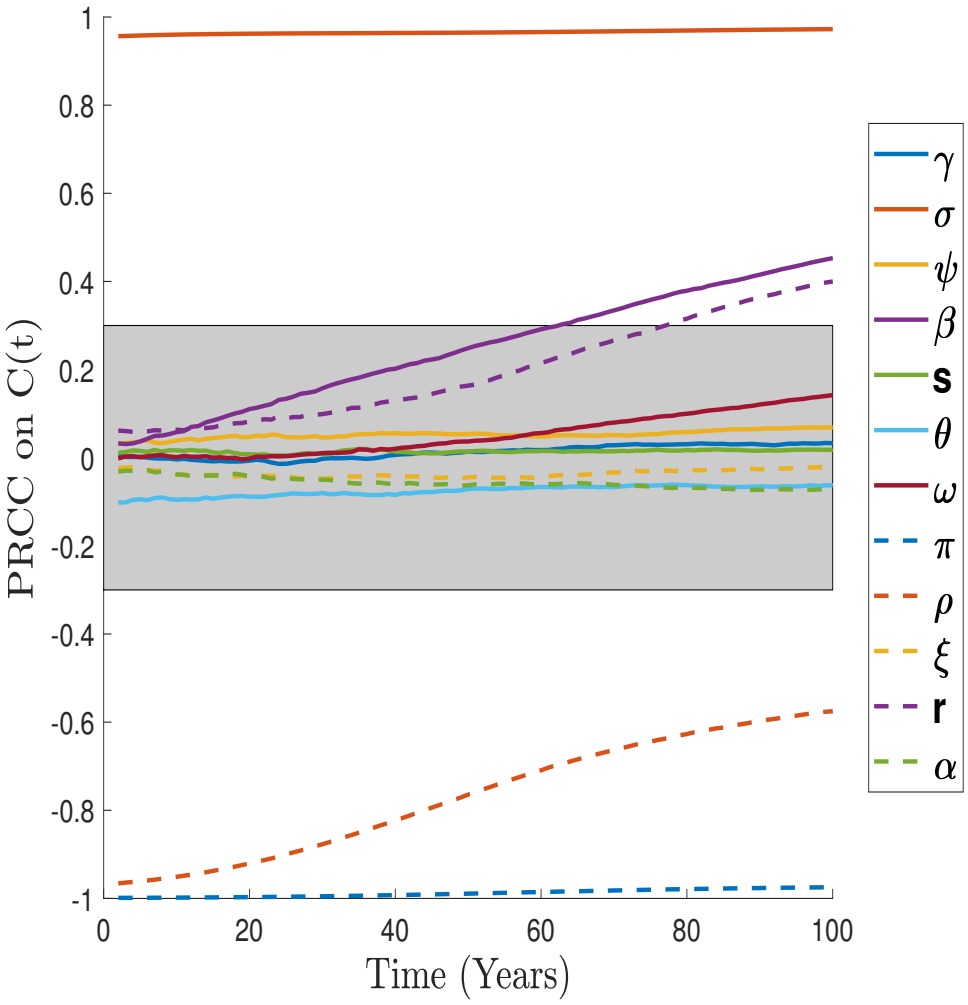

Figure 6: Sensitivity analysis PRCCs of parameters with respect to the atmospheric CO_2 concentration

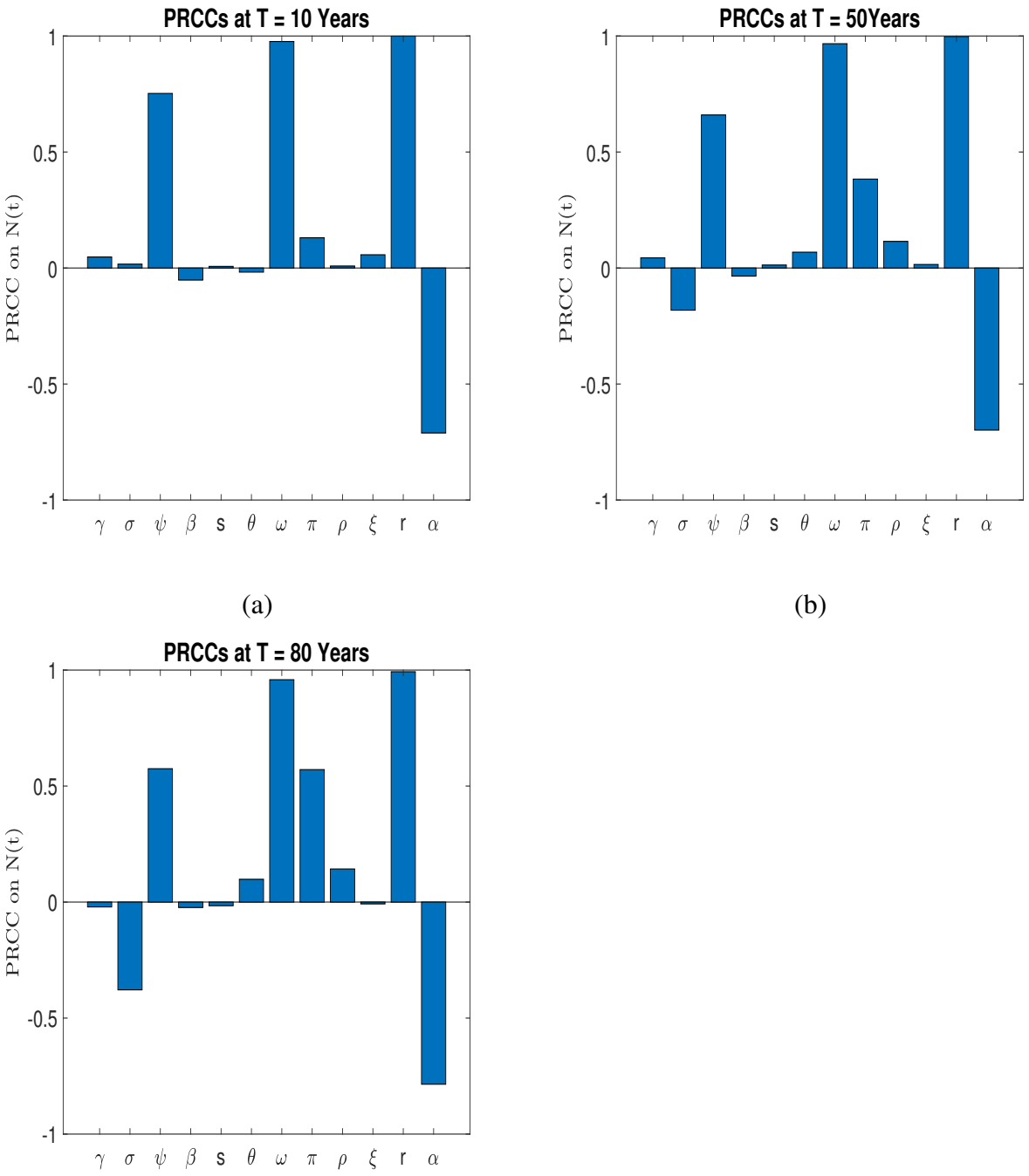

Figure 7: PRCCs of model parameters on human population at different time $T = 10$ years, $T = 50$ years and $T = 80$ years

4.5 Numerical simulation of the basic model

To comprehend the dynamics of atmospheric CO_2 due to vehicle emission, we performed a numerical simulation of the basic model (6) using parameters as listed in Table 3. With the aid of MATLAB R2021 we use a Runge Kutta order 4 numerical method to find the numerical solution of the system (6). From Fig. 8, it can be easily noted that, the atmospheric CO_2 concentration is influenced by human population, human economic activities, forest area and vehicle population. As human population increases, the demand for mobility of both human, goods and services increases, hence vehicle population is raised. This impacts to the rapid growth of atmospheric CO_2, since those vehicles are burning fossil fuels which is associated with the CO_2 emission. The atmospheric CO_2 depletes due to forest biomass through photosynthesis process and forest significantly depletes due to increased human population and human economic activities which is highly influenced by vehicle population growth rate β.

Human population grows and get stabilized as the atmospheric CO_2 starts to decline. But as number of vehicles increased, human economic activities get stimulated as depicted in Fig. 8, which results to depletion of human population due to adverse impacts of enhanced atmospheric CO_2 concentration such as global warming, droughts and other climate related problems. Hence, it is crucial to prioritize sustainable transportation practices to mitigate the negative effects of increased atmospheric CO_2.

4.5.1 Dynamics of atmospheric CO_2 with respect to vehicle population and human economic activities

In this section we simulated the model system (6) under different scenarios. First we observed the impact of increasing vehicle CO_2 emission rate γ on time evolution of atmospheric CO_2 and human population as depicted in Fig. 9 (b) and Fig. 9 (a) respectively. It can be easily noted that, at high vehicle emission rate, the volume of atmospheric CO_2 is high as the result, the human population starts to decline due to adverse impact caused by the enhanced atmospheric CO_2 like global warming, droughts and other climate related problems. From Fig. 9 we can observe that, when vehicle CO_2 emission rate is increased from 9.4×10^{-4} to 9.4×10^{-1}, the atmospheric CO_2 increased from 395.316 ppm to 2101.95 ppm and human population declined from 8.04 billions to 7.8804 billion people as depicted in Fig. 9.

Also, the increased human economic activities CO_2 emission rate (σ) which is triggered by

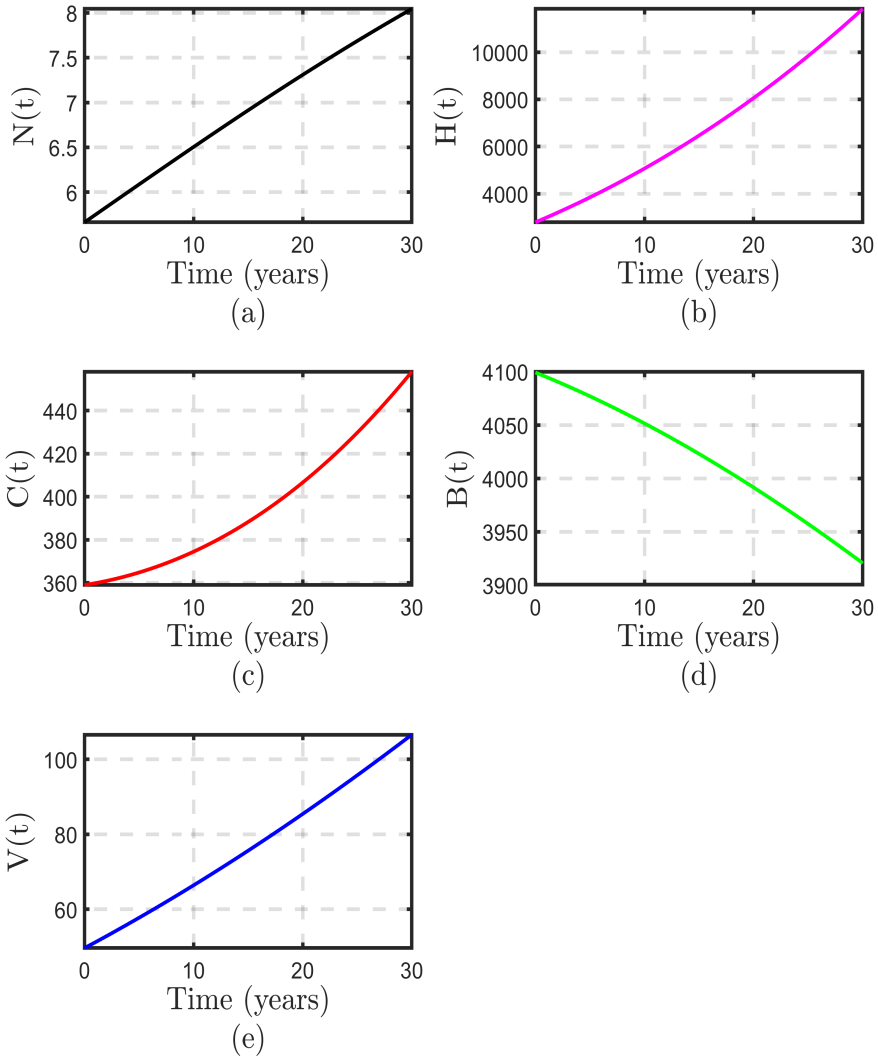

Figure 8: Interplay of atmospheric CO_2 concentration dynamics with human population, economic activities, vehicle population, and forest biomass

vehicle population growth rate (β) results to the significant increase in the atmospheric CO_2 concentration as shown in Fig. 11 and the decline of human population as depicted in Fig. 10. For instance the rise of σ from 0.0007897 to 0.01524 resulted to the increase of atmospheric CO_2 from 1315.92 ppm to 11229 ppm as the result human population starts to decline from 8.05 to 7.944 billion people at the end of 21^{st} century.

In the model system (6), forest biomass $B(t)$ acts as the sink for atmospheric CO_2. When deforestation rate ψ decline it will facilitate the growth of forest area as the result, the ability of forest to store CO_2 will be increased. Figure 12, portrays the impact of reducing deforestation

rate ψ on the forest biomass and time evolution of atmospheric CO_2 concentration. When the deforestation rate (ψ) is reduced by either providing education to society on using alternative energy sources like for home consumption and reforestation campaign the storage of CO_2 will be increased.

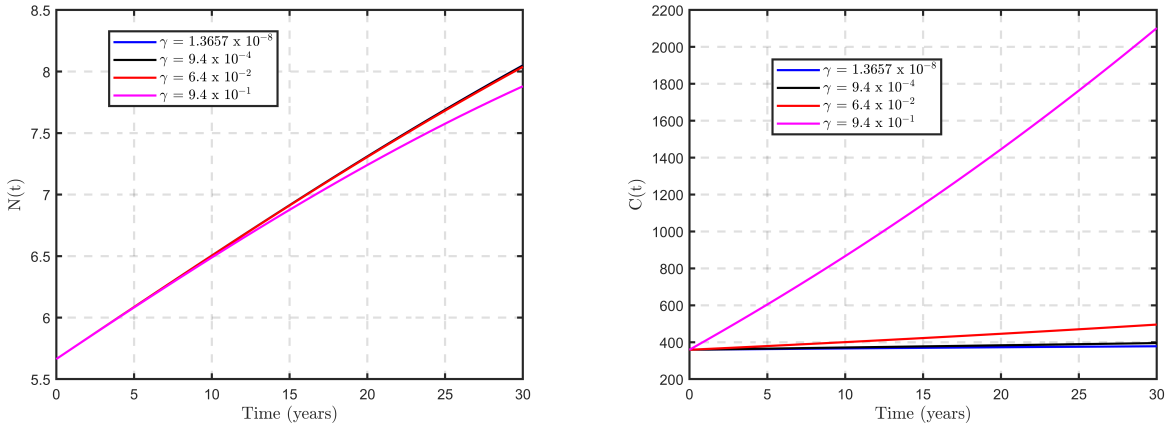

(a) (b)

Figure 9: Impact of varying vehicle CO_2 emission on human population, increase in vehicle CO_2 emission rate results to depletion of human population

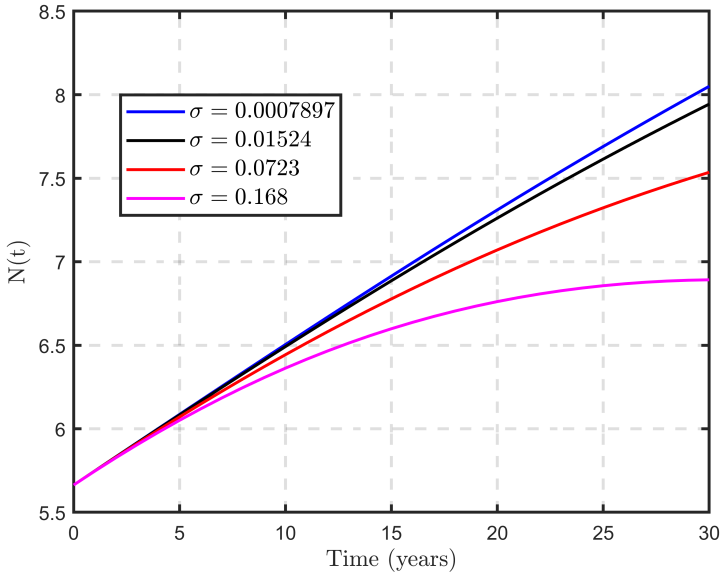

Figure 10: Impact of varying human economic activities CO_2 emission rate σ on time evolution of human population

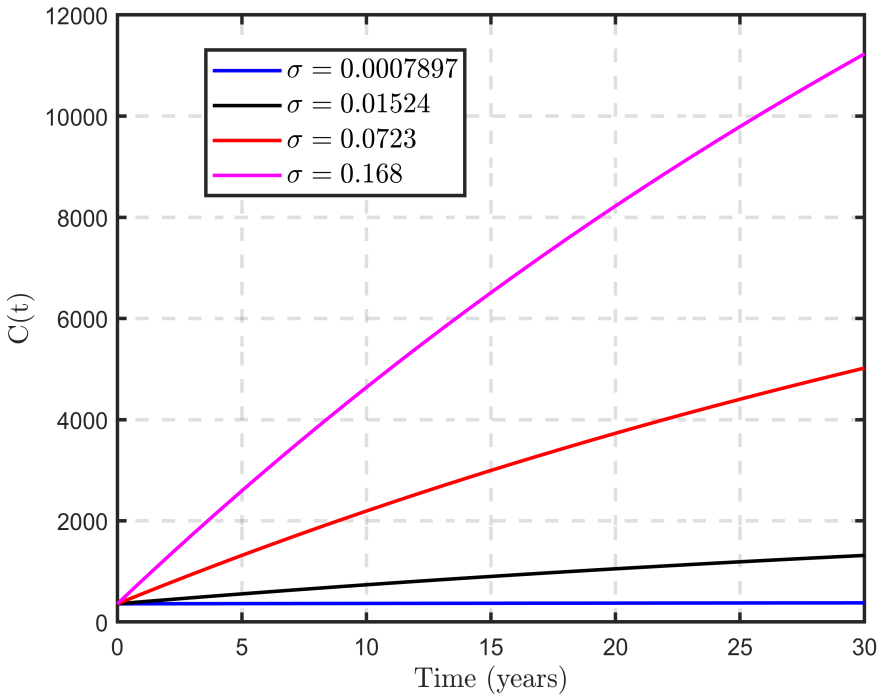

Figure 11: Impact of varying human economic activities CO_2 emission rate (σ) on time evolution of atmospheric CO_2 concentration

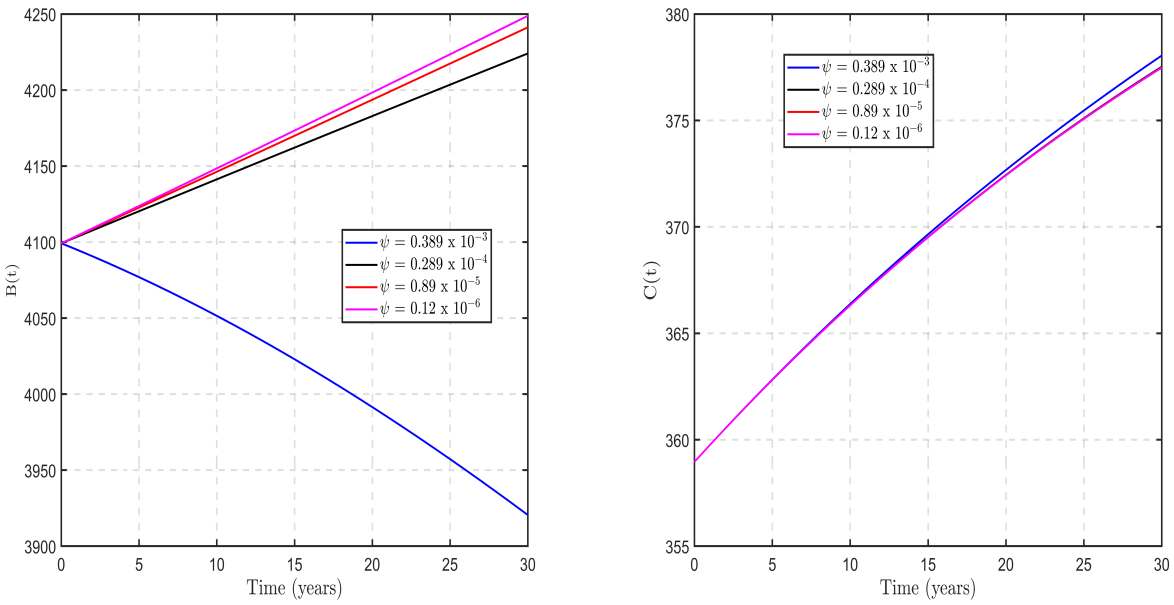

(a) (b)

Figure 12: Effects of decline in deforestation rate ψ on the evolution of atmospheric CO_2 concentration

4.6 Numerical simulation of optimal control problem

This section explores various optimal control strategies aimed at reducing atmospheric CO_2 emissions. The state system, costate system, and optimal characterization in Equations 49, 53 and 58–61 are solved numerically using the algorithm outlined in Mwanga *et al.* (2014). In numerical simulations, we assume a specific order for the weight constants: $a_1 > a_3 > a_5 > a_4 > a_2$, corresponding to controls $C(t)$, μ_1, μ_3, μ_4, and μ_2, respectively. This assumption is based on the associated costs of each control. For instance, the cost linked to μ_1 involves investing in incentives to encourage the use of vehicles powered by alternative energy sources like Clean Natural Gas (CNG) and electric vehicles. Meanwhile, the cost related to control μ_2 includes investments in tree planting and reforestation campaigns to enhance the forest's capacity to absorb CO_2. Similarly, the weight constant for control μ_3 represents investments in the production of vehicles that utilize clean energy sources, while that for control μ_4 signifies investments in green economy practices. Weights are chosen to be $a_1 = 1000$, $a_2 = 100$, $a_3 = 500$, $a_4 = 500$ and $a_5 = 400$.

To showcase the most effective strategies for mitigating future atmospheric CO_2 levels and their environmental impacts, the system (62) is solved numerically by taking $\mu_{1max} = 0.7$, $\mu_{2max} = 0.5$, $\mu_{3max} = 0.9$, $\mu_{4max} = 0.8$ and $T = 55$ years. All model parameters are as listed in Table 3 and starting time is fixed at 1994, the initial values of state variables are $N(0) = 5.66315$ billion people, $H(0) = 2787.67662$ billion US \$, $C(0) = 358.96$ ppm, $B(0) = 4099.2026$ million hectares, and $V(0) = 49.658288$ million vehicles. To solve numerically, we implement forward - backward sweep method for the model system (6) in MATLAB R2021 using parameters listed in Table 3. The method begins by solving the model system (6) forward in time using Runge Kutta fourth order method relying on the supplied initial control values. Then backward order Runge Kutta fourth order uses the obtained values of state variables and initial values of controls to solve the adjoint Equations (53). The control variables μ_1, μ_2, μ_3 and μ_4 are updated and used to solve the state and adjoint system. The following control strategies are assessed when they are implemented to control the atmospheric CO_2 concentration. Strategy 1: When reforestation efforts and green economy practices are implemented ($\mu_1 = 0$, $\mu_2 \neq 0$, $\mu_3 = 0$ and $\mu_4 \neq 0$), Strategy 2: When implementation of options for reducing CO_2 emission rates from operational vehicles and efficiency to cut down fossil fueled vehicles ($\mu_1 \neq 0$, $\mu_2 = 0$, $\mu_3 \neq 0$ and $\mu_4 = 0$) is considered and Strategy 3: When all controls are implemented

simultaneously ($\mu_1 \neq 0$, $\mu_2 \neq 0$, $\mu_3 \neq 0$, $\mu_4 \neq 0$).

Strategy 1: When reforestation efforts and green economy practices are implemented (μ_1 = 0, $\mu_2 \neq 0$, μ_3 = 0 and $\mu_4 \neq 0$)

In this strategy, reforestation efforts, coupled with a green economy practice, contribute to the reduction of carbon emissions. The growth of employment and income which is driven by public and private investments in activities, infrastructures, and assets will enable to reduce carbon emissions and pollution. Simulation results for this strategy are shown in Fig. 13. When $\mu_{1max} = 0.7$, $\mu_{2max} = 0.5$, $\mu_{1max} = 0.9$, and $\mu_{1max} = 0.8$, atmospheric CO_2 declined by 2.307%, from 374.475 ppm to 365.835 ppm, as shown in Fig.13 (a). Reforestation efforts (μ_2) is applied to its maximum for five years then started to decline while μ_4 is implemented to its maximum for approximately 9 years, after which they start to decline to zero in their final time, as depicted in Fig. 13 (d). From Fig. 13 (c), it can be observed that there is a slight impact of strategy 1 to the number of vehicles. This implies that emphasizing green economy efforts will encourage sustainable transportation practices, resulting in a reduced impact of the number of fossil fueled vehicles on atmospheric CO_2 concentration.

Strategy 2: When implementation of options for reducing CO_2 emission rate from operational vehicles and efficiency to cut down fossil fueled vehicles manufacture ($\mu_1 \neq 0$, μ_2 = 0, $\mu_3 \neq 0$ and μ_4 = 0)

In this strategy, the control variables μ_1 and μ_3 are used to optimize the objective function J. The control μ_3 is implemented to its maximum for 9 years, suggesting that in order to control CO_2 emissions from vehicles, cutting down fossil fueled vehicles manufacture should be done while the available vehicles in operation should be converted to Clean energy technologies as depicted in Fig. 14(d). From Figure 14(a), it can be observed that, the trend for atmospheric CO_2 is declined by 0.898%, from 374.475 ppm to 371.144 ppm, implying that, when this strategy is implemented, vehicles burning fossil fuels falls from 66.405 million vehicles to 58.8658 million vehicles as shown in Fig. 14(c).

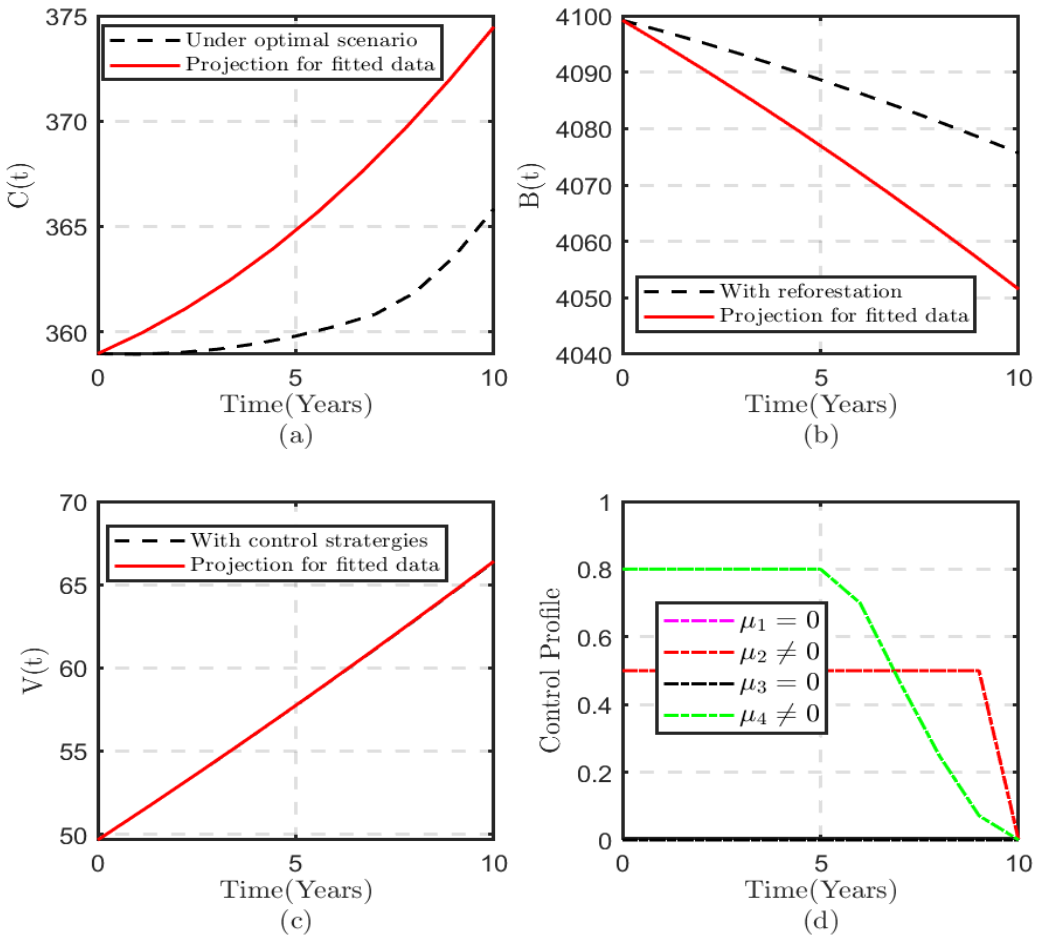

Figure 13: Time series for atmospheric CO_2, Forest biomass, vehicle population and optimal control profiles for strategy 1

Strategy 3: When all control strategies are implemented ($\mu_1 \neq 0$, $\mu_2 \neq 0$, $\mu_3 \neq 0$, $\mu_4 \neq 0$)

When all controls are taken into consideration, the future projection of atmospheric CO_2 level is illustrated in Fig. 15(a). From this plot it can be easily observed that, if the trend of CO_2 emissions without control continues, the atmospheric CO_2 concentration will reach to 374.475 ppm at the end of 21^{st} century, but if an optimal control strategy $\mu_{1max} = 0.7$, $\mu_{2max} = 0.5$, $\mu_{3max} = 0.9$ and $\mu_{4max} = 0.8$ the atmospheric Co_2 concentration will decline by 2.866% to 363.741 ppm, as depicted in Fig.15 (a). The optimal control profiles $\mu_1(t)$, $\mu_2(t)$, $\mu_3(t)$ and $\mu_4(t)$ in Fig.15 (d) shows that, under this optimal control strategy, mitigation options to cut down CO_2 emissions rate from vehicles in operations are implemented and fossil fueled vehicles are converted to clean energy source while reforestation efforts are implemented to its

maximum for the first 9 years then starts to decline. Also, the mitigation options to cut down fossil fueled vehicle production is implemented to its maximum for approximately 9 years then starts to decline. Furthermore, the efforts to practice green economy is implemented to its maximum for 8 years and thereafter started to decline. Comparing these three scenarios, it can be observed that, implementation of all four controls depletes more atmospheric CO_2. That implementation of mitigation options to cut down vehicle CO_2 emission rate, reforestation efforts, mitigation option to cut down fossil fueled vehicle manufacture together with efforts to implement green economy to cut CO_2 emissions from human economic activities results to 2.866% decline in atmospheric CO_2 concentration.

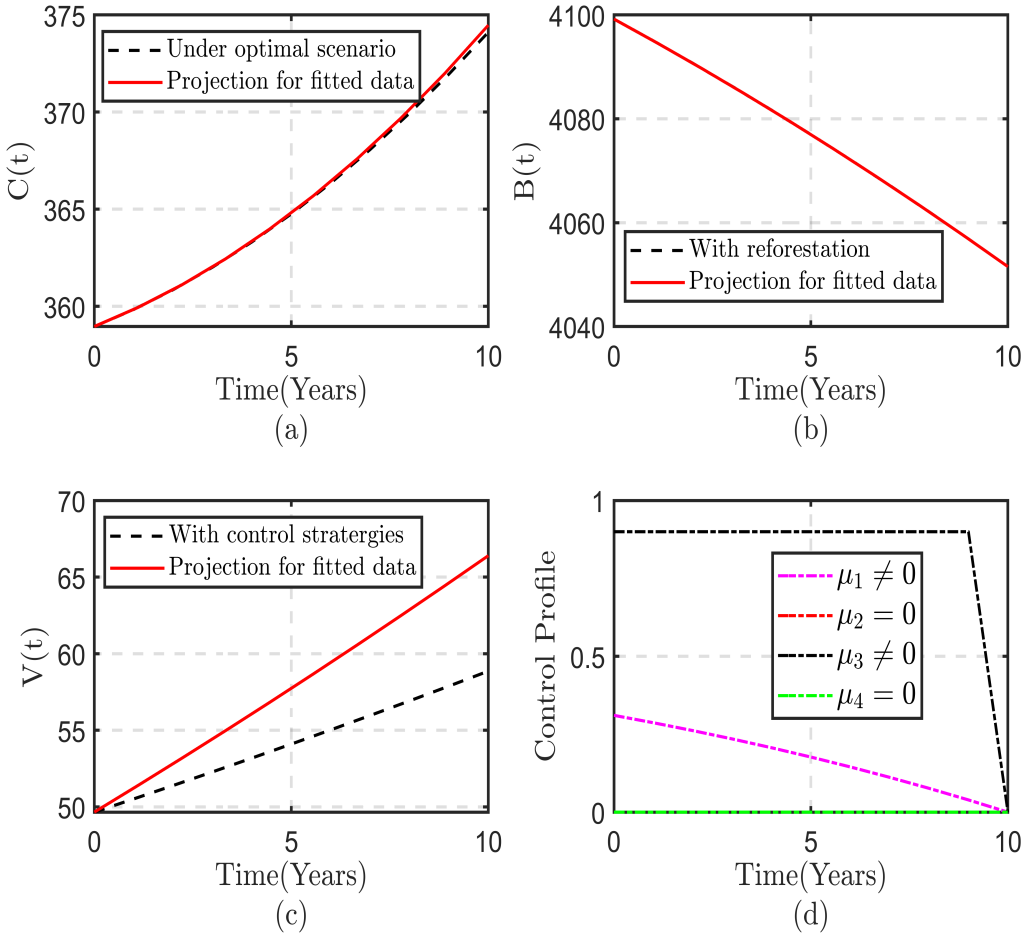

Figure 14: Trend for atmospheric CO_2, Forest biomass, Vehicle population and optimal control profiles for strategy 2

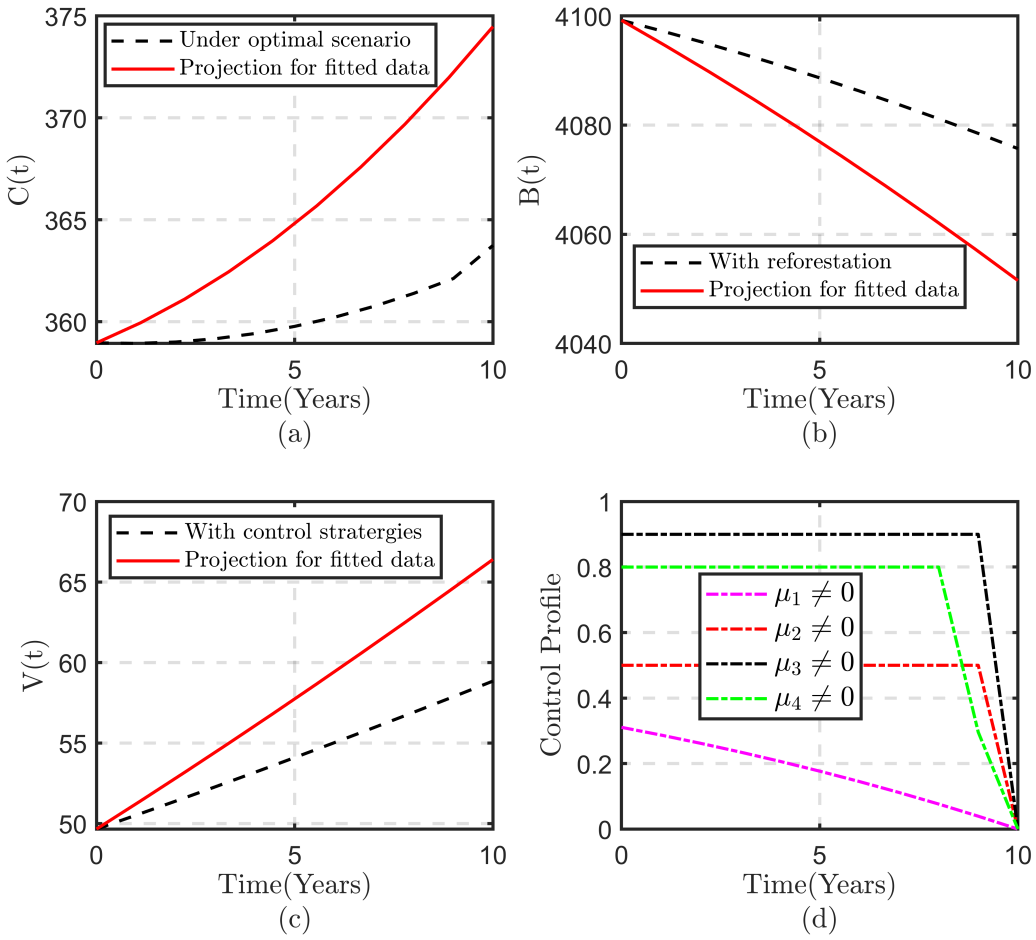

Figure 15: Time evolution of atmospheric CO_2, Forest biomass and Vehicle population with their corresponding optimal control profiles for implementation of strategy 3

CHAPTER FIVE

CONCLUSION AND RECOMMENDATIONS

5.1 Conclusion

From this study, it can be concluded that, the atmospheric CO_2 concentration is largely influenced by human activities which is highly accelerated by the transportation activities. Also, in this study we can conclude that human population is affected by the adverse impacts of increased atmospheric CO_2 concentration. The simulation of basic mathematical model revealed that, as human population increases, the demand for mobility is increased as the result atmospheric CO_2 concentration becomes high. Also, forest biomass is declining due to the increased human activities which promotes deforestation. Ecologically, the model analysis demonstrates four different scenarios. Firstly, the absence of human population lead to cessation of human related activities and only natural CO_2 emissions like volcanic eruption will exists and this CO_2 will naturally depleted. Secondly, the absence of human population makes the human related activities disappear and forest will grow up to its carrying capacity, since forest will not be harvested and naturally emitted CO_2 will be depleted by both forest biomass and naturally. Thirdly, revealed the absence of forest biomass in which this will exist if and only if the intrinsic human population growth rate "r" is greater than the mortality rate caused by the natural CO_2 emission. Lastly, the co-existence of both human population, economic activities, atmospheric CO_2 concentration, forest biomass and vehicle population. This scenario exists if the intrinsic human population growth rate is greater than the mortality rate due to natural CO_2 emission. The co-existence of all state variables is ecologically worth since plants need CO_2 for photosynthesis process, human requires oxygen gas (O_2) from plants for respiration process. Also, transportation activities are important for development of economic sector. Therefore for sustainable transportation activities and economic growth it is important to consider the conditions for stability of the interior equilibrium point which shows the existence of values of all state variables.

The co-existence of human population, economic activities, atmospheric CO_2, forest biomass and vehicles is important for sustainable development. The optimal control problem formulated helps to determine the best option to mitigate transport related CO_2 emission while meeting the

demand for mobility of goods, humans and services while minimizing the atmospheric CO_2 concentration. In conclusion, to attain a reduction in CO_2 emissions by 2.866%, it is imperative to implement green economy practices, pursue reforestation initiatives, reduce emissions from operational vehicles, and decrease the production of fossil fuel vehicles. These strategies are essential for addressing the challenges posed by climate change and promoting environmental sustainability.

5.2 Recommendations

Climate change issues will persist globally unless greenhouse gas (GHG) emissions, a primary contributor to global warming, are effectively controlled. In light of the findings from this study, we propose the following recommendations:

(i) The analysis of the model indicates that the atmospheric concentration of CO_2 increases in correlation with the rise in the vehicle population burning fossil fuels. To mitigate the emission of CO_2 from vehicles, it is imperative to adopt efficient technological solutions for running vehicles, particularly embracing clean energy technologies. Implementation of such efficient technological alternatives should be coupled with green economy practices and reforestation efforts to enhance the capacity of forests to sequester CO_2.

(ii) Drawing from the sensitivity analysis and simulation results, it becomes evident that the growth rate of the vehicle population (β) serves as a pivotal model parameter influencing economic activities. Significantly, it has a positive correlation with atmospheric CO_2 levels, suggesting that an increase in operational vehicles not only stimulates economic growth but also amplifies CO_2 production. This underscores the critical need to regulate CO_2 emissions from vehicles while simultaneously sustaining economic growth.

In light of these findings, this study strongly recommends that policymakers and governments prioritize sustainable transportation practices. This can be achieved through the implementation of technological innovations aimed at curbing emissions from vehicles and green economy strategy implementations to cut down emissions from economic activities without compromising the overall economic growth of a nation. Proactive measures in this regard will contribute to a balanced and sustainable trajectory, aligning environmental preservation with economic prosperity.

(iii) The government should intensify its commitment to achieving the United Nations Sustainable Development Goals (SDGs), specifically targeting the reduction of energy sources with adverse environmental impacts. Additionally, governmental policies should be designed to offer incentives to communities or individuals engaged in sustainable transportation practices. This strategic approach aims to inspire and motivate others to adopt similar eco-friendly activities. By aligning policies with the SDGs and fostering positive reinforcement through incentives, the government can play a pivotal role in promoting widespread adoption of sustainable transportation practices, contributing to a more environmentally conscious and resilient society.

(iv) Researchers can further extend this work by exploring the impacts of alternative transportation means and the utilization of shared mobility facilities, such as Bus Rapid Transit and Light Railway Transit, on the temporal evolution of atmospheric CO_2. Investigating these alternative modes of transportation can provide valuable insights into their effectiveness in reducing carbon emissions compared to conventional vehicle fleets. This extension would contribute to a more comprehensive understanding of sustainable transportation options and aid in the formulation of policies that promote environmentally friendly modes of commuting.

REFERENCES

Appiah, M., Li, F., & Korankye, B. (2021). Modeling the linkages among CO_2 emission, energy consumption, and industrialization in sub-Saharan African (SSA) countries. *Environmental Science and Pollution Research*, 28(29), 38506–38521.

Azizi, T., & Mugabi, R. (2020). Global sensitivity analysis in physiological systems. *Applied Mathematics*, 11(03),119–136.

Barisa, A., & Rosa, M. (2018). A system dynamics model for CO_2 emission mitigation policy design in road transport sector. *Energy Procedia*, 147, 419–427.

Bidah, S., Zakary, O., & Rachik, M. (2020). Stability and global sensitivity analysis for an agree-disagree model: Partial rank correlation coefficient and latin hypercube sampling methods. *International Journal of Differential Equations*, 2020, 1–14.

BTS (2019). World motor vehicle production. *https://www.bts.gov/content/world-motor-vehicle-production-selected-countries*. Online: Accessed: 2022-12-16.

Caetano, M. A. L., Gherardi, D. F. M., & Yoneyama, T. (2008). Optimal resource management control for CO_2 emission and reduction of the greenhouse effect. *Ecological Modelling*, 213(1), 119–126.

Devi, S., & Gupta, N. (2019). Dynamics of carbon dioxide gas (CO_2): Effects of varying capability of plants to absorb CO_2. *Natural Resource Modeling*, 32(1), e12174.

Etheridge, D. M., Steele, L. P., Langenfelds, R. L., Francey, R. J., Barnola, J.-M., & Morgan, V. I. (1996). Natural and anthropogenic changes in atmospheric CO_2 over the last 1000 years from air in antarctic ice and firn. *Journal of Geophysical Research: Atmospheres*, 101(D2), 4115–4128.

Fanuel, I. M., Mirau, S., Kajunguri, D., & Moyo, F. (2023). Conservation of forest biomass and forest–dependent wildlife population: Uncertainty quantification of the model parameters. *Heliyon*, 9(6) , e16948

FAO (2018).Forest Area (sq. km),food and agriculture organization, electronic files and web site. *https://data.worldbank.org/indicator/AG.LND.FRST.K2*. Online: Accessed: 2022-12-16.

Ferreira, R. V., Tavares, R. L. M., Medeiros, S. F. d., Silva, A. G. d., & Silva Júnior, J. F. d. (2020). Carbon stock and organic fractions in soil under monoculture and Sorghum bicolor–Urochloa ruziziensis intercropping systems. *Bragantia*, 79, 425–433.

Fleming, W. H., & Rishel, R. W. (2012). *Deterministic and stochastic optimal control.* Vol. 1. Springer Science & Business Media.

Freedman, H. I., & So, J. W.-H. (1985). Global stability and persistence of simple food chains. *Mathematical Biosciences*, 76(1), 69–86.

Gao, F., & Han, L. (2010). Implementing the Nelder-Mead simplex algorithm with adaptive parameters. *Computational Optimization and Applications*, 51(1), 259–277.

Helbing, D., Brockmann, D., Chadefaux, T., Donnay, K., Blanke, U., Woolley-Meza, O., Moussaid, M., Johansson, A., Krause, J., Schutte, S., & Perc, M. (2014). Saving Human Lives: What Complexity Science and Information Systems can Contribute. *Journal of Statistical Physics*, 158(3), 735–781.

Hussain, J., Khan, A., & Zhou, K. (2020). The impact of natural resource depletion on energy use and CO_2 emission in Belt & Road Initiative countries: A cross-country analysis. *Energy*, 19 (9), 117409.

IEA (2019). CO_2 emissions from fuel combustion 2019 edition. *IEA CO_2 emissions from fuel combustion database. Available at: http://wds. iea. org*.

Jaoua, N. (2019).Mathematical Model for CO_2 Emissions Reduction to Slow and Reverse Global Warming. *In:* Global Warming and Climate Change. IntechOpen.

Jawahar Farook, A., & Senthamarai Kannan, K. (2014). Stochastic modeling for carbon dioxide emissions. *Journal of Statistics and Management Systems*, 17(1), 97–112.

Lamb, W. F., Wiedmann, T., Pongratz, J., Andrew, R., Crippa, M., Olivier, J. G. J., Wiedenhofer, D., Mattioli, G., Al Khourdajie, A., House, J., Steven, J., & Minx, B. (2021). A review of trends and drivers of greenhouse gas emissions by sector from 1990 to 2018. *Environmental Research Letters*, 16(7), 073005.

Layek, G. C. *et al.* (2015). *An introduction to dynamical systems and chaos.* Vol. 449. Springer.

Léonidas, H., Toru, T., Fidel, N., Athanase, C. R., & Athanase, M. (2023). Comparative analysis of monocropping and mixed cropping systems on selected soil properties, soil organic carbon stocks, and simulated maize yields in drought-hotspot regions of Rwanda. *Heliyon*, 9(9), e19041.

Li, Y., Shang, J., Zhang, C., Zhang, W., Niu, L., Wang, L., & Zhang, H. (2021). The role of freshwater eutrophication in greenhouse gas emissions: A review. *Science of The Total Environment*, 768, 144582.

Majewska, A., & Gierałtowska, U. (2022). Impact of Economic Affluence on CO_2 Emissions in CEE Countries. *Energies*, 15(1), 322.

McMichael, A. J., Woodruff, R. E., & Hales, S. (2006). Climate change and human health: present and future risks. *The Lancet*, 367(9513), 859–869.

Misra, A. K., & Lata, K. (2015). A mathematical model to achieve sustainable forest management. *International Journal of Modeling, Simulation, and Scientific Computing*, 6(04), 1550040.

Misra, A. K., & Verma, M. (2013). A mathematical model to study the dynamics of carbon dioxide gas in the atmosphere. *Applied Mathematics and Computation*, 219(16), 8595–8609.

Misra, A. K., Verma, M., & Venturino, E. (2015). Modeling the control of atmospheric carbon dioxide through reforestation: Effect of time delay. *Modeling Earth Systems and Environment*, 1(3), 1–17.

Mohammadi, A., Burhan, A. A., & Mangal, R. (2020). Impact of Population and Economic Growth on CO_2 Emission (Case of Afghanistan). *Journal of Emerging Technologies and Innovative Research*, 7(10), 65–106.

Mwanga, G. G., Haario, H., & Nannyonga, B. K. (2014). Optimal control of malaria model with drug resistance in presence of parameter uncertainty. *Applied Mathematical Sciences*, 8(55), 2701–2730.

NOAA (2020).Trends in atmospheric carbon dioxide, mauna Loa CO_2 annual mean data. *https://gml.noaa.gov/ccgg/trends/data.html*. Online: Accessed: December 16, 2022.

Pal, S., & Ghosh, I. (2023). Dynamics of a coupled socio-environmental model: An application to global CO_2 emissions. *Ecological Modelling*, 478, 110279.

Pedreira, V. N., Brito, M. L., dos Santos, L. C. L., & Simonelli, G. (2022). Modeling of brazilian carbon dioxide emissions: A review. *Brazilian Archives of Biology and Technology*, 65, e22210594.

Pontryagin, L. S. (2018). *Mathematical theory of optimal processes.* Routledge.

Ritchie, H., Roser, M., & Rosado, P. (2020). *CO_2 and greenhouse gas emissions*. Our world in data. *https://ourworldindata.org/co2-and-greenhouse-gas-emissions*

Roosa, S. A., & Jhaveri, A. G. (2020). Carbon Reduction Technologies. *In:* Energy Management Handbook. River Publishers. pp. 561–581.

Tan, Z., & Gao, H. O. (2015). Traffic control for air quality management and congestion mitigation in complex urban vehicular tunnels. *Transportation Research Part C: Emerging Technologies*, 58, 13–28.

Tans, D. P. (2020). *Annual mean atmospheric CO2 values for Mauna Loa. NOAA/ESRL. https://datahub.io/core/co2-ppm.*

UNCCC (2023). UN Climate Change Conference - United Arab Emirates 30 Nov 2023. *https://unfccc.int/cop28*. Online: Accessed: December,16 2023.

Van Klooster, H. S. (1947). Jan Baptist van Helmont. *Journal of Chemical Education*, 24(7), 319.

Verma, M., & Misra, A. K. (2016). Optimal control of anthropogenic carbon dioxide emissions through technological options: A modeling study. *Computational and Applied Mathematics*, 37(1), 605–626.

Verma, M., & Verma, A. K. (2021). Effect of plantation of genetically modified trees on the control of atmospheric carbon dioxide: A modeling study. *Natural Resource Modeling*, 34(2), e12300.

Verma, M., Verma, A. K., & Misra, A. K. (2021). Mathematical modeling and optimal control of carbon dioxide emissions from energy sector. *Environment, Development and Sustainability*, 23(9), 13919–13944.

WBOD (2018). Population, total. *https://data.worldbank.org/indicator/SP.POP.TOTL*. Online: Accessed: December 16, 2022.

WBOD (2019). GDP (US Dollar), World Bank national accounts data, and OECD national accounts data files. *https://data.worldbank.org/indicator/NY.GDP.MKTP.CD*. Online: Accessed: December 16, 2022.

Yeh, J.-C., & Liao, C.-H. (2017). Impact of population and economic growth on carbon emissions in Taiwan using an analytic tool STIRPAT. *Sustainable Environment Research*, 27(1), 41–48.

Yoro, K. O., & Daramola, M. O. (2020). CO_2 emission sources, greenhouse gases, and the global warming effect. In *Advances in Carbon Capture* (pp. 3–28). Woodhead Publishing.

Zhao, X., Mahendra, A., Godfrey, N., Dalkmann, H., Rode, P., & Floater, G. (2016). *Unlocking the power of urban transport systems for better growth and a better climate. The New Climate Economy*.

APPENDICES

Appendix 1: MATLAB Codes

```
clc
close all
clear
global L K C0 s tau eta gamma sigma rho theta psi beta xi alpha
   omega pai r
%% parameter values
L=11;
K=750000;
C0=5;
s=0.03374;
tau=3.94;
eta=6.67e-7;
gamma=1.3657e-8;
sigma=0.0007897;
rho=3.86657e-7;
theta=0.0012025;
psi=0.389e-3;
beta=0.27534;
xi=1.50623e-5;
alpha=0.0000010551;
omega=0.00094457;
pai=0.016232;
r=0.0285;

ts=(1:1:250)';
S0=[5.66315,2787.67662,358.96,4099.2026,49.658288];
[t,z]=ode45(@(t,z)pet(t,z,L,K,C0,s,tau,eta,gamma,sigma,rho,theta,psi
   ,beta,xi,alpha,omega,pai,r),ts,S0)

N=z(:,1);
H=z(:,2);
C=z(:,3);
B=z(:,4);
V=z(:,5);


figure(1)
%subplot(321)
plot(t,N,'k-','LineWidth',2.5)
ylabel('N(t)','Interpreter','Latex','Fontsize',10)
xlabel({'Time(Years)','(a)'},'Interpreter','Latex','Fontsize',10)
grid on
grid(gca,'on');
set(gca,'GridLineStyle','--')

figure(2)
%subplot(322)
```

```
plot(t,H,'m-','LineWidth',2.5)
ylabel('H(t)','Interpreter','Latex','Fontsize',10)
xlabel({'Time(Years)','(b)'},'Interpreter','Latex','Fontsize',10)
grid on
grid(gca,'on');
set(gca,'GridLineStyle','--')


figure(3)
%subplot(323)
plot(t,C,'r-','LineWidth',2.5)
ylabel('C(t)','Interpreter','Latex','Fontsize',10)
xlabel({'Time(Years)','(c)'},'Interpreter','Latex','Fontsize',10)
grid(gca,'on');
set(gca,'GridLineStyle','--')
grid on

figure(4)
%subplot(324)
plot(t,B,'g-','LineWidth',2.5)
ylabel('B(t)','Interpreter','Latex','Fontsize',10)
xlabel({'Time(Years)','(d)'},'Interpreter','Latex','Fontsize',10)
grid on
grid(gca,'on');
set(gca,'GridLineStyle','--')

figure(5)
%subplot(325)
plot(t,V,'b-','LineWidth',2.5)
ylabel('V(t)','Interpreter','Latex','Fontsize',10)
xlabel({'Time(Years)','(e)'},'Interpreter','Latex','Fontsize',10)
grid on
grid(gca,'on');
set(gca,'GridLineStyle','--')


figure(6)
subplot(321)
plot(t,N,'k-','LineWidth',2.5)
ylabel('N(t)','Interpreter','Latex','Fontsize',10)
xlabel({'Time(Years)','(a)'},'interpreter','LaTex','FontSize',10)
grid on
grid(gca,'on');
set(gca,'GridLineStyle','--')

subplot(322)
plot(t,H,'m-','LineWidth',2.5)
ylabel('H(t)','Interpreter','Latex','Fontsize',10)
xlabel({'Time(Years)','(b)'},'interpreter','LaTex','FontSize',10)
grid on
grid(gca,'on');
```

```
set(gca,'GridLineStyle','--')



subplot(323)
plot(t,C,'r-','LineWidth',2.5)
ylabel('C(t)','Interpreter','Latex','Fontsize',10)
xlabel({'Time(Years)','(c)'},'interpreter','LaTex','FontSize',10)
grid(gca,'on');
set(gca,'GridLineStyle','--')
grid on


subplot(324)
plot(t,B,'g-','LineWidth',2.5)
ylabel('B(t)','Interpreter','Latex','Fontsize',10)
xlabel({'Time(Years)','(d)'},'interpreter','LaTex','FontSize',10)
grid on
grid(gca,'on');
set(gca,'GridLineStyle','--')


subplot(325)
plot(t,V,'b-','LineWidth',2.5)
ylabel('V(t)','Interpreter','Latex','Fontsize',10)
xlabel({'Time(Years)','(e)'},'interpreter','LaTex','FontSize',10)
grid on
grid(gca,'on');
set(gca,'GridLineStyle','--')



function dy=pet(t,var,L,K,C0,s,tau,eta,gamma,sigma,rho,theta,psi,
   beta,xi,alpha,omega,pai,r)
dy=zeros(5,1);
dy(1)= r*var(1).*(1 - var(1)/L) - alpha*var(3).*var(1) + psi*omega*
   var(1).*var(4);

dy(2)= s*var(1) + tau*var(5) - eta*var(2);

dy(3)= C0 + gamma*var(5) + sigma*var(2) - rho*var(4).*var(3) - pai*
   var(3);

dy(4)= theta*var(4).*(1 - var(4)/K) - psi*var(1).*var(4);

dy(5)= beta*var(1) - xi*var(5);
end
```

Listing 1: MATLAB code for basic model

MATLAB Codes for Parameter Estimations

```
1
2  %% Script file
3  clc;
4  close all;
5  %% parameter initial guess
6  xi=1.0676e-5;
7  psi=0.26e-3;
8  gamma=0.0019e-5;
9  sigma=0.576e-3;
10 rho=4.8e-4;
11 pai=0.016;
12 theta=  0.00114579083555226;
13 beta=0.2678;
14 r=0.026;
15 alpha=0.000001;
16 omega=0.001;
17 s=0.035;
18 p0=[xi psi gamma sigma rho pai theta beta r alpha omega s];
19 ts=(1:1:23)';
20 %% function to minimize error/residue
21 fun = @giov_objective;
22 [p, fval]=fminsearch(fun,p0);
23 %% optimized parameters
24 xi=p(1);
25 psi=p(2);
26 gamma=p(3);
27 sigma=p(4);
28 rho=p(5);
29 pai=p(6);
30 theta=p(7);
31 beta=p(8);
32 r=p(9);
33 alpha=p(10);
34 omega=p(11);
35 s=p(12);
36 p=[xi psi gamma sigma rho pai beta r alpha omega s];
37 %% model with updated parameter
38 p=[xi;psi;gamma;sigma;rho;pai;theta;beta;r;alpha;omega;s];
39 S0=[5.66315,2787.67662,358.96,4099.2026,49.658288];
40 [t,S]=ode45(@(t,S)giov_func(t,S,p),ts,S0);
41 %% Read dats from excel file world_data2.csv as S_m
42 noise_mean=0;
43 noise_std=0.5;
44 noise=noise_mean+noise_std*randn(size(S_m));
45 %% experimental data at each time point when gaussian noise added
46 S_measured=S_m +noise;
47 H=S-S_measured;
48 %% computations of correlation coefficients for both state variables
49 r_1 =corrcoef(S_measured(:,1),S(:,1))
50 r_2 =corrcoef(S_measured(:,2),S(:,2))
```

```
r_3 =corrcoef(S_measured(:,3),S(:,3))
r_4 =corrcoef(S_measured(:,4),S(:,4))
r_5 =corrcoef(S_measured(:,5),S(:,5))
%% Computations of coefficient of determination
R_sq1 = r_1.^2
R_sq2 = r_2.^2
R_sq3 = r_3.^2
R_sq4 = r_4.^2
R_sq5 = r_5.^2
%% olotting actual data and the model solution with optimal
   parameters
subplot(3,2,1)
plot(t,S(:,1),'r-','linewidth',2.0)
hold on
plot(t,S_measured(:,1),'bo','linewidth',1.5)
legend('Model fit','Real data','Interpreter','Latex','Fontsize',16)
ylabel({'Human population','(Billions)'},'Interpreter','Latex','
   Fontsize',16)
xlabel({'Time [Years]','(a)'},'Interpreter','Latex','Fontsize',16)
xticklabels({'1994','1999','2004','2009','2014','2019','Interpreter'
   ,'Latex','Fontsize',16})
grid on

subplot(3,2,2)
plot(t,S(:,2),'r-','linewidth',2.0)
hold on
plot(t,S_measured(:,2),'bo','linewidth',1.5)
legend('Model fit','Real data','Interpreter','Latex','Fontsize',16)
ylabel({'Economic Activities','(in billions US \$)'},'Interpreter','
   Latex','Fontsize',16)
xlabel({'Time [Years]','(b)'},'Interpreter','Latex','Fontsize',16)
xticklabels({'1994','1999','2004','2009','2014','2019','Interpreter'
   ,'Latex','Fontsize',16})
grid on

subplot(3,2,3)
plot(t,S(:,3),'r-','linewidth',2.0)
hold on
plot(t,S_measured(:,3),'bo','linewidth',1.5)
legend('Model fit','Real data','Interpreter','Latex','Fontsize',16)
ylabel({'Atmospheric $CO_2$ concentration','(in ppm)'},'Interpreter'
   ,'Latex','Fontsize',16)
xlabel({'Time [Years]','(c)'},'Interpreter','Latex','Fontsize',16)
xticklabels({'1994','1999','2004','2009','2014','2019','Interpreter'
   ,'Latex','Fontsize',16})
grid on

subplot(3,2,4)
plot(t,S(:,4),'r-','linewidth',2.0)
hold on
plot(t,S_measured(:,4),'bo','linewidth',1.5)
```

```
legend('Model fit','Real data','Interpreter','Latex','Fontsize',16)
ylabel({'Forest Biomass','(in KHa)'},'Interpreter','Latex','Fontsize
    ',16)
xlabel({'Time [Years]','(d)'},'Interpreter','Latex','Fontsize',16)
xticklabels({'1994','1999','2004','2009','2014','2019','Interpreter'
    ,'Latex','Fontsize',16})
grid on

subplot(3,2,5)
plot(t,S(:,5),'r-','linewidth',2.0)
hold on
plot(t,S_measured(:,5),'bo','linewidth',1.5)
legend('Model fit','Real data','Interpreter','Latex','Fontsize',16)
ylabel({'Vehicle population','(in millions)'},'Interpreter','Latex',
    'Fontsize',16)
xlabel({'Time [Years]','(e)'},'Interpreter','Latex','Fontsize',16)
xticklabels({'1994','1999','2004','2009','2014','2019','Interpreter'
    ,'Latex','Fontsize',16})
grid on

num_points=numel(S_measured);
mse=sum((S-S_measured).^2)/num_points;
R_mean=mean(S_measured);
RMSEN=(sqrt(mse)/R_mean)*100;
fprintf('Root Mean Sqared Normalized Error (RMSNE): %.4f\n',RMSEN);

D=(S_measured-R_mean).^2;
D_sum=sum(D);
squared_error=(S-S_measured).^2;
E_sum=sum( squared_error);
NSE=1- (E_sum/D_sum);
fprintf('Nash-Sutcliffe effciency index (NSE): %.4f\n',NSE);
options = optimset('Display','iter', 'TolFun', 1e-6, 'MaxIter', 100)
    ;

%% bootstraping
numBootstraps = 20;
bootstrappedParams = zeros(numBootstraps, length(p0));

for i = 1:numBootstraps
bootstrappedData = datasample(S_measured, length(S_measured));
bootstrappedParams(i, :) = fminsearch(@(p) giov_objective(p, t,
    bootstrappedData), p0,options);
end
confidenceIntervals = prctile(bootstrappedParams, [2.5, 97.5]);

%% Display Results
disp('Estimated Parameters:');
disp(p);
disp('Confidence Intervals:');
disp(confidenceIntervals);
```

```
140
141 %% Calculate RMSNE
142 num_points = numel(S_measured);
143 mse = sum((S - S_measured).^2) / num_points;
144 R_mean = mean(S_measured);
145 RMSNE = (sqrt(mse) / R_mean) * 100;
146 fprintf('Root Mean Squared Normalized Error (RMSNE): %.4f\n', RMSNE)
    ;
147
148 %% Calculate NSE
149 D = (S_measured - R_mean).^2;
150 D_sum = sum(D);
151 squared_error = (S - S_measured).^2;
152 E_sum = sum(squared_error);
153 NSE = 1 - (E_sum / D_sum);
154 fprintf('Nash-Sutcliffe efficiency index (NSE): %.4f\n', NSE);
```

Listing 2: Script file for Parameter Estimations

```
1         function dy=giov_func(~,var,p)
2         dy=zeros(5,1);
3         %%known parameters
4         L=11;
5         K=750000;
6         C0=5;
7         tau=3.94;
8         eta=6.67e-7;
9         %% unkown parameters
10        xi=p(1);
11        psi=p(2);
12        gamma=p(3);
13        sigma=p(4);
14        rho=p(5);
15        pai=p(6);
16        theta=p(7);
17        beta=p(8);
18        r=p(9);
19        alpha=p(10);
20        omega=p(11);
21        s=p(12);
22        %% ode system
23        dy(1)= r*var(1).*(1 - var(1)/L) - alpha*var(3).*var(1) +
             omega*psi*var(1).*var(4);
24        dy(2)= s*var(1) + tau*var(5) - eta*var(2);
25        dy(3)= C0 + gamma*var(5) + sigma*var(2) - rho*var(4).*var(3)
              - pai*var(3);
26        dy(4)= theta*var(4).*(1 - var(4)/K) - psi*var(1).*var(4);
27        dy(5)= beta*var(1) - xi*var(5);
28        end
```

Listing 3: Function file for defining a system ordinary differential Eqns

```
function obj=giov_objective(p,~,~)
%% initial condition at t=0
S0=[5.66315,2787.67662,358.96,4099.2026,49.658288];
%% time points for the experiment (measured data point for
   time)
ts=(1:1:23)';
%% ode solver to solve the ode
[~,S]=ode45(@(t,S)giov_func(t,S,p),ts,S0);
noise_mean=0;
noise_std=0.5;
noise=noise_mean+noise_std*randn(size(S_m));
S_measured=S_m +noise;
%% objective function to minimize the sum of square of
   residue
A=(S-S_measured).^2;
obj=sum(A,'all');
end
```

Listing 4: Function file for defining an objective function

Research Outputs

(i) Publication

Donald, P., Mayengo, M.,& Lambura, A.G. (2024). Mathematical modeling of vehicle carbon dioxide emissions, *Heliyon 10 (2), e23976*.

(ii) Poster presentation

Donald, P., Mayengo, M., & Lambura, A.G. (2024). *Mathematical models for vehicle carbon dioxide emissions*.

Heliyon 10 (2024) e23976

Contents lists available at ScienceDirect

Heliyon

journal homepage: www.cell.com/heliyon

Research article

Mathematical modeling of vehicle carbon dioxide emissions

Pita Donald [a,b,*], Maranya Mayengo [a], Aristide G. Lambura [c]

[a] School of Computational and Communication Science and Engineering, Nelson Mandela African Institution of Science and Technology (NM-AIST), P.O. Box 447, Arusha, Tanzania

[b] Department of Mathematics, Humanities and Social Sciences, National Institute of Transport (NIT), P.O. Box 705, Dar es Salaam, Tanzania

[c] Department of Computer Systems and Mathematics, Ardhi University (ARU), P.O. Box 35176, Dar es Salaam, Tanzania

ARTICLE INFO

Keywords:
Mathematical model
Vehicular emission
Greenhouse gas
Atmospheric carbon dioxide
Climate change
Sustainable transportation

ABSTRACT

The demand for transportation, driven by an increasing global population, is continuously rising. This has led to a higher number of vehicles on the road and an increased reliance on fossil fuels. Consequently, the rise in atmospheric carbon dioxide (CO_2) levels has contributed to global warming. Therefore, it is important to consider sustainable transportation practices to meet climate change mitigation targets. In this research paper, a non-linear mathematical model is developed to study the dynamics of atmospheric CO_2 concentration in relation to human population, economic activities, forest biomass, and vehicle population. The developed model is analyzed qualitatively to understand the long-term behavior of the system's dynamics. Model parameters are fitted to actual data of world population, human economic activities, atmospheric CO_2, forest biomass, and vehicle population. It is shown that increased vehicular CO_2 emissions have a potential contribution to the increase in atmospheric CO_2 and the decline of human population. Numerical simulations are carried out to verify the analytical findings and we performed global sensitivity analysis to explore the impacts of different sensitive parameters on the CO_2 dynamics.

1. Introduction

Greenhouse gases, with carbon dioxide (CO_2) being a prominent example, play a significant role in the greenhouse effect, a key driver of climate change. These gases are emitted by diverse economic sectors, including energy generation, industrial processes, building operations, transportation activities, agricultural practices, forestry, and other land use activities (AFOLU). The expanding global population and corresponding economic development have led to an increased demand for energy, primarily sourced from fossil fuels [1–4]. This heightened energy demand has resulted in higher carbon dioxide (CO_2) emissions, exacerbating the challenges posed by climate change [5–7].

The transportation sector is a significant contributor to CO_2 emissions due to the combustion of fossil fuels, which contributes to the concentration of atmospheric CO_2 [8–11]. Urban transport alone accounted for 23% of total energy-related emissions, and the global transportation sector contributes approximately 25% of total CO_2 emissions from fossil fuel combustion [10,12]. Consequently, climate-related issues such as ozone layer depletion, droughts, and global warming have become more pronounced.

* Corresponding author at: School of Computational and Communication Science and Engineering, Nelson Mandela African Institution of Science and Technology (NM-AIST), P.O. Box 447, Arusha, Tanzania.
E-mail address: donaldp@nm-aist.ac.tz (P. Donald).

https://doi.org/10.1016/j.heliyon.2024.e23976
Received 18 June 2023; Received in revised form 21 November 2023; Accepted 2 January 2024

Available online 8 January 2024

Table 1
Model parameters and description.

Parameter	Description
r	Intrinsic human population growth rate
L	Human population carrying capacity
α	Mortality rate coefficient due to enhanced CO_2
s	Economic activities growth rate due to population
τ	Human economic activities growth rate due to vehicle population
η	Human economic activities depletion rate constant
C_0	Emission rate of CO_2 from natural and respiration processes
γ	CO_2 vehicle emission rate constant
σ	Human economic activities CO_2 emission rate
ρ	CO_2 depletion rate coefficient due to forest biomass
π	Natural CO_2 depletion rate coefficient
θ	Forest biomass intrinsic growth rate coefficient
K	Forest area carrying capacity
ψ	Deforestation rate coefficient
β	Vehicle's population growth rate due to demand for mobility
ξ	Vehicle depletion rate coefficient
ω	Human population growth rate coefficient due forest harvesting

At the forefront of contemporary discourse, complexity sciences play a pivotal role in preserving human lives. This discourse encompasses the strategic application of mathematical modeling as a potent instrument within this paradigm [13]. Recent studies have employed non-linear mathematical models to investigate the dynamics of atmospheric CO_2 in relation to forest biomass. Notably, [14–16] have explored these models. These investigations have delved into diverse strategies, including genetically engineered plants and incentives for energy conservation through education, aimed at curtailing CO_2 emissions. Additionally, [17] has contributed to the discourse by scrutinizing the dynamics of atmospheric CO_2 from an energy sector perspective, highlighting the significance of adopting low-carbon energy sources to mitigate costs. Furthermore, [18,19] have employed non-linear mathematical models to manage atmospheric CO_2 levels through reforestation, considering variables such as forest biomass, human population, and reforestation efforts. Likewise, [15] have utilized a non-linear mathematical model to study atmospheric CO_2 concentration, taking into account plants' capacity to absorb atmospheric CO_2.

However, non of these studies considered the dynamics of atmospheric CO_2 concentration due to vehicle emissions. Therefore, this study comes up with a mathematical model that encompasses the interplay or dynamics between human population, human economic activities, forest biomass, vehicle population and atmospheric CO_2 concentration in a global scale, and investigate the impact of vehicle population on the dynamics of atmospheric CO_2 concentration and human population. The structure of this paper is well-organized, with sections dedicated to formulating the mathematical model, qualitative analysis, quantitative analysis, and concluding the findings.

2. Model formulation

The system of non-linear ordinary differential equations is used to describe the dynamics of atmospheric CO_2 concentration. The model is made up of five distinct compartments, namely, human population (N), human economic activities (H), atmospheric CO_2 concentration (C), forest biomass (B) and vehicle population (V) at a time t. It is assumed that the human population grows logistically and depletes due to the adverse impact of increased atmospheric CO_2 concentration by a rate α [14,20]. Also, it is assumed that human population increases due to consumption of forest resources by a rate ω [14]. Using these assumptions, the dynamics of human population is governed by the equation (1) and parameter descriptions are in Table 1

$$\dot{N} = rN\left(1 - \frac{N}{L}\right) + \omega\psi NB - \alpha CN \tag{1}$$

Human economic activities are assumed to expand in response to population growth, as it drives increased demand for goods and services, and depletes naturally by a rate η. The growth of human activities is assumed to be influenced by the number of vehicles by the rate τ. As number of vehicle increases, it stimulates various economic sectors and promotes overall economic growth. This, in turn, leads to an expansion of human activities and their impact on the environment. Additionally, we assume that the growth of human economic activities is quantified by the Gross Domestic Product (GDP). The GDP serves as an indicator of economic performance and reflects the overall value of goods and services produced within a country. As GDP increases, it signifies a higher level of economic activity, including industrial, commercial, and agricultural sectors. The dynamics of human economic activities can be modeled by the equation (2) and its parameters are detailed in Table 1.

$$\dot{H} = sN + \tau V - \eta H \tag{2}$$

The atmospheric CO_2 concentration is assumed to increase due to the growing number of vehicles and human activities by rates γ and σ respectively. Additionally, CO_2 concentration in the atmosphere is naturally depleted through ocean sinking and absorbed by forest through photosynthesis process [21,4]. The growth rate of atmospheric CO_2 resulting from natural processes, such as

respiration of living organisms, volcanic eruptions, and changes in ocean circulation, is assumed to be constant [18]. The dynamics of atmospheric CO_2 is governed by equation (3) and parameters are described in a Table 1.

$$\dot{C} = C_0 + \gamma V + \sigma H - \rho BC - \pi C \tag{3}$$

It is presumed that forest biomass adheres to the principles of logistic growth and depletes due to human population growth. Its dynamics is governed by equation (4) and parameters are explained in a Table 1.

$$\dot{B} = \theta B\left(1 - \frac{B}{K}\right) - \psi N B \tag{4}$$

In the region of consideration, the vehicle population is assumed to have a growth rate of β and naturally depletes, by the rate ξ. Vehicle population dynamics is modeled by equation (5).

$$\dot{V} = \beta N - \xi V \tag{5}$$

Consequently, we formulate the following system of equations of non linear differential equation as presented in a system (6).

$$\begin{cases} \dot{N} = rN\left(1 - \frac{N}{L}\right) + \omega\psi N B - \alpha C N \\ \dot{H} = sN + \tau V - \eta H \\ \dot{C} = C_0 + \gamma V + \sigma H - \rho BC - \pi C \\ \dot{B} = \theta B\left(1 - \frac{B}{K}\right) - \psi N B \\ \dot{V} = \beta N - \xi V \end{cases} \tag{6}$$

Where

$$N(0) \geq 0, H(0) \geq 0, C(0) > 0, B(0) \geq 0, V(0) \geq 0 \tag{7}$$

3. Qualitative analysis

3.1. Boundedness of model solution

In this section, we demonstrate that the solutions of a system (6) with the initial condition (7) remain bounded. We achieve this by employing a well-established comparison theorem for differential equations [22]. In Lemma (1), we determine the region of attraction, which is an invariant region attracting all solutions of the model system (6) with the initial condition (7).

Lemma 1. *The set* $\Omega = \{(N, H, C, B, V) \in \mathbb{R}^5 : 0 \leq N \leq N_m; 0 \leq H \leq H_m; 0 < C \leq C_m; 0 \leq B \leq B_m;\ 0 \leq V \leq V_m$, *where* $N_m = L + \frac{\omega\psi KL}{r}$, $H_m = \frac{sN_m}{\eta}$, $C_m = \frac{\eta C_0 + s\sigma N_m}{\eta(\rho K + \pi)}$, $B_m = K$, $V_m = \frac{\beta N_m}{\xi}$ *establish the region of attraction for the system (6), which attracts all solutions originating from within the positive orthant's interior.*

Proof for Lemma (1) is appended in Appendix B.

3.2. Equilibrium analysis

The long-term behavior of the system (6) was established by using stability theory. The feasible equilibrium points are obtained and their stability properties are established. The model system (6) has two non-negative trivial solutions $E_1\left(0, 0, \frac{C_0}{\pi}, 0, 0\right)$ and $E_2\left(0, 0, \frac{\theta C_0}{K\rho + \pi}, K, 0\right)$ and two non-trivial solutions $E_3\left(N_3, H_3, C_3, 0, V_3\right)$ and $E^*(N^*, H^*, C^*, B^*, V^*)$.

It can be noted that the existence of E_1 and E_2 is obvious. Further more the existence of equilibria E_3 and E^* depend on the satisfaction of condition (8).

$$\frac{r}{\alpha} - \frac{C_0}{\pi} > 0 \tag{8}$$

Existence of E_3

To prove the existence of E_3 we solved the system (9) to obtain algebraic equations for N_3, H_3, C_3 and V_3 [17]. Consider the system (9) below,

$$\left.\begin{aligned} r\left(1-\frac{N_3}{L}\right)-\alpha C_3 &= 0\\ sN_3+\tau V_3-\eta H_3 &= 0\\ C_0+\gamma V_3+\sigma H_3-\pi C_3 &= 0\\ \beta N_3-\xi V_3 &= 0 \end{aligned}\right\}. \tag{9}$$

From system (9) we have the following equations

$$V_3=\frac{\beta N_3}{\xi}. \tag{10}$$

$$C_3=\frac{\eta\xi C_0+(\gamma\beta\eta+\sigma(s\xi+\tau\beta))N_3}{\pi\xi\eta}=f(N_3). \tag{11}$$

$$H_3=\frac{s\xi N_3+\tau\beta N_3}{\eta\xi}. \tag{12}$$

On the other hand, the first equation provides $g(N_3)$ such that

$$g(N_3)=r\left(1-\frac{N_3}{L}\right)-\alpha f(N_3). \tag{13}$$

By using equation (13), we analyze $g(N_3)$ in three different scenarios as follows:

(a) When $N_3=L+\dfrac{\omega\psi KL}{r}$ we have the following

$$-\left(\omega\psi KL+\frac{\eta\xi C_0 r+(\gamma\beta\eta+\sigma(s\xi+\tau\beta))(rL+\omega\psi KL)}{\pi r\xi\eta}\right)<0.$$

(b) At $N_3=0$, a function $g(N_3)$ is given by

$$g(0)=\alpha\left(\frac{r}{\alpha}-\frac{C_0}{\pi}\right).$$

Since $g\left(L+\dfrac{\omega\psi KL}{r}\right)<0$, there exist a positive root N_3 in the interval of $0<N_3<L+\dfrac{\omega\psi KL}{r}$ if and only if $g(0)>0$. Clearly, this requirement is met upon satisfaction of condition (8).

(c) For uniqueness of $N=N_3$, we need to prove that $g'(N_3)<0$. Considering equation (13) and some algebraic simplifications, it can be easily shown that

$$g'(N_3)=-\left(\frac{r}{L}+\alpha\frac{\gamma\beta\eta+\sigma(s\xi+\tau\beta)}{\pi\xi\eta}\right)<0.$$

Thus, a unique positive root, say $N=N_3$ of the equation (13) lies on interval $0<N_3<L+\dfrac{\omega\psi KL}{r}$. Substituting $N=N_3$ into equations (10)–(12) we get the appropriate values of $V=V_3$, $C=C_3$ and $H=H_3$. Hence, it can be concluded that an equilibrium point E_3 exists, whenever the condition (8) holds.

Existence of E^*

Interior equilibrium point E^* of the system (6) can be obtained by solving the system (14).

$$\left.\begin{aligned} r\left(1-\frac{N^*}{L}\right)-\alpha C^*+\omega\psi B^* &= 0\\ sN^*+\tau V^*-\eta H^* &= 0\\ C_0+\gamma V^*+\sigma H^*-\rho B^*C^*-\pi C^* &= 0\\ \theta\left(1-\frac{B^*}{K}\right)-\psi N^* &= 0\\ \beta N^*-\xi V^* &= 0 \end{aligned}\right\} \tag{14}$$

The solution of the system (14) establishes the following results

$$V^*=\frac{\beta N^*}{\xi} \tag{15}$$

$$H^*=\frac{(s\xi+\tau\beta)N^*}{\xi\eta} \tag{16}$$

$$B^*=\frac{K}{\theta}\left(\theta-\psi N^*\right) \tag{17}$$

$$C^* = \frac{\eta C_0 \xi + \eta\gamma\beta N^* + \sigma N^*(s\xi + \tau\beta)}{\eta\xi(\rho B^* + \pi)} \tag{18}$$

$$h(N^*, B^*) = r\left(1 - \frac{N^*}{L}\right) - \frac{\alpha}{\eta\xi\pi}\left(\xi\eta C_0 + \xi\gamma\beta N^* + \sigma N^*(s\xi + \tau\beta)\right) + \omega\psi B^* \tag{19}$$

From equation (19) when no forest resources ($B^* = 0$) we get the following function of N^*

$$f(N^*) = r\left(1 - \frac{N^*}{L}\right) - \frac{\alpha}{\eta\xi\pi}\left(\xi\eta C_0 + \xi\gamma\beta N^* + \sigma N^*(s\xi + \tau\beta)\right). \tag{20}$$

By using equation (20) $f(N^*)$ can be analyzed as follows,

(a) We evaluate a function $f(N^*)$ at $N^* = 0$ to get the following

$$f(0) = \alpha\left(\frac{r}{\alpha} - \frac{C_0}{\pi}\right) > 0$$

(b) When $N^* = L + \dfrac{\omega\psi KL}{r}$ we have the following

$$-\left[\omega\psi K + \frac{\alpha}{\eta\xi\pi r}\left[r\xi\eta C_0 + (rL + \omega\psi KL)(\xi\gamma\beta + (s\xi + \tau\beta)\sigma)\right]\right] < 0$$

There exists a positive root $N = N^*$ of equation (20) in the interval $(0, L + \dfrac{\omega\psi KL}{r})$ under condition (8).

(c) For uniqueness of $N = N^*$, we need $f'(N^*) < 0$, that is

$$f'(N^*) = -\left(\frac{r}{L} + \frac{\alpha}{\eta\xi\pi}(\xi\gamma\beta + \sigma(s\xi + \tau\beta))\right) < 0$$

Thus, a unique positive root, say N^* of the equation (20) lies on interval $0 < N^* < L + \dfrac{\omega\psi KL}{r}$. Substituting the obtained value of N^* into equations (15), (16) and (17) and performing algebraic simplifications we get the appropriate values of V^*, B^* and H^*. Since the values of N^* and B^* are known, then to obtain the value of C^* we substitute N^* and B^* into equation (18) and we conclude that an interior point E^* exists under condition (8).

3.3. Stability analysis

In this section the behaviors of different equilibrium points of the model system are analyzed. From the system (6) the Jacobian matrix is given by

$$J = \begin{pmatrix} r\left(1 - \frac{N}{L}\right) - \frac{rN}{L} - \alpha C + \omega\psi B & 0 & -\alpha N & \omega\xi N & 0 \\ s & -\eta & 0 & 0 & \tau \\ 0 & \sigma & -\rho B - \pi & -\rho C & \gamma \\ -\psi B & 0 & 0 & \theta\left(1 - \frac{B}{K}\right) - \frac{\theta B}{K} - \psi N & 0 \\ \beta & 0 & 0 & 0 & -\xi \end{pmatrix}.$$

At the equilibrium point $E_1\left(0, 0, \dfrac{C_0}{\pi}, 0, 0\right)$ the corresponding Jacobian matrix J_{E_1}, resulted from evaluating matrix J through E_1 is given by

$$J_{E_1} = \begin{pmatrix} \alpha\left(\frac{r}{\alpha} - \frac{C_0}{\pi}\right) & 0 & 0 & 0 & 0 \\ s & -\eta & 0 & 0 & \tau \\ 0 & \sigma & -\pi & \frac{-\rho C_0}{\pi} & \gamma \\ 0 & 0 & 0 & \theta & 0 \\ \beta & 0 & 0 & 0 & -\xi \end{pmatrix}.$$

The eigenvalues of a matrix J_{E_1} are $\lambda_1 = -\xi$, $\lambda_2 = \theta$, $\lambda_3 = -\eta$, $\lambda_4 = -\pi$ and $\lambda_5 = \dfrac{r}{\alpha} - \dfrac{C_0}{\pi} > 0$. The equilibrium point E_1 is unstable since it have at least one positive eigenvalues, that is $\lambda_2 > 0$ and $\lambda_5 > 0$.

Similarly, evaluating matrix J at E_2, the following matrix is established.

$$J_{E_2}=\begin{pmatrix} \frac{K^2\omega\psi\rho+K\pi\psi\omega+Kr\rho+\pi r-\alpha C_0}{\rho K+\pi} & 0 & 0 & 0 & 0 \\ s & -\eta & 0 & 0 & \tau \\ 0 & \sigma & -K\rho-\pi & \frac{-C_0\rho}{\rho K+\pi} & \gamma \\ -\psi K & 0 & 0 & -\theta & 0 \\ \beta & 0 & 0 & 0 & -\xi \end{pmatrix}.$$

The eigenvalues of J_{E_2} are $\lambda_1=-\xi$, $\lambda_2=-\theta$, $\lambda_3=-\eta$, $\lambda_4=-(K\rho+\pi)$, and $\lambda_5=\frac{K^2\omega\psi\rho+K\pi\psi\omega+Kr\rho+\pi r-\alpha C_0}{\rho K+\pi}$. Clearly, upon utilizing condition (8), $\lambda_5>0$ making E_2 unstable.

At the equilibrium point E_3, we establish a matrix J_{E_3}, such that

$$J_{E_3}=\begin{pmatrix} -\frac{rN_3}{L} & 0 & -\alpha N_3 & \omega\psi N_3 & 0 \\ s & -\eta & 0 & 0 & \tau \\ 0 & \sigma & -\pi & -\rho C_3 & \gamma \\ 0 & 0 & 0 & -\left(\psi N_3-\theta\right) & 0 \\ \beta & 0 & 0 & 0 & -\xi \end{pmatrix}.$$

$$N_3>\frac{\theta}{\psi} \tag{21}$$

Upon satisfaction of condition (21) all the entries at the main diagonal will be negative, following [15], we utilize the Gershgorin's Theorem by columns of the matrix to deduce sufficient conditions for local stability of E_3. As such, E_3 is proved to be asymptotically stable upon satisfaction of conditions in equation (22).

$$\begin{cases} \frac{L}{r}(s+\beta)<N_3<\frac{\pi}{\alpha} \\ \sigma<\eta \\ \frac{\rho C_m+\theta}{\psi(\omega+1)}<N_3<\frac{\rho C_m-\theta}{\psi(\omega-1)} \\ \tau+\gamma<\xi \end{cases} \tag{22}$$

Where C_m is defined in Lemma 1

Theorem 2. *The equilibrium point E_3, if exists, is locally asymptotically stable if conditions (22) are satisfied.*

At the interior equilibrium point E^*, the Jacobian matrix J, was evaluated to get a matrix J_{E^*}, such that

$$J_{E^*}=\begin{pmatrix} -\frac{rN^*}{L} & 0 & -\alpha N^* & \omega\psi N^* & 0 \\ s & -\eta & 0 & 0 & \tau \\ 0 & \sigma & -\rho B^*-\pi & -\rho C^* & \gamma \\ -\psi B^* & 0 & 0 & -\frac{\theta B^*}{K} & 0 \\ \beta & 0 & 0 & 0 & -\xi \end{pmatrix}.$$

Clearly, all entries in the main diagonal of J_{E^*} are negative. Following [15], we use the Gershgorin's Theorem by columns of the matrix to deduce the local stability of E^*. As such, E^* is proved to be locally asymptotically stable upon satisfaction of the following set of conditions

$$\begin{cases} N^*>\max\left\{\frac{L}{r}(\beta-\psi K),\frac{L}{r}(\psi K-\beta)\right\} \\ \sigma<\eta \\ N^*<\frac{\rho K-\pi}{\alpha} \\ \frac{\rho C_m-\theta}{\omega\psi}<N^*<\frac{\theta+\rho C_m}{\omega\psi} \\ \tau+\gamma<\xi \end{cases} \tag{23}$$

Where C_m is defined in lemma (1).

Theorem 3. *The interior equilibrium point E^*, if exists, is locally asymptotically stable if conditions (23) are satisfied.*

Theorem 4. *The interior equilibrium point E^*, if exists, is globally asymptotically stable in Ω if conditions (24) are satisfied.*

$$\left.\begin{aligned} r &> \min\left\{\frac{81\beta^2 L\gamma^2}{16\xi^2(\rho K+\pi)}, \frac{9\sigma^2 s^2}{16\eta(\rho K+\pi)}\right\} \\ L &< \max\left\{\frac{4(\rho K+\pi)}{9\alpha^2}, \frac{4\xi^2 s^2}{81\tau^2\beta^2}\right\} \end{aligned}\right\} \tag{24}$$

The proof of theorem (4) is presented in Appendix A.

3.4. Ecological interpretation of stability analysis

Equilibrium points E_1 and E_2 represent different situations regarding the extinction of the human population and the presence or absence of forest biomass. The point E_1 signifies the extinction of forest biomass, while E_2 represents a situation where forest biomass exists. The absence of human population would lead to the cessation of human-related activities, resulting in a lack of stabilization in atmospheric CO_2 concentration. Only natural processes such as volcanic eruptions will contribute to CO_2 emissions, resulting in a natural depletion of atmospheric CO_2 concentration. However, the analysis reveals further that the forest will rapidly grow up to its carrying capacity, acting as a sink for CO_2 absorption. The atmospheric CO_2 concentration will solely depend on natural processes and will naturally deplete.

The equilibrium point E_3 illustrates a situation where forest biomass no longer exists. In such a scenario, the emitted CO_2 will undergo some degree of natural absorption, while the remaining portion will persist in the atmosphere. This state is achieved when the natural growth rate of the human population exceeds the mortality rate resulting from the natural release of CO_2.

The interior equilibrium point E^* takes into account the coexistence of human population, economic activities, atmospheric CO_2 concentration, forest area, and vehicle population. To achieve this balance, the natural growth rate of the human population needs to exceed the mortality rate caused by natural CO_2 emissions. Moreover, specific conditions for the global stability of E^* must be met to ensure the stability of the atmospheric CO_2 concentration. When these conditions are satisfied, the forest biomass can absorb the existing atmospheric CO_2, safeguarding the environment, while the remaining CO_2 gradually decreases. These interpretations emphasize how human actions and natural processes interact, highlighting the critical importance of maintaining the necessary conditions to uphold the stability of atmospheric CO_2 concentration and environmental well-being.

4. Quantitative analysis

4.1. Parameter estimation and model fitting

The parameter estimation process was done by adjusting the model parameters to best fit the time series data of world population [23], atmospheric CO_2 concentration [24–26], forest area [27], number of vehicles produced [28], and Gross Domestic Product (GDP) [29]. The specific values of the parameters were obtained through the least squares method, which minimizes the sum of squared differences between the model predictions and the actual data. We use a MATLAB in-built function *(fminsearch)* that implements unconstrained nonlinear minimization (Nelder-Mead) to get candidates that serve as local minimizers for the sum of squared residuals [30]. The selection of initial parameter values was guided by the fulfillment of conditions outlined in the qualitative analysis section. In addition to the data-driven parameter estimation, values of $L = 11$, $C_0 = 5$ and $K = 750000$ were obtained from [31], [18] and [32] respectively. For the intrinsic human population growth rate (r), data from [23] was considered, where a range of 0.02 to 0.03 per year is considered [31]. This range provides an estimate for the value of r that is consistent with the available data and existing literature. The initial time is set to 1994, and the starting values are $N(0) = 5.66315$ billion people, $H(0) = 2,787.67662$ billion US$, $C(0) = 358.96$ ppm, $B(0) = 4,099.2026$ million hectares, and $V(0) = 49.658288$ million vehicles.

To test the validity of the model, R-squared values are employed [31]. The R-squared values for real data and model predictions of human population, human economic activities, atmospheric CO_2 concentration, forest biomass, and vehicle production are 0.955471914, 0.94694, 0.981052, 0.9535782, and 0.9275, respectively. These values indicate a strong correlation between the real data and the model predictions. The real and model projections of the variables N, H, C, B and V are shown in Fig. 1. It is evident from the figure that there is a close alignment between the model projections and the actual data, which ensures the validity of the model.

Furthermore, we applied statistical metrics to assess the performance of our model, including the Root Mean Squared Error Normalized (RMSEN) and the Nash-Sutcliffe Efficiency index (NSE). RMSEN, as it approaches zero, serves as a positive indicator of the model's effectiveness. To classify model performance, we follow the criteria established in previous research [33,34], where RMSEN is considered excellent if it is less than or equal to 10%, good between 10% and 20%, reasonable between 20% and 30%, and poor if it exceeds 30%.

On the other hand, the coefficient of efficiency (NSE) quantifies the overall deviation between real and predicted values from the actual data (R_i) and its mean (R). The NSE value can range from $-\infty$ to $+1$, with higher values indicating efficient model predictions. By using Formula (26), we calculated NSE to be 0.9343, suggesting efficient model predictions. Additionally, employing Formula (25), we obtained an RMSEN value of 2.6027%, further supporting the assessment of excellent model predictions.

In Equation (25), R_i represents the actual data value, R denotes the mean of actual data points, S_i represents the model's predicted data points, and n signifies the number of observations.

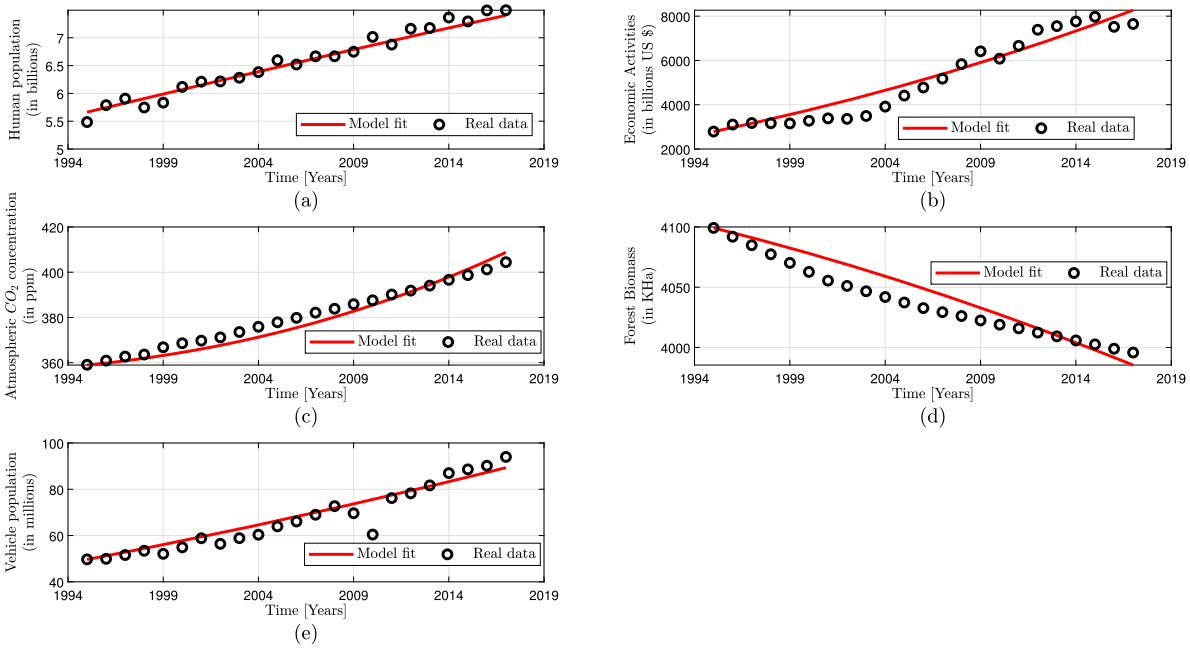

Fig. 1. Comparison between model fit and real data of (a) Human population, (b) Economic activities, (c) Atmospheric CO_2 concentration, (d) Forest biomass and (e) Vehicle population. The curve illustrates that there is a close alignment between the model solution and the observed data.

Table 2
Estimated model parameters, 95% confidence intervals, initial guess for parameters and their respective source.

Parameter	Baseline	Source	Interval	Estimated
r	0.026	[31]	[0.022645 0.03378]	0.0285245
α	0.000001	[32]	$[7.3998\times10^{-7}\ 1.2967\times10^{-6}]$	0.0000010551
τ	3.94	Assumed	-	3.94
s	0.035	[19]	[0.01752 0.04611]	0.03374
γ	4.9337×10^{-7}	Assumed	$[1.6407\times10^{-8}\ 2.3026\times10^{-8}]$	1.3657×10^{-8}
σ	0.000576	Assumed	[0.0005178 0.00079]	0.0007897
η	6.67×10^{-7}	Assumed	-	6.67×10^{-7}
π	0.016	[32]	[0.009668 0.0221]	0.016232
θ	0.0523	Assumed	[0.000909 0.001425]	0.0012025
β	0.0729	Assumed	[0.27216 0.30054]	0.27534
ψ	0.26×10^{-3}	Assumed	[0.0003480.0004031]	0.38874×10^{-3}
ρ	4.8×10^{-9}	[32]	$[0.8662\times10^{-6}\ 1.461\times10^{-6}]$	3.86657×10^{-7}
ξ	1.0676×10^{-6}	Assumed	$[8.374\times10^{-6}\ 1.05005\times10^{-5}]$	1.50623×10^{-5}
ω	0.001	Assumed	[0.00072517 0.0013074]	0.00094457

$$RMSEN = 100\times\frac{1}{R}\sqrt{\frac{1}{n}\times\sum_{i=1}^{n}(R_i-S_i)^2} \tag{25}$$

$$NSE = 1-\frac{\sum_{i=1}^{n}\left(R_i-S_i\right)^2}{\sum_{i=1}^{n}\left(R_i-R\right)^2} \tag{26}$$

In addition, to assess the robustness of model fitting, we computed 95% confidence intervals for the parameter estimates, as presented in Table 2. These confidence intervals strongly suggest a 95% likelihood of containing the true parameter value. To construct these confidence intervals, we employed a bootstrapping resampling technique with 1000 different data samples, each of the same size as the original datasets. We then re-estimated model parameters for each data sample. It is worth noting that the true parameter value is encompassed within the calculated intervals in 95% of the cases. The narrow width of these confidence intervals underscores the reliability of the model's parameter estimates. Notably, the value of r falls within the range specified by [31], providing further support for the credibility of the parameter estimation. The combination of these tests confirms the robustness of the model's parameter estimates, affirming its suitability for predictive purposes.

4.2. Parameter sensitivity analysis

In order to grasp the impact of model parameters on the system output, we conducted a global sensitivity analysis (GSA) employing partial ranking correlation coefficient (PRCC) which use Latin Hypercube sampling Monte Carlo simulation (LHS). This approach allows us to assess how changes in individual parameters can influence the overall model output [35,36]. A positive PRCC indicate a positive correlation between model parameters and its output. Meaning that increase in the magnitude of a model parameter value will lead to a significant increase in the model output, and a decrease in parameter value will result to a reduced model output. Conversely, a negative PRCC suggest an inverse relationship between parameter value and the model predictions [37]. Observing Fig. 2(a), it is evident that atmospheric CO_2 concentration is significantly accelerated by the growth rate of the vehicle population, denoted as β, and the emission rate of human activities, represented by σ, which is heavily influenced by β and the intrinsic growth rate of the human population, depicted in Fig. 2(c). Furthermore, the PRCC values for the mortality rate due to adverse impacts of enhanced atmospheric CO_2 (α), γ, σ, and β suggest that an increase in these values will lead to a decline in the human population. Conversely, increasing values of r, π, ω, θ, and ψ are associated with an increase in the human population, as illustrated in Fig. 2(b). Also, high values of human population intrinsic growth rate r, lead to the increased demand for mobility as depicted in Fig. 2(d) as the result deforestation will be increased as shown in Fig. 2(e). Analyzing the PRCC values, we pinpointed several highly influential parameters, notably the growth rate of the vehicle population (β), the CO_2 emission rate from human activities (σ) which is triggered by vehicle population, and the intrinsic growth rate of the human population (r). These findings strongly indicate that taking measures to reduce atmospheric CO_2 concentration and addressing the adverse effects of increased emissions from transportation could be pivotal in promoting environmentally friendly transportation practices.

4.3. Numerical simulation

To validate feasibility of the model analysis, we utilized MATLAB R2021a and Maple 2015 software. The chosen set of parameters from Table 2 satisfied the condition (8) for the existence of interior equilibrium point E^*. The eigenvalues of the Jacobian matrix corresponding to the equilibrium point E^* were calculated to be $-3.160388, -0.224952, -0.87302, -5.85509 \times 10^{-7}$, and -0.15062, all of which are negative. This indicates that the equilibrium point E^* is locally asymptotically stable and the condition (24) for global stability of E^* is satisfied for estimated parameter values. Furthermore, the solution trajectories of the model (6) are plotted in Fig. 3 with different starting values. It can be observed that all trajectories initiated inside the region Ω converge towards the interior equilibrium point E^*. This demonstrates the nonlinear stability behavior of the point E^* in the $N(t) - V(t) - B(t)$ and $N(t) - B(t) - C(t)$ space, as depicted in Fig. 3.

To investigate the impact of increased vehicular CO_2 emissions on the human population, we manipulated the most sensitive parameter, denoted as β (as depicted in Fig. 2(c)), within our model. As shown in Fig. 4(a), doubling the vehicle population growth rate has a noticeable effect on the temporal evolution of atmospheric CO_2 concentration, illustrated in Fig. 4(b). The data clearly shows that as the vehicle population increases, atmospheric CO_2 concentration rises.

When we assess the implications of this heightened transportation activity, with the vehicle population growth rate doubled (as shown in Fig. 4(a)), it stimulates economic growth, increasing it from $64,670.4$ billion US dollars to $1,071,774$ billion US dollars (as depicted in Fig. 4(c)). Simultaneously, atmospheric CO_2 levels increase from 1578 ppm to 2299.83 ppm (as seen in Fig. 4(b)). This results in a reduction in the human population, declining from 10.5255 billion to 10.3976 billion after 100 years as shown in Fig. 4(d).

5. Conclusion

At present time, the control of CO_2 emission along with fulfilling demand for mobility of both humans, goods and services is one of the important issues from ecological and environmental perspectives. The rapid increase in population influences the growth of atmospheric CO_2 concentration and hence climate change issues become more pronounced. In the present study, we have proposed and analyzed a non-linear mathematical model for vehicular CO_2 emission in relation to human population, economic activities, forest biomass and vehicle population.

The proposed model is useful to predict the long-term impact of vehicle CO_2 emission on atmospheric CO_2 evolution and human population. To verify the validity of a model, the model is simulated by using the real world datasets and model parameters fitted to these datasets. All conditions for existence and stability of the interior equilibrium point are satisfied by the estimated data. Numerical simulation shows that an increase in the vehicle CO_2 emission rate results to an increase of atmospheric CO_2 concentration as a result human population depletes due to adverse impact of enhanced atmospheric CO_2 concentration.

In addition, we conducted a global sensitivity analysis of the model parameters using PRCC. The analysis revealed that the atmospheric CO_2 concentration is significantly influenced by the growth rate of the vehicle population (β), the intrinsic human population growth rate (r), and the CO_2 emissions from human activities triggered by the growth in the vehicle population. Furthermore, we identified a connection between the decline in human population and the adverse impacts of increased atmospheric CO_2 concentration and the CO_2 emission rate from human activities (σ). These findings underscore the importance of considering sustainable transportation practices to mitigate the negative impacts on human population caused by an elevated atmospheric CO_2 concentration.

Therefore, to reduce the atmospheric CO_2 concentration, efforts to lower the emission from vehicles are advised so as to attain the seventh and thirteenth Sustainable Development Goals (SDG'S). The present study is not merely confined to consider the impact

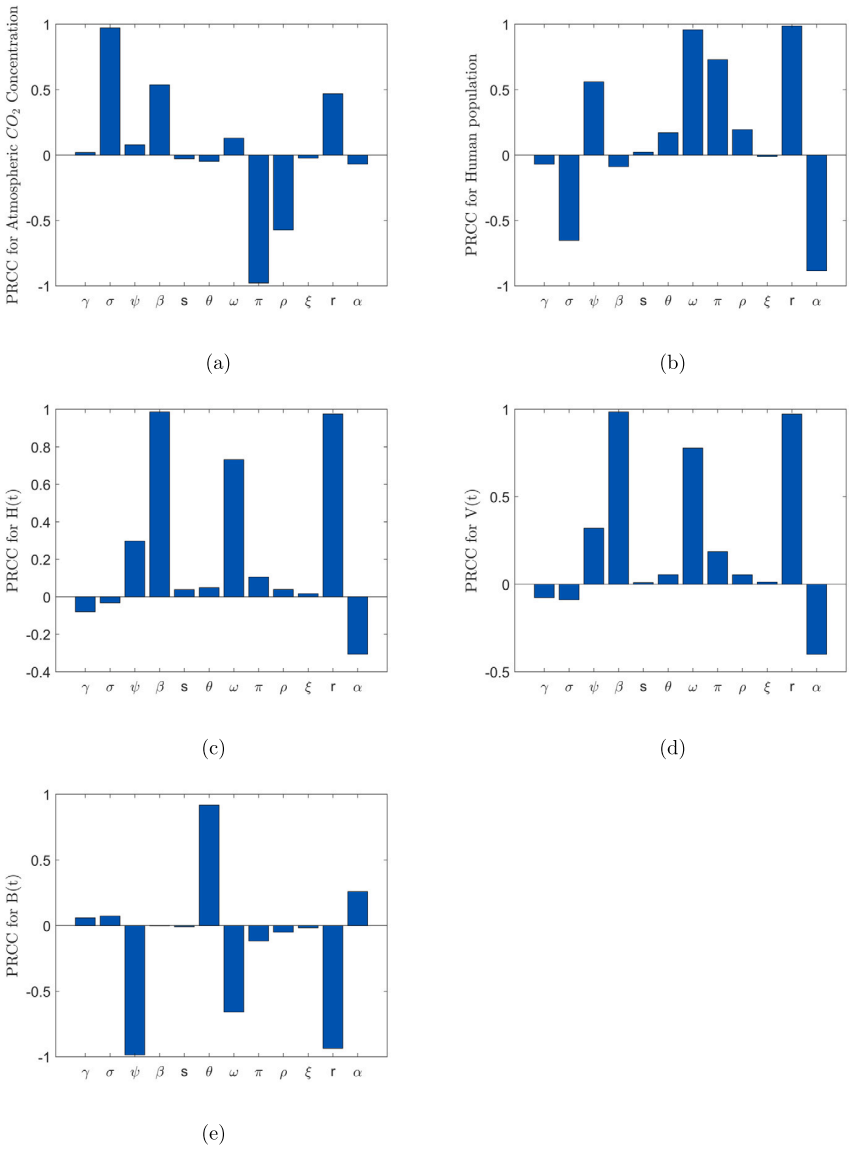

Fig. 2. Sensitivity analysis of model dynamics conducted through 1000 simulations using Latin Hypercube Sampling (LHS). Partial Rank Correlation Coefficients (PRCCs) with respect to atmospheric CO_2 concentration, human population, human economic activities, vehicle population, and forest biomass are presented in graphs (a), (b), (c), (d), and (e), respectively.

of electric vehicles, shared mobility facilities such as Bus rapid Transit (BRT) and alternative transportation modes on atmospheric CO_2 dynamics. Instead, it offers a foundational structure for predicting the long-term effects of atmospheric CO_2 concentration in relation to transport related emissions and human population with the help of analytical results. This will enable the development of strategies to alleviate the potential negative consequences of increased levels of carbon dioxide (CO_2). The present study can be extended to include the impact of electric vehicles, shared mobility facilities and alternative transportation modes on atmospheric CO_2 dynamics.

CRediT authorship contribution statement

Pita Donald: Writing – review & editing, Writing – original draft, Validation, Methodology, Investigation, Formal analysis, Conceptualization. **Maranya Mayengo:** Writing – review & editing, Writing – original draft, Supervision, Methodology, Investigation, Formal analysis, Conceptualization. **Aristide G. Lambura:** Writing – review & editing, Writing – original draft, Supervision, Methodology, Formal analysis, Conceptualization.

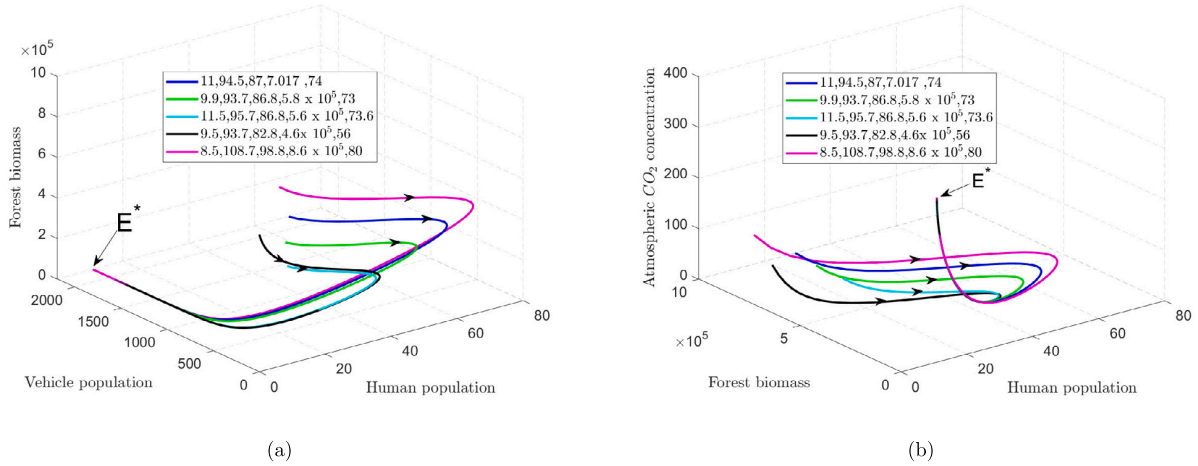

Fig. 3. Graphical representation for global stability of an interior equilibrium point E^* in $N-V-B$ Fig. 3 (a) and $N-V-C$ Fig. 3 (b). All solution trajectories with different initial start are attracted to the interior equilibrium point E^*.

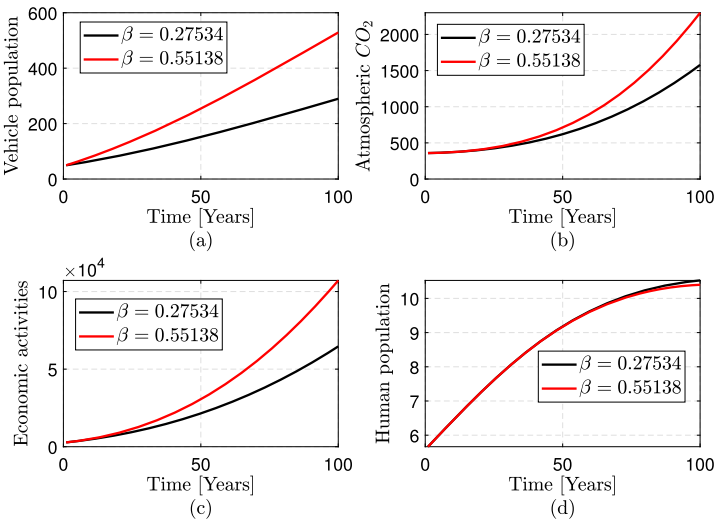

Fig. 4. Impact of increased transportation activities on time evolution of atmospheric CO_2 Fig. 4(b), economic activities Fig. 4(c), and human population Fig. 4(d). As vehicle population is doubled, results to an increase in the atmospheric CO_2 concentration and decline in human population.

Declaration of competing interest

The authors assert that they do not have any identifiable financial conflicts of interest or personal relationships that could have potentially influenced the findings presented in this paper.

Data availability

The data that support the findings of this study are available at the repositories listed below.

1. World Bank Open Data (WBOD). population, total. https://data.worldbank.org/indicator/SP.POP.TOTL, Accessed: 2022-12-16
2. World Bank Open data (WBOD): GDP (current US dollar), World Bank national accounts data, and OECD National Accounts data files https://data.worldbank.org/indicator/NY.GDP.MKTP.CD, Accessed: 2022-12-16
3. Food and Agriculture Organization (FAO), electronic files and web site, https://data.worldbank.org/indicator/AG.LND.FRST.K2., Accessed: 2022-12-16
4. National Oceanic and Atmospheric Administration (NOAA). Trends in Atmospheric Carbon Dioxide, Mauna Loa CO2 annual mean data. https://gml.noaa.gov/ccgg/trends/data.html, Accessed: 2022-12-16 & Our Word in Data (OWD), CO2 emissions https://ourworldindata.org/co2-emissions

5. Beureau of Transportation Statistics (BTS). World Motor Vehicle Production. https://www.bts.gov/content/world-motor-vehicle-production-selected-countries, Accessed: 2022-12-16

Funding

No any fund received in accomplishing this study.

Acknowledgements

Authors are thankful to the handling editor and reviewer for their useful suggestions which improved the quality of this paper. Also, we gratefully acknowledge The Nelson Mandela African Institution of Science and Technology (NM-AIST) and National Institute of Transport (NIT).

Appendix A. Proof of Theorem 4

To analyze the global stability of the interior equilibrium E^*, we use Lyapunov stability theory. Consider the following scalar valued positive definite function

$$\begin{aligned} U &= \left(N - N^* - N^* \ln \frac{N^*}{N}\right) + \frac{1}{2}k_1 (H - H^*)^2 + \frac{1}{2}k_2 (C - C^*)^2 \\ &\quad + \frac{1}{2}k_3 \left(B - B^* - B^* \ln \frac{B^*}{B}\right) + \frac{1}{2}k_4 (V - V^*)^2 \end{aligned} \tag{A.1}$$

Where k_1, k_2, k_3 and k_4 are suitable positive constants to be determined later.
Differentiating U with respect to t;

$$\frac{dU}{dt} = \frac{\partial U}{\partial N}\left(\frac{dN}{dt}\right) + \frac{\partial U}{\partial H}\left(\frac{dH}{dt}\right) + \frac{\partial U}{\partial C}\left(\frac{dC}{dt}\right) + \frac{\partial U}{\partial B}\left(\frac{dB}{dt}\right) + \frac{\partial U}{\partial V}\left(\frac{dV}{dt}\right) \tag{A.2}$$

Performing algebraic operations we get the following;

$$\begin{aligned} \frac{dU}{dt} &= -\frac{r}{L}(N - N^*)^2 - \eta k_1 (H - H^*)^2 - k_2 (\rho K + \pi)(C - C^*)^2 - \frac{\theta k_3}{K}(B - B^*)^2 \\ &\quad -\xi k_4 (V - V^*)^2 + \alpha (C - C^*)(N - N^*) + \psi \left(\omega - k_3\right)(B - B^*)(N - N^*) \\ &\quad +s k_1 (H - H^*)(N - N^*) + \tau k_1 (V - V^*)(H - H^*) + \gamma k_2 (V - V^*)(C - C^*) \\ &\quad +\sigma k_2 (H - H^*)(C - C^*) + \beta k_4 (N - N^*)(V - V^*) \end{aligned} \tag{A.3}$$

Choosing $k_3 = \omega$ we have the following;

$$\begin{aligned} \frac{dU}{dt} &= -\frac{r}{L}(N - N^*)^2 - \eta k_1 (H - H^*)^2 - k_2 (\rho K + \pi)(C - C^*)^2 - \frac{\theta k_3}{K}(B - B^*)^2 \\ &\quad -\xi k_4 (V - V^*)^2 + \alpha (C - C^*)(N - N^*) + s k_1 (H - H^*)(N - N^*) \\ &\quad +\tau k_1 (V - V^*)(H - H^*) + \gamma k_2 (V - V^*)(C - C^*) \\ &\quad +\sigma k_2 (H - H^*)(C - C^*) + \beta k_4 (N - N^*)(V - V^*) \end{aligned} \tag{A.4}$$

Choosing $k_1 = \frac{\eta r}{s^2 L}$, $k_2 = 1$, $k_3 = \omega$ and $k_4 = \frac{\xi r}{\beta^2 L}$, $\frac{dU}{dt}$ is negative definite under conditions (24), hence the Theorem (4) is proved.

Appendix B. Proof of Lemma 1

From the fourth equation of model system (6), we have

$$\frac{dB}{dt} \leq \theta B \left(1 - \frac{B}{K}\right). \tag{B.1}$$

By comparing the above differential inequality with the differential equation

$$\frac{dB}{dt} = \theta B \left(1 - \frac{B}{K}\right). \tag{B.2}$$

and using comparison theorem, we have

$$B(t) \leq \frac{K}{1 + \left(\frac{K}{B(0)} - 1\right) e^{-\theta t}}. \tag{B.3}$$

Let $\epsilon > 0$ be given. Then $\exists_{t_0 \geq 0}$ such that

$$B(t) \leq K + \epsilon \qquad \forall_{t \geq t_0}. \tag{B.4}$$

This gives

$$\limsup_{t\to\infty} B(t) \le B_m. \tag{B.5}$$

Now from the first equation of the model system (6), we have

$$\frac{dN}{dt} \le (r + \omega\psi(K+\epsilon))N - \frac{rN^2}{L} \qquad \forall_{t\ge t_0}. \tag{B.6}$$

Using the same argument as previously, $\exists_{t_1\ge t_0}$ such that

$$N(t) \le (r + \omega\psi(K+\epsilon))\frac{L}{r} + \epsilon = N_\epsilon \quad , \quad \forall_{t\ge t_1\ge t_0}. \tag{B.7}$$

Hence

$$\limsup_{t\to\infty} N(t) \le N_m. \tag{B.8}$$

From second equation in the model system (6), we get

$$\frac{dH}{dt} \le sN_\epsilon - \eta H \qquad \forall_{t\ge t_1}. \tag{B.9}$$

Then we have

$$H(t) \le \frac{sN_\epsilon}{\eta} + \epsilon = H_\epsilon \quad , \quad \forall_{t\ge t_2\ge t_1}. \tag{B.10}$$

Hence

$$\limsup_{t\to\infty} H(t) \le H_m. \tag{B.11}$$

From third equation of the model system (6)

$$\frac{dC}{dt} \le C_0 + \sigma H\epsilon - \rho(K+\epsilon)C - \pi C \qquad \forall_{t\ge t_2}. \tag{B.12}$$

$\exists_{t_3\ge t_2}$ such that

$$C(t) \le \frac{C_0 + \sigma H_\epsilon}{\rho(K+\epsilon)+\pi} + \epsilon = C_\epsilon \qquad \forall_{t\ge t_3\ge t_2}. \tag{B.13}$$

Hence

$$\limsup_{t\to\infty} C(t) \le C_m. \tag{B.14}$$

Similarly, it can be easily shown that $\limsup_{t\to\infty} V(t) \le \frac{\beta N_m}{\xi}$. Thus, the Lemma 1 is proved.

Appendix C. Supplementary material

Supplementary material related to this article can be found online at https://doi.org/10.1016/j.heliyon.2024.e23976.

References

[1] J.-C. Yeh, C.-H. Liao, Impact of population and economic growth on carbon emissions in Taiwan using an analytic tool STIRPAT, Sustain. Environ. Res. 27 (1) (2017) 41–48, https://doi.org/10.1016/j.serj.2016.10.001.

[2] A. Majewska, U. Gierałtowska, Impact of economic affluence on CO2 emissions in CEE countries, Energies 15 (1) (2022) 322, https://doi.org/10.3390/en15010322.

[3] J. Hussain, A. Khan, K. Zhou, The impact of natural resource depletion on energy use and CO2 emission in Belt Road Initiative countries: a cross-country analysis, Energy 199 (2020) 117409, https://doi.org/10.1016/j.energy.2020.117409.

[4] S. Pal, I. Ghosh, Dynamics of a coupled socio-environmental model: an application to global CO2 emissions, Ecol. Model. 478 (2023) 110279, https://doi.org/10.1016/j.ecolmodel.2023.110279.

[5] A. Mohammadi, A.A. Burhan, R. Mangal, Impact of population and economic growth on CO2 emission (case of Afghanistan), J. Emerg. Technol. Innov. Res. (2020).

[6] M. Appiah, F. Li, B. Korankye, Modeling the linkages among CO2 emission, energy consumption, and industrialization in sub-Saharan African (SSA) countries, Environ. Sci. Pollut. Res. 28 (29) (2021) 38506–38521, https://doi.org/10.1007/s11356-021-12412-z.

[7] T. Boden, G. Marland, R. Andres, Global, regional, and national fossil-fuel co2 emissions, 1751 - 2006 (published 2009), https://doi.org/10.3334/CDIAC/00001, 2009.

[8] W.F. Lamb, T. Wiedmann, J. Pongratz, R. Andrew, M. Crippa, J.G.J. Olivier, D. Wiedenhofer, G. Mattioli, A.A. Khourdajie, J. House, S. Pachauri, M. Figueroa, Y. Saheb, R. Slade, K. Hubacek, L. Sun, S.K. Ribeiro, S. Khennas, S. de la Rue du Can, L. Chapungu, S.J. Davis, I. Bashmakov, H. Dai, S. Dhakal, X. Tan, Y. Geng, B. Gu, J. Minx, A review of trends and drivers of greenhouse gas emissions by sector from 1990 to 2018, Environ. Res. Lett. 16 (7) (2021) 073005, https://doi.org/10.1088/1748-9326/abee4e.

[9] Y. Li, J. Shang, C. Zhang, W. Zhang, L. Niu, L. Wang, H. Zhang, The role of freshwater eutrophication in greenhouse gas emissions: a review, Sci. Total Environ. 768 (2021) 144582, https://doi.org/10.1016/j.scitotenv.2020.144582.
[10] X. Zhao, A. Mahendra, N. Godfrey, H. Dalkmann, P. Rode, G. Floater, Unlocking the power of urban transport systems for better growth and a better climate, in: The New Climate Economy, 2016.
[11] V.N. Pedreira, M.L. Brito, L.C.L. dos Santos, G. Simonelli, Modeling of Brazilian carbon dioxide emissions: a review, Braz. Arch. Biol. Technol. 65 (2022), https://doi.org/10.1590/1678-4324-2022210594.
[12] IEA, CO2 emissions from fuel combustion 2019 edition, IEA CO2 emissions from fuel combustion database, Available at http://wds.iea.org, 2019.
[13] D. Helbing, D. Brockmann, T. Chadefaux, K. Donnay, U. Blanke, O. Woolley-Meza, M. Moussaid, A. Johansson, J. Krause, S. Schutte, M. Perc, Saving human lives: what complexity science and information systems can contribute, J. Stat. Phys. 158 (3) (2014) 735–781, https://doi.org/10.1007/s10955-014-1024-9.
[14] A.K. Misra, K. Lata, A mathematical model to achieve sustainable forest management, Int. J. Model. Simul. Sci. Comput. 06 (04) (2015) 1550040, https://doi.org/10.1142/s1793962315500403.
[15] S. Devi, N. Gupta, Dynamics of carbon dioxide gas: effects of varying capability of plants to absorb CO2, Nat. Resour. Model. 32 (1) (2018) e12174, https://doi.org/10.1111/nrm.12174.
[16] A.K. Misra, M. Verma, A mathematical model to study the dynamics of carbon dioxide gas in the atmosphere, Appl. Math. Comput. 219 (16) (2013) 8595–8609, https://doi.org/10.1016/j.amc.2013.02.058.
[17] M. Verma, A.K. Verma, A.K. Misra, Mathematical modeling and optimal control of carbon dioxide emissions from energy sector, Environ. Dev. Sustain. 23 (9) (2021) 13919–13944, https://doi.org/10.1007/s10668-021-01245-y.
[18] A.K. Misra, M. Verma, E. Venturino, Modeling the control of atmospheric carbon dioxide through reforestation: effect of time delay, Model. Earth Syst. Environ. 1 (3) (Sep. 2015), https://doi.org/10.1007/s40808-015-0028-z.
[19] M.A.L. Caetano, D.F.M. Gherardi, T. Yoneyama, Optimal resource management control for CO2 emission and reduction of the greenhouse effect, Ecol. Model. 213 (1) (2008) 119–126, https://doi.org/10.1016/j.ecolmodel.2007.11.014.
[20] A.J. McMichael, R.E. Woodruff, S. Hales, Climate change and human health: present and future risks, Lancet 367 (9513) (2006) 859–869, https://doi.org/10.1016/s0140-6736(06)68079-3.
[21] S.A. Roosa, A.G. Jhaveri, Carbon reduction technologies, in: Energy Management Handbook, Publishers, River, 2020, pp. 561–581.
[22] H.I. Freedman, J.W.-H. So, Global stability and persistence of simple food chains, Math. Biosci. 76 (1) (1985) 69–86, https://doi.org/10.1016/0025-5564(85)90047-1.
[23] WBOD, Population, total [dataset]: https://data.worldbank.org/indicator/SP.POP.TOTL, 2018. (Accessed 16 December 2022).
[24] D.M. Etheridge, L.P. Steele, R.L. Langenfelds, R.J. Francey, J.-M. Barnola, V.I. Morgan, Natural and anthropogenic changes in atmospheric CO2 over the last 1000 years from air in Antarctic ice and firn, J. Geophys. Res., Atmos. 101 (D2) (1996) 4115–4128, https://doi.org/10.1029/95jd03410.
[25] H. Ritchie, M. Roser, P. Rosado, CO2 and greenhouse gas emissions, in: Our World in Data, 2020.
[26] NOAA, Trends in atmospheric carbon dioxide, mauna Loa co2 annual mean data [dataset], https://gml.noaa.gov/ccgg/trends/data.html, 2020. (Accessed 16 December 2022).
[27] FAO, Forest area (sq. km), food and agriculture organization, electronic files and web site [dataset], https://data.worldbank.org/indicator/AG.LND.FRST.K2, 2020. (Accessed 16 December 2022).
[28] BTS, World motor vehicle production [dataset], https://www.bts.gov/content/world-motor-vehicle-production-selected-countries, 2019. (Accessed 16 December 2022).
[29] WBOD, Gdp (current us dollar), world bank national accounts data, and oecd national accounts data files [dataset], https://data.worldbank.org/indicator/NY.GDP.MKTP.CD, 2019. (Accessed 16 December 2022).
[30] F. Gao, L. Han, Implementing the Nelder-Mead simplex algorithm with adaptive parameters, Comput. Optim. Appl. 51 (1) (2010) 259–277, https://doi.org/10.1007/s10589-010-9329-3.
[31] M. Verma, A.K. Verma, Effect of plantation of genetically modified trees on the control of atmospheric carbon dioxide: a modeling study, Nat. Resour. Model. 34 (2) (Feb. 2021), https://doi.org/10.1111/nrm.12300.
[32] M. Verma, A.K. Misra, Optimal control of anthropogenic carbon dioxide emissions through technological options: a modeling study, Comput. Appl. Math. 37 (1) (2016) 605–626, https://doi.org/10.1007/s40314-016-0364-2.
[33] R.V. Ferreira, R.L.M. Tavares, S.F. d. Medeiros, A.G.d. Silva, J.F.d. Silva Júnior, Carbon stock and organic fractions in soil under monoculture and Sorghum bicolor–Urochloa ruziziensis intercropping systems, Bragantia 79 (2020) 425–433.
[34] H. Léonidas, T. Toru, N. Fidel, C.R. Athanase, M. Athanase, Comparative analysis of monocropping and mixed cropping systems on selected soil properties, soil organic carbon stocks, and simulated maize yields in drought-hotspot regions of Rwanda, Heliyon (2023).
[35] T. Azizi, R. Mugabi, Global sensitivity analysis in physiological systems, Appl. Math. 11 (03) (2020) 119–136, https://doi.org/10.4236/am.2020.113011.
[36] S. Bidah, O. Zakary, M. Rachik, Stability and global sensitivity analysis for an agree-disagree model: partial rank correlation coefficient and Latin hypercube sampling methods, Int. J. Differ. Equ. 2020 (2020) 1–14, https://doi.org/10.1155/2020/5051248.
[37] I.M. Fanuel, S. Mirau, D. Kajunguri, F. Moyo, Conservation of forest biomass and forest–dependent wildlife population: uncertainty quantification of the model parameters, Heliyon 9 (6) (2023).

Poster presentation

Mathematical models for vehicle carbon dioxide emission

Pita Mwaitolage Donald[1,2], *Dr. Maranya Mayengo* [1], *Dr. Aristide Lambura* [3]

[1] *Department of Applied Mathematics and Computational Sciences, The Nelson Mandela African Institution of Science and Technology, P.O.BOX 447 Arusha*

[2] *Department of Mathematics and Technical Education, The National Institute of Transport P.O.BOX 705 Dar es Salaam*

[3] *Department of Computer Systems and Mathematics, Ardhi University, P.O.BOX 35176, Dar es Salaam*

Introduction

Carbon dioxide (CO_2) is one of the greenhouse gas that contribute to the global warming [1,2]. This gas is derived from energy sector, industrial processes, building operations, transportation activities, agricultural practices, forestry, and other land use activities (AFOLU). Urban and global transport contribute 23% and 25% of total energy-related emissions respectively [3]. A deterministic mathematical model is formulated and analyzed to study the dynamics of atmospheric CO_2 concentration in relation to vehicle CO_2 emissions. Furthermore an optimal control problem was formulated and solved, it was revealed that, the atmospheric CO_2 concentration depletes as technological innovations for running vehicles is implemented along with reforestation efforts.

Model formulation

A system of non-linear ode is formulated and analyzed to capture the dynamic relationship between human population (N), Human economic activities (H), Atmospheric CO_2 concentration (C), Forest biomass (B) and Vehicle population (V).

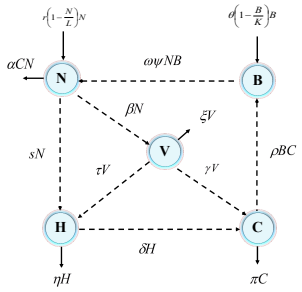

Figure 5: Schematic representation of the model, with variables human population (N), Human economic activities (H), Atmospheric CO_2 (C), Forest biomass (B) and Vehicles (V)

The following is a system of non-linear ordinary differential equation for vehicle CO_2 emission.

$$\begin{cases} \dot{N} - rN\left(1-\frac{N}{L}\right) + \omega\psi NB - \alpha CN \\ \dot{H} - sN + \tau V - \eta H \\ \dot{C} - C_0 + \gamma V + \delta H - \rho BC - \pi C \\ \dot{B} - \theta B\left(1-\frac{B}{K}\right) - \psi NB \\ \dot{V} - \beta N - \xi V \end{cases} \tag{2}$$

Where

$$N(0) \geqslant 0, H(0) \geqslant 0, C(0) > 0, B(0) \geqslant 0, V(0) \geqslant 0 \tag{3}$$

The steady states of the system Eq. 2 are representing four different scenarios. Where $E_1\left(0,0,\frac{C_0}{\pi},0,0\right)$ shows the non existence of human population and forest biomass, hence cessation of human related activities. $E_2\left(0,0,\frac{\theta C_0}{K\rho+\pi},K,0\right)$ indicates the absence of human population, hence human related activities distinct and forest will grow up to its carrying capacity, the naturally emitted CO_2 will deplete by both natural processes and through photosynthesis process. Also, two non-trivial solutions $E_3(N_3,H_3,C_3,0,V_3)$ and $E^*(N^*,H^*,C^*,B^*,V^*)$ exists if condition 4 holds.

$$r > \alpha\frac{C_0}{\pi} \tag{4}$$

That is E_3 and E^*, exists if the intrinsic human population growth rate is greater than the mortality rate due to the adverse impact caused by natural CO_2 emissions such as volcanic eruptions.

The equilibrium point E^* is ecologically significant, since it consider the co existence of all variables. For sustainable transportation practices the conditions for global stability of E^* is to be considered.

Parameter Estimation

The system of non-linear ordinary differential equations was fitted to actual data points spanning 29 years, utilizing the least square method. To enhance the accuracy of the parameter estimates, bootstrapping sampling techniques were applied 1000 times, resulting in the establishment of 95% confidence intervals for the parameter estimates. It is noteworthy that all model parameters Eq.1 were found to lie within the constructed confidence intervals.

$$\begin{aligned} &L = 11, r = 0.0285, \alpha = 0.00000106, \tau = 3.94, s = 0.03374, \\ &\gamma = 1.37\times10^{-8}, \sigma = 0.0007897, \eta = 6.67\times10^{-7}, \pi = 0.0162, \\ &\theta = 0.001203, \beta = 0.27534, \psi = 0.389\times10^{-3}, \rho = 3.87\times10^{-7} \\ &\xi = 1.506\times10^{-5}, \omega = 0.0009446, K = 75000, C_0 = 5. \end{aligned} \tag{1}$$

R^2 values for model prediction and the actual data for N, H, C, B and V are 0.955, 0.9469, 0.98, 0.95, and 0.9275 , respectively, suggesting a strong correlation between model prediction and the actual data. To assess the performance of the model, the Root Mean Squared Error Normalized (RMSEN) and the Nash-Sutcliffe Efficiency index (NSE) was computed to be 2.6027% and 0.9343 indicating excellent model prediction.

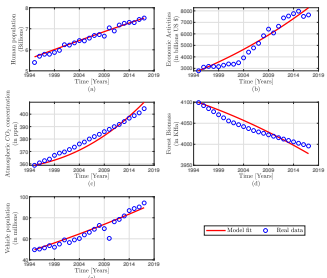

Figure 1: Model fitting to the actual data, showing strong correlation between model prediction and actual data

Optimal control problem

We introduced control parameters μ_1 for the efficiency of mitigation options to cut down CO_2 emission rate per unit vehicle in operations, μ_2 is the reforestation rate , μ_3 is the efficiency of mitigation options to cut down fossil fueled vehicle production and μ_4 represents Eco-efficiency or green economy implementation rate to cut down CO_2 emissions from human economic activities.

$$\begin{cases} \dot{N} = rN\left(1-\frac{N}{L}\right) - \alpha CN + (1-\mu_2)\omega\psi NB \\ \dot{H} = sN + \tau V - \eta H \\ \dot{C} = C_0 + (1-\mu_1)\gamma V + (1-\mu_4)\sigma H - \rho BC - \pi C \\ \dot{B} = \theta B\left(1-\frac{B}{K}\right) - (1-\mu_2)\psi NB \\ \dot{V} = (1-\mu_3)\beta N - \xi V \end{cases} \tag{5}$$

The ad-joint system is given by Eq. 6

$$\begin{cases} \dot{\lambda}_1 - \left(\frac{2rN}{L} - r - (1-\mu_2)\psi\omega B + \alpha C\right)\lambda_1 - \lambda_2 s + \\ (1-\mu_2)\psi\lambda_4 B - (1-\mu_3)\beta\lambda_5 \\ \dot{\lambda}_2 - \eta\lambda_2 - (1-\mu_4)\sigma\lambda_3 \\ \dot{\lambda}_3 - -a_1 + \alpha\lambda_1 N + \rho\lambda_3 B + \pi\lambda_3 \\ \dot{\lambda}_4 - \rho\lambda_3 C - \omega\psi\lambda_1 N - \left(\theta - \frac{2\theta B}{K} - (1-\mu_2)\psi N\right)\lambda_4 \\ \dot{\lambda}_5 - \xi\lambda_5 - \tau\lambda_2 - (1-\mu_1)\gamma\lambda_3 \end{cases} \tag{6}$$

We intend to minimize the atmospheric CO_2 concentration with its associated implementation cost by using objective functional Eq.7

$$J - min_{\mu_i \epsilon U}\int_0^T \left[a_1C(t) + a_2\mu_1^2(t) + a_3\mu_2^2(t) + a_4\mu_3^2(t) + a_5\mu_4^2(t)\right]dt \tag{7}$$

We find optimal controls $\mu_1^*, \mu_2^*, \mu_3^*$ and μ_4^* such that:

$$J(\mu_1^*,\mu_2^*,\mu_3^*,\mu_4^*) = \min_U J(\mu_1,\mu_2,\mu_3,\mu_4)$$

Results and discussion

Model analysis revealed that, the increased vehicle CO_2 emissions leads to the depletion of human population due to the adverse impacts of enhanced atmospheric CO_2 concentration. From numerical simulation of optimal control problem, it can be easily observed that, implementation of mitigation options to cut down vehicle CO_2 emission rate, reforestation efforts, mitigation option to cut down fossil fueled vehicle manufacture together with efforts to implement green economy to cut CO_2 emissions from human economic activities results to 2.866% decline in atmospheric CO_2 concentration.

Numerical simulation

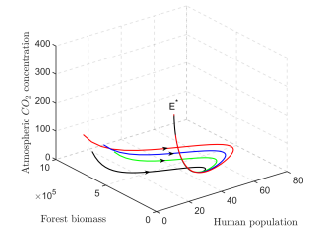

Figure 2: Graphical representation of non linear stability of equilibrium point E^*

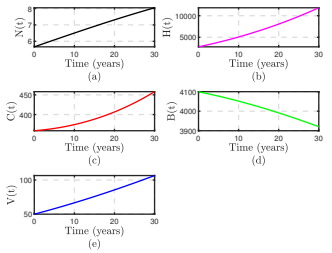

Figure 3: Basic Model numerical simulation, As vehicle population is increasing, then results to an increased atmospheric CO_2

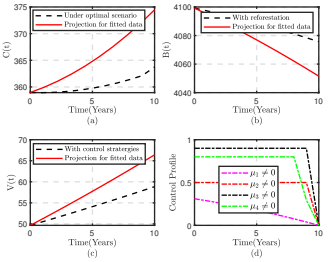

Figure 4: Optimal control for atmospheric CO_2 when efficient technological innovations for running vehicles are implemented along with reforestation efforts.

Ecological interpretation

From an ecological standpoint, it is crucial to examine the equilibrium point, denoted as E^*. This point signifies the simultaneous existence of all state variable values necessary for ecological balance. The existence of this equilibrium point hinges upon the condition that the intrinsic human population growth rate exceeds the mortality rate induced by the adverse effects of naturally emitted CO_2.

References

Verma, M., Vema, A.K.,& Misra, B. (2021). Mathematical modeling and optimal control of carbon dioxide emissions from energy sector. *Environment, Development and Sustainability* 23(9), 13919–13944.

Verma, M., & Vema, A.K. (2018). optimal control of anthropogenic carbon dioxide emissions through technological options, A modeling study. *Natural Resource Modeling* 37(1), 605–626.

Devi, S., & Gupta, N. (2019). Dynamics of carbon dioxide gas (CO_2): Effects of varying capability of plants to absorb CO_2. *Natural Resource Modeling*, 32(1), e12174.